

## 2. EXPLANATORY NOTES<sup>1</sup>

Shipboard Scientific Party<sup>2</sup>

### INTRODUCTION

The “Explanatory Notes” chapter documents the primary procedures and methods employed by the various shipboard laboratories during Leg 206. This information concerns only shipboard methods described in the Leg 206 *Initial Reports* volume of the *Proceedings of the Ocean Drilling Program* (ODP). Methods for shore-based analysis of Leg 206 samples and data will be described in the individual scientific contributions to be published in scientific journals and in the *Scientific Results* volume.

### Authorship

All shipboard scientists contributed to the completion of this volume. The separate sections of the chapters were, however, written by an individual or groups of scientists as given below (listed in order of seniority where appropriate and alphabetically otherwise):

Principal Results: Shipboard Scientific Party

Background and Objectives: Wilson, Teagle

Operations: Grout, Acton

Sedimentary lithostratigraphy: Coggan, Jiang, Teagle, Acton, Alt,  
Banerjee, Cooper, Crispini, Laverne, Tartarotti, Umino

Biostratigraphy: Jiang

Sediment geochemistry: Ziegler

Paleomagnetism: Acton, Wilson, Sandwell

Physical properties: Kerneklian, Barr

Downhole measurements: Einaudi, Kalberkamp, Barr

Basement stratigraphy: Umino, Cooper, Nichols, Teagle

Igneous petrology: Cooper, Umino, Nichols, Teagle

Igneous geochemistry: Nichols, Cooper, Umino, Teagle

Alteration: Alt, Laverne, Banerjee, Coggan, Teagle

<sup>1</sup>Examples of how to reference the whole or part of this volume.

<sup>2</sup>Shipboard Scientific Party addresses.

Structure: Tartarotti, Crispini  
Microbiology: Banerjee  
Digital imaging: Barr, Einaudi, Kalberkamp  
Underway geophysics: Wilson  
Thin section descriptions: Umino, Laverne, Alt, Crispini, Tartarotti,  
Banerjee, Coggon

## Numbering of Sites, Holes, Cores, and Samples

Drilling sites are numbered consecutively from the first site drilled by the *Glomar Challenger* in 1968. At a site, multiple holes can be drilled by removing the drill pipe from the seafloor, moving the ship a short distance, and then drilling a new hole. For all ODP drill sites, a letter suffix distinguishes each hole drilled at the same site. The first hole drilled is assigned the site number modified by the suffix “A,” the second hole takes the site number and suffix “B,” and so forth.

The cored interval is measured in meters below seafloor (mbsf). The depth below seafloor is determined by subtracting the water depth estimated from the initial drill pipe measurement, which gives the length of pipe from the rig floor to the seafloor (measured in meters below rig floor), from the total drill pipe measurement. Each cored interval is generally 9.5 to 9.6 m long, which is the length of a core barrel. Coring intervals may be shorter and may not necessarily be adjacent if separated by drilled intervals.

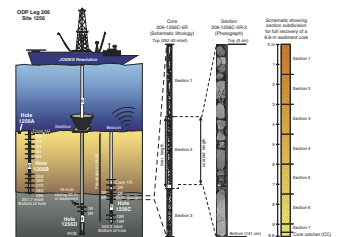
A recovered core is divided into 1.5-m sections that are numbered serially from the top. When full recovery is obtained, the sections are numbered from 1 through 7, with the last section possibly being shorter than 1.5 m (Fig. F1); rarely, an unusually long core may require more than seven sections. When less than full recovery is obtained, there will be as many sections as needed to accommodate the length of the core recovered. By convention, material recovered from the core catcher of a sedimentary core is placed in a separate section during the core description, labeled core catcher (CC), and placed below the last section recovered in the liner. The core catcher is placed at the top of the cored interval in cases where material is only recovered in the core catcher.

When the recovered core is shorter than the cored interval, the top of the core is equated with the top of the cored interval by convention to achieve consistency in handling analytical data derived from the cores. Samples removed from the cores are designated by distance measured in centimeters from the top of the section to the top and bottom of each sample removed from that section. A full identification number for a sample consists of the following information: leg, site, hole, core number, core type, section number, piece number (for hard rock), and interval in centimeters measured from the top of section. For example, a sample identification of “206-1256C-9R-2, 80–85 cm” would be interpreted as representing a sample removed from the interval between 80 and 85 cm below the top of Section 2, Core 9 (R designates that this core was taken with the rotary core barrel) of Hole 1256C from Leg 206 (Fig. F1).

All ODP core identifiers indicate core type. The following abbreviations are used:

H = hydraulic piston corer (also referred to as advanced hydraulic piston corer or advanced piston corer [APC]).

F1. ODP labeling scheme, p. 50.



- X = extended core barrel (XCB).
- R = rotary core barrel (RCB).
- G = ghost core (material from the junk basket for Leg 206).
- W = wash core.
- M = miscellaneous material.

## **Core Handling**

### **Sedimentary Cores**

As soon as a core is retrieved on deck, it goes through a sequence of processing steps. Usually, a sample is first taken from the core catcher and given to the paleontology laboratory for an initial age assessment. The core is then placed on a long horizontal rack. For safety monitoring, small (~5 cm<sup>3</sup>) plugs of sediment are also usually taken from the end of one section per core for headspace gas analysis. Gas samples may also be taken by piercing the core liner, typically at voids, and withdrawing gas into a syringe (referred to as vacutainer samples). Next, the core is marked into section lengths, each section is labeled, and the core is cut into sections. Interstitial water (IW) whole-round samples are then taken at intervals requested by scientists and approved by the sample allocation committee; whole-round samples for microbiology studies may also be taken (following sterile handling procedures as outlined in individual sample requests) at this stage if they have been requested. For some of the cores that contain gas, several small holes are drilled into the core liners to allow gas to escape.

Each section is then sealed at the top and bottom with color-coded plastic caps—blue to identify the top of a section and clear for the bottom. A yellow cap is placed on the section ends from which a whole-round sample has been removed, and the sample code (e.g., IW) is written on the yellow cap. The caps are usually attached to the liner by coating the end liner and the inside rim of the cap with acetone, and then the caps are taped to the liners. The core sections are then carried into the laboratory, where the individual sections are again labeled using an engraver to permanently mark the full designation of the section. The length of the core liner and core in each section and the core catcher sample are measured to the nearest centimeter. The core-liner length and curated length are typically identical for sedimentary sections, although small variations can occur when, for example, core material extrudes beyond the core liner in gassy sediments. Both lengths are logged into the ODP database program.

After a core has equilibrated to room temperature, which usually takes ~1–3 hr, each whole-round core section is run through the multi-sensor track (MST), and thermal conductivity measurements are made on soft-sediment cores. Whole-round samples for shore-based studies of paleomagnetism, consolidation, shear strength, and other elastic properties may be taken at this stage if they have been requested.

Cores of soft material are split lengthwise into working and archive halves. The softer cores are split with a wire or saw, depending on the degree of induration. Harder cores are split with a band saw or diamond saw. The wire-cut cores are split from bottom to top, so investigators should be aware that older material could have been transported up the core on the split face of each section.

## **Igneous Cores**

Igneous rock cores are handled differently from sediment cores. Once on deck, the core catcher sample is placed at the bottom of the core liner and total core recovery is calculated by pushing the rock pieces together and measuring to the nearest centimeter. The core then is cut into 1.5-m-long sections and transferred into the laboratory.

The contents of each section are transferred into 1.5-m-long sections of split core liner, where the bottom of oriented pieces (i.e., pieces that clearly could not have rotated top to bottom about a horizontal axis in the liner) is marked with a red wax pencil. This is done to ensure that orientation is not lost during the splitting and labeling processes. Important primary features of the cores also are recorded at this time. A plastic spacer is used to separate individual pieces and/or reconstruct contiguous groups of pieces in the core liner. These spacers may represent a substantial interval of no recovery. The length of each section is then recorded and entered into the database as the curated length. The curated length will commonly differ by a few centimeters from the liner length measured on the catwalk. At this point, cores are marked by a shipboard petrologist for splitting and the outer cylindrical surfaces of the whole-round pieces are scanned with a digital core scanner, called the DMT CoreScan, which was rented for use during Leg 206 (see [“Digital Imaging,”](#) p. 34). Each piece of core is then split into archive and working halves, with the positions of spacers maintained for both halves. Each piece is numbered sequentially from the top of each section, beginning with number 1; reconstructed groups of pieces are assigned the same number, but they are lettered consecutively. Pieces are labeled only on the outer cylindrical surfaces of the core. If the piece is oriented, an arrow is added to the label pointing to the top of the section.

## **All Cores**

For both sedimentary and igneous cores, the archive half is described visually (see [“Visual Core Descriptions,”](#) p. 9, in [“Lithostratigraphy”](#)). Smear slides are made from small amounts of sediment samples taken from the archive half. Digital images of the archive halves are made on the Geotek digital imaging system installed prior to Leg 198. Sedimentary archive-half sections are run through the archive multisensor track (AMST) for color reflectance spectroscopy measurements and susceptibility measurements with a point susceptibility meter and then through the cryogenic magnetometer for magnetic remanence measurements. Finally, the archive half is photographed using black-and-white and color film. Close-up photographs (color and black and white) are taken of particular features for illustrations in the summary of each site, as requested by individual scientists.

The working half of the core is sampled for both shipboard and shore-based laboratory studies. Samples are routinely taken for shipboard physical properties; paleomagnetic, thin section, and geochemical analyses; and microbiological and molecular investigations as described in the sections below. Each extracted sample is logged into the sampling computer database program by the location and the name of the investigator receiving the sample. Records of all removed samples are kept by the curator at ODP. The extracted samples are sealed in plastic vials, cubes, or bags and labeled. Special sampling and handling procedures are followed when required for postcruise investigations.

Following the initial scientific measurements and sampling, both halves of igneous cores are shrink-wrapped in plastic to prevent rock pieces from vibrating out of sequence during transit. The working and archive halves of sedimentary and igneous cores are then put into labeled plastic tubes, sealed, and transferred to cold-storage space aboard the drilling vessel. At the end of Leg 206, the cores were transferred from the ship in refrigerated containers to cold storage at the ODP Gulf Coast Repository at Texas A&M University in College Station, Texas.

## LITHOSTRATIGRAPHY

### Visual Core Description

Visual core description (VCD) forms (Fig. F2), or “barrel sheets,” drafted in AppleCORE software (version 8.1m), summarize the data obtained during shipboard observation and analysis of each sediment core. Detailed observations of each section were recorded initially by hand on blank AppleCORE templates with two sections per page. This information was subsequently entered into the AppleCORE software, which generates a simplified, annotated graphical description (barrel sheet) for each core. These barrel sheets are linked to corresponding core photographs in the volume Core Descriptions (see the “[Core Descriptions](#)” contents list). The following text explains the ODP conventions used for compiling each part of the core description form and the exact protocols adopted by the Leg 206 shipboard scientific party.

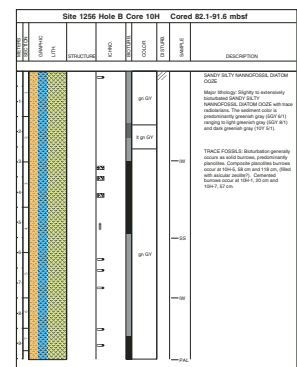
Shipboard scientists, none of whom specialized in sedimentology, were responsible for visual core logging and smear slide analysis. Mineral abundance and identifications were augmented by X-ray diffraction (XRD) analysis. Data describing biostratigraphy (age), geochemistry (CaCO<sub>3</sub>, organic carbon [C<sub>org</sub>], and major and trace element concentrations), paleomagnetism, and physical properties (wet bulk density and porosity) were integrated with the sedimentological information.

### Core Designation

Cores are designated using leg, site, hole, core number, and core type as discussed previously (see “[Numbering of Sites, Holes, Cores, and Samples](#),” p. 2, in “Introduction”). The cored interval is specified in terms of meters below seafloor. On the basis of drill pipe measurements, reported by the Transocean coring technician and the ODP operations manager, depths are corrected for the height of the rig floor dual elevator stool above sea level to give true water depth and correct meters below sea level.

Site, hole, and depth in meters below seafloor are given at the top of the barrel sheet, with depth positions of core sections indicated along the left margin. Columns on the barrel sheets include Graphic Lithology, Sedimentary Structures, Fossils (ichnofossils), Bioturbation, Color, Sediment Disturbance, Sample Types, and Remarks. These columns are discussed below, followed by an outline of the lithostratigraphic classification used during Leg 206.

F2. Examples of barrel sheets, p. 51.



## Graphic Lithology

Lithologies of the core intervals recovered are represented on barrel sheets by graphic patterns in the Graphic Lithology column (Figs. F2, F3). For intervals containing homogeneous mixtures of multiple lithologies, symbols are arranged within the column from left to right in order of their relative abundance. Graphic lithologies are used for components that compose 10% or more of the total sediment, with only the three most abundant components shown. The width of each pattern in the column approximates the relative abundance of that component. Relative abundances reported in this volume are useful for general characterization of the sediment, but they are not precise, quantitative data.

## Sedimentary Structures

Sedimentary structures formed by natural processes and not as a result of drilling disturbance are represented on the barrel sheet in the Structure column (Fig. F4). Structures formed by both biogenic and physical processes are included. These include varying degrees of bioturbation, types of trace fossils, parallel laminations, and soft-sediment deformation structures.

## Ichnofossils

Symbols are used to denote the location of clearly identifiable ichnofossils (Fig. F4).

## Bioturbation

The extent of general bioturbation is indicated in the Bioturbation column. Using a scheme similar to that proposed by Droser and Bottjer (1986), five levels of bioturbation were recognized. Bioturbation intensity is classified as abundant (>75%), common (50%–75%), moderate (10%–50%), rare (<10%), and barren (none); these levels are illustrated with graphic symbols in the Bioturbation column (Fig. F4).

## Color

Color is determined qualitatively using the Munsell rock color charts (Rock-Color Chart Committee, 1991) and is described immediately after the cores are split to avoid color changes associated with drying and oxidation. Color is generalized in the Color column with acronyms like “dk mo Br,” which is dark mottled brown (Table T1).

## Disturbance

Symbols are used to denote sediment disturbance induced by the coring process (Fig. F4). Symbols are positioned at the location in the section where that feature is observed. If the feature extends over an interval, the symbol appears centered on a vertical line to denote the stratigraphic extent of occurrence.

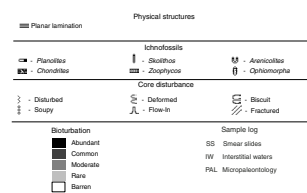
## Sample Types

Sample material taken for shipboard sedimentologic and chemical analysis consisted of pore water from whole-round samples, “toothpick” samples (smear slides), and discrete samples for XRD, paleomag-

F3. Graphic lithology symbols, p. 52.



F4. Barrel sheet symbols, p. 53.



T1. Color column acronyms, p. 74.



netic, and physical property analyses. Typically, one to two smear slides (or thin sections) were made per core and one pore water and two physical property samples were taken per core. XRD samples were taken from the interstitial pore water squeeze cakes and from unique locations to better characterize the lithologic components. Data such as grain size and relative abundance of sedimentary components from smear slides are summarized in data tables that are independent of the AppleCORE sheets. An up-to-date list of samples that have been taken from the cores can be obtained from the ODP Janus database.

### Remarks

The written description for each core contains a brief overview of major and minor lithologies that are present, as well as notable features (e.g., sedimentary structures).

### Sediment Classification

Lithologic names consist of a principal name based on composition, degree of lithification, and/or texture as determined from visual description and smear slide observations. For a mixture of components, the principal name is preceded by major modifiers (in order of increasing abundance) that refer to components making up 25% or more of the sediment. Minor components that represent between 10% and 25% of the sediment follow the principal name after a “with” in order of increasing abundance. Thus, an unconsolidated sediment containing 30% nannofossils, 25% clay minerals, 20% foraminifers, 15% quartz silt, and 10% manganese nodules would be described as a clayey nannofossil ooze with manganese nodules, quartz silt, and foraminifers. These naming conventions follow the ODP sediment classification scheme (Mazzullo et al., 1988), with the exception that during Leg 206 a separate “mixed sediment” category was not distinguished. During Leg 206, we did not encounter neritic sediments or chemical sediments and do not address these categories below.

Sediment was classified on the basis of composition estimated by visual examination of the core, smear slides, and thin sections and by shipboard measurements of carbonate content (see “Bulk Sediment Sampling and Chemical Analyses,” p. 16, in “Geochemistry”) and shipboard XRD analyses (see “Sample Types,” p. 6, in “Visual Core Descriptions”). In volcanoclastic sediments, the term “ash” (or “tuff” if lithified) is used in place of “sand,” whereas “lapilli” is used for granule and cobble size categories. Larger volcanic clasts (breccia) were not encountered, but discrete pumice lapilli are noted as “pumice clasts.” Size divisions for grains are those of Wentworth (1922) (Fig. F5). Size-textural qualifiers were not used for pelagic sediment names (e.g., nannofossil clay implies that the dominant component is detrital clay rather than clay-sized nannofossils).

Terms that describe lithification vary depending upon the dominant composition:

1. Sediment derived predominantly from calcareous pelagic organisms (e.g., calcareous nannofossils and foraminifers):
  - Ooze = sediment can be deformed with a finger.
  - Chalk = sediment can be scratched easily by a fingernail.
  - Limestone = sediment cannot be scratched easily.

F5. Sedimentary grain-size divisions, p. 54.

Millimeters (mm)	Micrometers (µm)	Phi (φ)	Wentworth size class	Rock type
4000	4000	4.0	Boulder	Conglomerate/ Breccia
200	200	4.0	Cobble	
64	64	4.0	Pebble	
4	4	4.0	Gravel	
2.00	2.00	4.0	Very coarse sand	Sandstone
1.00	1.00	4.0	Coarse sand	
0.50	500	4.0	Medium sand	
0.25	250	4.0	Fine sand	
0.125	125	4.0	Very fine sand	
0.0625	63	4.0	Silt	
0.031	31	4.0	Coarse silt	Siltstone
0.0156	15.6	4.0	Medium silt	
0.0078	7.8	4.0	Fine silt	
0.0039	3.9	4.0	Very fine silt	
0.0020	2.0	4.0	Clay	Claystone

2. Sediment derived predominantly from siliceous microfossils (diatoms, radiolarians, and siliceous sponge spicules):
  - Ooze = sediment can be deformed with a finger.
  - Radiolarite/spiculite/diatomite = sediment cannot be easily deformed manually.
  - Porcellanite = siliceous limestone/claystone that has a dull luster and is less hard and compact than chert (Keene, 1975). It may contain a mix of opal, quartz, clay minerals, and carbonate. Note that the terms “porcellanite” and “chert” do not imply crystallinity of the silica.
  - Chert = sediment displays a glassy luster. It may contain a mix of opal, quartz, clay minerals, and carbonate. Note that the terms “porcellanite” and “chert” do not imply crystallinity of the silica.
3. Sediment derived predominantly from siliciclastic material: if the sediment can be deformed easily with a finger, no lithification term is added and the sediment is named for the dominant grain size. For more consolidated material, the lithification suffix “-stone” is appended to the dominant size classification (e.g., “clay” vs. “claystone”).
4. Sediment composed of sand-sized volcanoclastic grains: if the sediment can be deformed easily with a finger, the interval is described as ash. For more consolidated material, the rock is called tuff. The term “lapilli” is used for coarse-grained material.

## **IGNEOUS ROCKS**

### **Core Curation and Shipboard Sampling**

To preserve important features and structures, core sections containing igneous rocks were examined before the core was split. Contacts were examined for evidence of chilling, baking, and alteration. Each piece was numbered sequentially from the top of each core section and labeled on the outside surface. Broken core pieces that could be fitted together were assigned the same number and were lettered consecutively from the top down (e.g., 1A, 1B, and 1C). Composite pieces sometimes occupied more than one section. Plastic spacers were placed between pieces with different numbers. The presence of a spacer may represent a substantial interval without recovery. If it was evident that an individual piece had not rotated about a horizontal axis during drilling, an arrow was added to the label pointing to the top of the section.

Nondestructive physical property measurements, such as magnetic susceptibility, natural gamma ray (NGR) emission, and digital imaging of the exterior of the whole-core pieces were made before the core was split (see “**Physical Properties**,” p. 29). The pieces were split with a diamond-impregnated saw in such a way that important compositional and structural features were preserved in both the archive and working halves. After splitting, the archive half was described on VCD forms and photographed. Digital images of the core were taken using the Geotek digital imaging scanner before describing. To minimize contamination of the core with platinum group elements and gold, the describers removed jewelry from their hands and wrists before handling. After the core was split and described, the working half was sampled for shipboard physical properties, paleomagnetic studies, thin sections, XRD,





each section of core that includes (1) the leg, site, hole, core number, core type, and section number; (2) the depth of the top of the section in meters below seafloor; (3) the unit number (consecutive downhole; subunits are designated by letters after the unit number, e.g., 1, 2a, 2b, etc.) (sedimentary units within the basement were also numbered consecutively downhole but were numbered separately from igneous units and were distinguished from them with the letter "S;" e.g., S1, S2); (4) the rock name; (5) a summary description of the unit as it appears in the section, including a brief rock name and the rock type (e.g., pillow basalt or sheet flow); (6) the piece numbers included in the unit; (7) the type of contacts; (8) the Munsell color; (9) the phenocryst minerals, abundance, and size; (10) the groundmass grain size; (11) vesicle abundance; (12) the nature of the alteration; (13) information about abundance and filling of veins; (14) a description of structures in the rock; and (15) any additional comments.

Units and subunits were named on the basis of the groundmass texture and the abundance of primary minerals. Basalts were described based on the identification of phenocrysts in hand sample:

Aphyric = <1% phenocrysts.  
Sparsely phyric = 1%–5% phenocrysts.  
Moderately phyric = 5%–10% phenocrysts.  
Highly phyric = >10% phenocrysts.

Rock names were further classified by the types of phenocrysts, where present (e.g., sparsely plagioclase-olivine phyric, in which the amount of olivine exceeds the amount of plagioclase). In cases where the groundmass grain size was fine grained or larger, we did not use these modifiers because it was difficult to distinguish phenocrysts from groundmass crystals in hand sample. (e.g., we used "fine-grained basalt" rather than "aphyric fine-grained basalt"). Rock color was determined on a wet, cut surface of the rock using the Munsell color chart. Groundmass character was determined by measuring average groundmass grain size (width of elongated grains) with a binocular microscope. Grain size was identified as

mg = medium grained (average groundmass grain size is 1 mm or greater).  
fg = fine grained (grains are 0.2–1 mm).  
μx = microcrystalline (groundmass crystals are 0.1–0.2 mm).  
cx = cryptocrystalline (crystals are <0.1 mm).  
G = glassy.

An estimate of the percentage of vesicles and their average sizes was made and included in the comments on the VCDs. Mineral abundance was used in determining the rock name. The igneous unit and contact logs are included (see Table T3).

Pillow basalts were identified by curved chilled margins oblique to the vertical axis of the core or, when these margins were absent, by variolitic texture, curved fractures, and microcrystalline or cryptocrystalline grain size. For glassy or chilled pieces lacking definitive indications of pillows (for example, with subhorizontal chilled margins), we designated the units as "flow margins," which could be interpreted either as pillow basalts or as the tops or bottoms of sheet flows or massive flows. Sheet flows were identified by sections of core <3 m thick with the same

lithology and grain size that increased toward the center of the unit. Massive units were identified by continuous intervals >3 m thick of similar lithology that increased in grain size toward their center. Other rock types distinguished were dikes, pillow breccias, breccias, and hyaloclastites.

### **Igneous Unit and Contact Logs**

The first step in describing the core was the selection of unit boundaries, as described in “**Visual Core Descriptions**,” p. 9. Subunits are designated in the VCD, and their descriptions are included within the overall written description of the unit. The igneous unit and contacts log (Table T3) provides information about the unit boundaries and a brief description of each unit. The table lists for each unit the core number; section number; piece number(s); location (in meters below seafloor) of the upper contact, calculated from the curated depth of the top of the core and the length of the pieces in the core above the upper contact; the type of the upper contact (listed in Table T3); the minimum thickness of the unit, calculated from the piece lengths; and the rock type of each unit.

### **Thin Sections**

Thin sections of igneous rocks were studied to complete and refine the hand-specimen observations. This included textural features that were not identified in hand specimen; precise determination of grain size of phenocrysts and groundmass; the mineralogy, abundance, and kind of glomerocrysts; the presence of inclusions within phenocrysts; and the presence of spinel, oxides, and sulfides. Crystal sizes of all primary phases were measured. In addition, mineral morphologies, grain sizes, and textural features were described. The terms hetero-granular (different crystal sizes), seriate (continuous range in grain size), porphyritic (indicating presence of phenocrysts), glomerophytic (containing clusters of phenocrysts), hypocrySTALLINE (100% crystals) to hypohyaline (100% glass), variolitic, intergranular (olivine and pyroxene grains between plagioclase laths), intersertal, subophitic, and ophitic were used to describe the textures of the mesostasis. The same terminology was used for thin section descriptions and the megascopic descriptions. An example of the thin section description form is given in Figure F8, with key in Table T4. Thin section descriptions are included in this volume (see the “**Core Descriptions**” contents list) and are also available from the ODP Janus database. Digital photomicrographs were taken during the cruise to document features described in the thin sections. A list of available images, any of which can be obtained from the ODP Data Librarian, is given in Table T30, p. 372, in the “Site 1256” chapter.

### **Alteration**

All igneous rocks recovered during Leg 206 have undergone alteration. On the hard rock VCD forms, rocks were graded according to whether they are fresh (<2% by volume alteration products) or have slight (2%–10%), moderate (10%–50%), high (50%–90%), or complete (90%–100%) alteration. Alteration and vein core description logs on a piece-by-piece scale were tabulated to provide a consistent characterization of the rocks and to quantify the different alteration types (see Tables T5, T6). Descriptions are based mostly on hand-specimen observa-

**F8.** Example thin section form, p. 57.

The form is a grid with multiple columns and rows. The columns are labeled with various parameters such as 'Sample ID', 'Section Number', 'Core Number', 'Depth (m)', 'Rock Type', 'Alteration', 'Comments', etc. The rows are numbered 1 through 10, providing space for detailed descriptions of each thin section.

**T5.** Example alteration log, p. 78.

**T6.** Example vein log, p. 79.

tions, and specific secondary minerals are not generally distinguished, except where crystal morphology allows unequivocal identification. Where additional mineralogical evidence is available from either thin section descriptions and/or X-ray diffractograms, these identifications were integrated into the alteration and vein logs and the VCDs.

We recorded the following information in the logs:

1. Alteration log (e.g., Table T5). This log was used to record the bulk rock alteration. Each entry records the igneous unit; identifiers for the core, section, piece, and subpiece; the locations of top and bottom of each piece; the length of each piece; and the depth below seafloor for the top of the core. The alteration type (as represented by rock color and calibrated by thin section observations), the abundance (in percent) and mineral fillings of vesicles, the abundance (in percent) of glass, and the percent alteration of glass are documented for each piece or groups of pieces. A column for comments is included.
2. Vein log (e.g., Table T6). This log was used to record the presence, location, width, and mineral content of veins observed on the cut surface of the cores. Each entry records the igneous unit and the identifiers for the core, section, piece, and subpiece. For each vein the location of the top and bottom of the feature is recorded, and the mineral fillings, vein width (in millimeters), presence or absence of a related alteration halo, and the width (in millimeters) of the halo on one side of the vein are recorded. For breccia, interflow sediment, and vein nets, recorded data include the centimeter interval, the percentages of nonbasalt material (veins, cement, and sediment), and the percentages of secondary minerals within the latter. A column for comments is included.

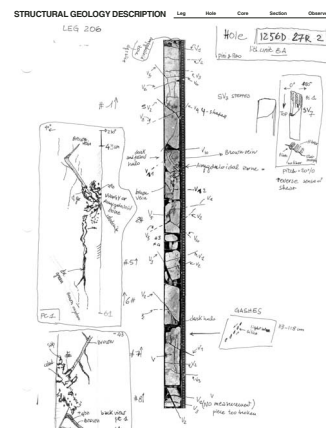
## STRUCTURAL GEOLOGY

This section outlines the techniques used for macroscopic and microscopic description of structural features observed in hard rock basement cores. Conventions for structural studies established during previous hard rock drilling legs (Leg 118, Shipboard Scientific Party, 1989; Leg 131, Shipboard Scientific Party, 1991; Leg 135, Shipboard Scientific Party, 1992c; Leg 140, Shipboard Scientific Party, 1992b; Leg 141, Shipboard Scientific Party, 1992a; Leg 147, Shipboard Scientific Party, 1993b; Leg 148, Shipboard Scientific Party, 1993a; Leg 153, Shipboard Scientific Party, 1995; Leg 176, Shipboard Scientific Party, 1999) were generally followed during Leg 206. However, several minor changes in nomenclature and procedure have been adopted.

### Graphical Representation and Terminology

All material from both working and archive halves was examined, although the sketches of the structures and orientation measurements were made on the archive half. The most representative structural features in the cores recovered during Leg 206 are summarized on the VCD form (see the “Core Descriptions” content list). For each section, more detailed structural information is described and sketched on a separate “Structural Geology Description” form (Fig. F9). Structural data were tabulated in two spreadsheet logs, “Structural Log” and “Breccia Log”

F9. Example structural description form, p. 58.



(Tables T7, T8), with reference to the structural geology checklist (Table T9).

To maintain consistency of core descriptions we used a set of structural feature “identifiers.” Brittle deformation identifiers include joint, vein, shear vein, fault, and breccia. Identification of these features is based on the presence of fractures, filling phases, and evidence of shear displacement. The terminology adopted generally follows that of Ramsay and Huber (1987), Twiss and Moores (1992), and Passchier and Trouw (1996) and is consistent with the terminology used during Leg 153 for brittle deformation (Shipboard Scientific Party, 1995). Some of the terms commonly used in the structural description are sketched in Figure F10:

- J = joints (fractures where the two sides show no differential displacement [relative to the naked eye or 10× pocket lens] and have no filling material).
- V = veins (extensional open fractures filled with epigenetic minerals).
- SV = shear veins (obliquely opening veins with minor shear displacement, filled with slickenfibers or overlapping fibers).
- F = faults (fractures with kinematic evidence for shear displacement across the discontinuity or with an associated cataclasite; we adopted the term microfault when the scale of the offset is millimetric).

This subdivision of the structures does not imply that all features fall into distinct and exclusive categories. We prefer to use the term veins for all the healed fractures, avoiding the usual subdivision based on fracture width (e.g., Ramsay and Huber [1987] defined veins as having >1 mm filling material), mainly to be consistent with the vein log (see “Alteration,” p. 11, in “Igneous Rocks”). There are not rigid boundaries between the adopted structural categories; where necessary, details specific of structural features are illustrated with comments and sketches.

In the VCD and Structural Log, the term “late magmatic vein” is used for texturally and/or compositionally distinct mineral products of late magmatic fluids that cut the primary features of the basalts. Ductile and brittle-ductile structures comprise folds, tension gashes, and shear veins, and most of them are related to magmatic and late magmatic events.

Brecciated core intervals are described in detail in a separate Breccia Log (Table T8), which records the compositional and textural features of the breccias. Where common types of breccia can be unambiguously recognized, such as hyaloclastite or jigsaw-puzzle breccia, a note was added in the Comments column. Data on the composition and alteration of both veins and breccias were integrated with the Alteration and Vein Logs (see “Alteration,” p. 11, in “Igneous Rocks”).

### Geometrical Reference Frame

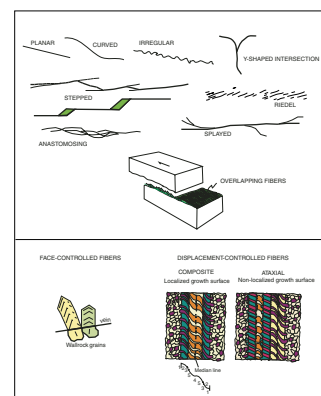
Structures are measured on the archive half relative to the core reference frame used by ODP. The plane normal to the axis of the borehole is referred to as the horizontal plane. On this plane, a 360° net is used with a pseudo-south (180°) pointing into the archive half and a pseudo-north (0°) pointing out of the archive half and perpendicular to the cut

T7. Example Structural Log, p. 80.

T8. Example Breccia Log, p. 82.

T9. Structural geology checklist, p. 83.

F10. Vein morphology and fiber growth examples, p. 59.





surface of the core (Fig. F11). The cut surface of the core, therefore, is a vertical plane striking  $90^{\circ}$ – $270^{\circ}$ .

Apparent dip angles of planar features were measured on the cut face of the archive half of the core. To obtain a true dip value, a second apparent dip reading was obtained where possible in a section perpendicular to the core face (second apparent orientation). The dip and the dip direction with respect to the archive half of the core are recorded on the spreadsheet together with second plane measurements. If the feature intersected the upper or lower surface of the core piece, measurements of the strike were made directly in the core reference frame and combined with the apparent dip measurements to calculate the true dip values. The two apparent dips and dip directions (or one apparent direction combined with the strike) measured for each planar feature are used to calculate the true orientation using the “LinesToPlane” Macintosh program by S.D. Hurst.

### Thin Section Description

Thin sections of basement rocks recovered during Leg 206 were examined in order to (1) confirm macroscopic descriptions of brittle structures; (2) characterize the microstructure of the rocks; (3) provide information on the kinematics of brittle and brittle-ductile deformation; (4) identify time relationships between deformation, magmatic, and alteration processes; (5) assess the role of fluid in contributing to deformation; and (6) document major structural zones and downhole variations. The microstructural notes were entered into the “Thin Section Description Form” spreadsheet database (see Fig. F8). For the description of microstructures we applied mostly the terminology of Passchier and Trouw (1996). Shipboard thin sections were generally oriented; the orientation is given relative to the core reference frame and was marked on each thin section by an arrow pointing upward and a short tick pointing toward “west” from the base of the arrow. Marking two directions is necessary in order to achieve complete orientation of thin sections cut parallel to the cut surface of the core. Digital photomicrographs were taken during the cruise to document features described in the thin sections. A list of available images, any of which can be obtained from the data librarian at ODP is given in Table T30, p. 372, in the “Site 1256” chapter.

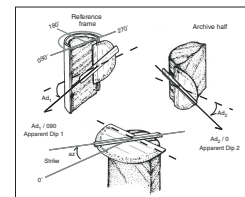
## GEOCHEMISTRY

### Interstitial Water Sampling and Chemical Analyses

Shipboard interstitial water analyses were performed on 5- to 10-cm-long whole-round sections from Section 2 of each core. Samples were cut and capped immediately after core retrieval on deck. After extrusion from the core liner in the chemistry laboratory, the surface of each whole-round section was trimmed with a spatula to remove potential contamination related to coring. When whole-round samples were collected more quickly than they could be squeezed, the samples were capped on both ends and stored in the refrigerator for up to several hours.

Interstitial water was collected using the trace metal noncontaminating titanium squeezer, modified after the standard ODP stainless steel squeezer of Manheim and Sayles (1974). Pressure up to 205 MPa

F11. Orientation conventions, p. 60.





(30,000 psi) was applied using a hydraulic press. Interstitial water was passed through a prewashed Whatman number 50 filter fitted above a titanium screen and subsequently extruded into a plastic syringe attached to the bottom of the squeezer assembly. All interstitial water samples were double-filtered through 0.45- $\mu\text{m}$  sterile Acrodisc filters. Aliquots for future shore-based analyses of strontium isotopes were placed in polytubes and heat-sealed. Aliquots for sulfur isotopes were placed in polytubes then poisoned with cadmium acetate solution (1 mL of 1-M  $\text{Cd}[\text{C}_2\text{H}_3\text{O}_2]_2$  to 10 mL of interstitial water sample) and heat-sealed. Aliquots for future shore-based analyses of interstitial water  $\delta^{13}\text{C}$  were poisoned with powdered mercuric chloride (~3-5 mg to 4.5 mL of interstitial water sample), and aliquots for future shore-based analysis of trace metals were acidified with concentrated nitric acid (100  $\mu\text{L}$  of  $\text{HNO}_3$  to 4 mL of interstitial water sample). Both were placed in individual glass vials and double-sealed with parafilm.

Interstitial water was routinely analyzed for salinity and total dissolved solids with a Goldberg optical handheld refractometer (Reichert) and for pH and alkalinity by Gran titration with a Brinkmann pH electrode and a Metrohm autotitrator. Chloride concentrations were determined by titration with  $\text{AgNO}_3$ . Silica, phosphate, and ammonium determinations were carried out by colorimetry using a Milton Roy Spectronic spectrophotometer using the analytical techniques described by Gieskes et al. (1991).

Sulfate was analyzed by ion chromatography (ICr) using the Dionex DX 120 ion chromatograph. Potassium, calcium, and magnesium concentrations were not determined by ICr because of an unidentified problem that persisted even after changing the cation column and the suppressor. These elements were analyzed by ICP-AES.

The major and minor cation concentrations (K, Ca, Mg, Na, Li, B, Sr, Ba, Mn, and Fe) were determined using the Jobin-Yvon Ultrace ICP-AES following the procedure outlined by Murray et al. (2000). In preparation for analysis by ICP-AES, 10-mL aliquots of interstitial water were acidified with 10 mL of nitric acid ( $\text{HNO}_3$ ) and diluted tenfold with matrix solution (2.25%  $\text{HNO}_3$  containing 9 ppm Y) for minor elements and diluted fiftyfold for major elements. Analytical blanks were prepared in an identical manner by analyzing nanopure water acidified and diluted with matrix solution to ensure a matrix match with the interstitial water samples. Sodium was determined using a charge balance calculation, where  $\sum_{\text{cations}} = \sum_{\text{anions}}$ .

Dissolved organic carbon concentrations were measured using a TOC-5000A analyzer. After interstitial water was extracted from the squeeze cake, ~1.5 mL of the water was removed and quickly frozen to preserve the sample until an analysis could be made. Samples were diluted fivefold (1 mL of sample to 5 mL of nanopure water) and acidified to a pH of ~2 using 53 mL of 2-N hydrochloric acid (HCl). Samples were then purged with purified air for 3 min (50 mL/min) and analyzed by triple injections of 25  $\mu\text{L}$  of sample.

International Association of Physical Sciences of Organization (IAPSO) standard seawater was used for calibrating most techniques. The reproducibility of these analyses, expressed as a percent of the standard deviation (1  $\sigma$ ) divided by the average of several IAPSO values, is summarized in Table T10. Accuracy of individual analysis is within the accepted deviation range for the accepted IAPSO values.

---

T10. Interstitial water analyses,  
p. 84.

---

## Bulk Sediment Sampling and Chemical Analyses

Bulk sediment samples, taken from interstitial water squeeze cakes, were routinely analyzed during Leg 206. Approximately 50 g of sample were ground in an agate mortar to a fine powder after freeze-drying. Sediment samples were analyzed for calcium carbonate using a Coulometrics 5011 carbon dioxide coulometer and for total carbon using a Carlo Erba 1500 CNS analyzer. Organic carbon was calculated from the difference between total carbon and inorganic carbon.

Elemental analyses for bulk sediment samples were measured by ICP-AES as outlined by Murray et al. (2000). Samples and standards ( $0.1000 \pm 0.0002$  g) were mixed with lithium metaborate ( $\text{LiBO}_2$ ) flux ( $0.4000 \pm 0.0004$  g). Analytical blanks were prepared with  $0.4000 \pm 0.0004$  g  $\text{LiBO}_2$  flux to ensure matrix matching. A solution of 0.172-mM LiBr wetting agent (10 mL) was added to the samples, standards, and blanks to prevent the cooled bead from sticking to the sides of the crucible. This mixture was fused for 3 min at  $900^\circ\text{C}$  in a NT-2100 Bead Sampler prior to dissolution in 50 mL of 10%  $\text{HNO}_3$ . For complete dissolution, 1 hr of shaking with the Burrell wrist-action shaker was required. A 5-mL aliquot of the resulting solution was filtered ( $0.20 \mu\text{m}$ ) and diluted with 35 mL of 10%  $\text{HNO}_3$ , resulting in a 4000-fold dilution of the original powder. Concentrations of the major elements (Si, Ti, Al, Fe, Mn, Mg, Ca, Na, K, and P) are presented as weight percent of oxides and trace elements (V, Cr, Sr, Y, Zr, and Ba) as parts per million (ppm). Phosphorous and zirconium were difficult to measure (analytical uncertainty  $\geq 30\%$ ) and are not presented in the initial results.

For these measurements, analyses of certified standards (BCSS-1 [marine mud], BHVO-2 [Hawaiian basalt], JCH-1 [Japanese chert], JLS-1 [Japanese limestone], MAG-1 [marine mud], and NIST-1C [argillaceous limestone]) were used to develop a six-point calibration curve for the major and trace elements. These standards were chosen because they are most representative of the lithologies at Site 1256. The results of BHVO-2 were poor and were taken out of the calibration. The drift was monitored with a synthetic solution composed of multiple natural samples and spikes of a few trace elements as needed. A certified standard (SCO-1 [Cody Shale]) was also analyzed as an unknown to check accuracy and consistency between analyses. The reproducibility of this analysis, expressed as a percent of the standard deviation ( $1 \sigma$ ) divided by the average of six (three times per run) determinations of an unknown sample, is summarized in Table T11. The analytical uncertainty for the bulk sediments is relatively high. Because of this and because the supply of argon was limited and intended for use with hard rock analyses, sediment analyses were only allotted a minimum number of runs. The quality of the analyses is, however, acceptable for observing general lithologic trends in the sediment column.

The sediment samples analyzed by ICP-AES were ignited before dissolution to release volatile phases ( $\text{H}_2\text{O}$ ,  $\text{CO}_2$ , and  $\text{SO}_2$ ) and to fully oxidize all iron to ferric iron. The ICP-AES analyses of these ignited powders should total 100% if the dilution measurements are perfect, but this was not the case and sample totals were consistently below 100%. Inorganic carbon ( $\text{CO}_3^{2-}$ ) is independently measured by coulometry, and the amount of CaO required to balance the inorganic carbon should approximately match the concentration of CaO measured by ICP-AES. As this was also not the case, the assumption was made that all the calcium present in the sediments is present as calcium carbonate

---

T11. Sediment chemistry analyses, p. 85.

---

and that there are only trace concentrations of other elements (Mg, Sr, and Fe) in the carbonate. Following this assumption, the ICP-AES data were normalized such that the CaO concentrations were consistent with the amount required to balance the inorganic carbon determined by coulometry. The volatile components (H<sub>2</sub>O and CO<sub>2</sub>) were then combined with the ICP-AES analyses and the data normalized to 100 wt%. These normalized data are reported in “*Inorganic Geochemistry*,” p. 36, in “The Sedimentary Overburden (Holes 1256A, 1256B, and 1256C)” in the “Site 1256” chapter (see Table T23, p. 361, in the “Site 1256” chapter).

### Hard Rock Sampling and Geochemical Analyses

Representative samples from selected igneous units were analyzed for major and trace elements during Leg 206 using ICP-AES. Approximately 20-cm<sup>3</sup> samples were cut from the core with a diamond saw blade. All outer surfaces were ground on a diamond-impregnated disk to remove surface contamination and altered rinds resulting from drilling. Each cleaned sample was placed in a beaker containing trace metal-grade methanol and was ultrasonicated for 15 min. The methanol was decanted, the samples were ultrasonicated twice in deionized water for 10 min, and then were ultrasonicated 10 min in nanopure DI water. The clean pieces were then dried for 10–12 hr at 65°C.

The clean, dry, whole-rock samples were fragmented to chips <1 cm by crushing them between two disks of Delrin plastic in a hydraulic press. They were then ground to a fine powder in a tungsten carbide (WC) mill by a SPEX 8510 shatterbox. A 1.0000 ± 0.0005-g aliquot of the sample powder was weighed on a ScienTech balance and ignited to determine weight loss on ignition (LOI).

ODP *Technical Note 29* (Murray et al., 2000) describes in detail the shipboard procedure for dissolution of rocks and ICP-AES analysis of samples. The following protocol is an abbreviated form of this with minor changes and additions. After determination of LOI, 100.0 ± 0.2-mg aliquots of the ignited whole-rock powders were weighed and mixed with 400.0 ± 0.5 mg of LiBO<sub>2</sub> flux that had been preweighed on shore. Standard rock powders and full procedural blanks (400 mg LiBO<sub>2</sub>) were included with the unknowns in each ICP-AES run. In addition, a grinding blank of pure SPEX SiO<sub>2</sub> was included in Runs 1 and 2 as a check on grinding contamination contributed by the WC mills (Table T12). The grinding blank was processed using the shatterbox that appeared dirtiest and is therefore a “worst-case” scenario. All samples and standards were weighed to ±0.20 mg on the ScienTech balance, and weighing errors are estimated to be ~0.02 mg.

We added 10 mL of 0.172-mM aqueous LiBr solution to the flux and rock powder mixture as an antiwetting agent to prevent the cooled bead from sticking to the crucible. Samples were then individually fused in Pt-Au (95-5) crucibles for ~3 min at a maximum temperature of 1050°C in a Bead Sampler NT-2100. After cooling, beads were transferred to 125-mL high-density (HD) polypropylene bottles and dissolved in 50 mL 10% HNO<sub>3</sub>, aided by shaking with a Burrell wrist-action bottle shaker for 1 hr. From Run 2 onward, the samples were ultrasonicated for ~1 hr after shaking to ensure complete dissolution of the glass bead. After digestion of the glass bead, all of the solution was passed through a 0.45-µm filter into a clean 60-mL wide-mouth HD polypropylene bottle. Next, 2.5 mL of this solution was transferred to a

---

T12. Analyses of blanks, p. 86.

---

plastic vial and diluted with 17.5 mL of 10% HNO<sub>3</sub> to bring the total volume to 20 mL. The final solution-to-sample dilution factor for this procedure was ~4000-fold.

Major (Si, Ti, Al, Fe, Mn, Mg, Ca, Na, K, and P) and trace (Sc, V, Cr, Ni, Sr, Y, Zr, Nb, and Ba) element concentrations of standards and samples were determined with the JY2000 Ultrace ICP-AES, which routinely measures wavelengths between ~100 and 800 nm. Specific analytical conditions for each sample run during Leg 206 are provided in Table T13.

The JY2000 plasma was ignited at least 30 min before each sample run to allow the instrument to warm up and stabilize. After the warm-up period, a zero-order search was performed to check the mechanical zero of the diffraction grating. After the zero-order search, the mechanical step positions of emission lines were tuned by automatically searching with a 0.002-nm window across each emission peak using the BAS-148 standard (basalt standard created during Leg 148, Hole 504B; Bach et al., 1996), or the BAS-206 (basalt interlaboratory standard created during this leg) prepared in 10% HNO<sub>3</sub>. During the initial setup an emission profile was selected for each peak, using BAS-148, to determine peak-to-background intensities and to set the locations of background points for each element. The JY2000 software uses these background locations to calculate the net intensity for each emission line. The photomultiplier voltage was optimized by automatically adjusting the gain for each element using BAS-148.

ICP-AES data presented in “**Hard Rock Geochemistry**,” p. 64, in “Basement Formed at Superfast Spreading Rate (Holes 1256C and 1256D)” in the “Site 1256” chapter were acquired using either the Gaussian or Maximum mode of the Windows 5 JY2000 software. The Gaussian mode fits a curve to points across a peak and integrates the area under the curve to determine element intensity and was used for Si, Ti, Al, Fe, Ca, Na, K, Sc, V, Sr, Zr, and Nb. Maximum mode was used for elements with asymmetric emission peaks (Mn, Mg, P, Y, Cr, Ni, and Ba), and intensity is integrated using the maximum intensity detected. Each unknown sample was run at least twice, nonsequentially, within a given sample run.

A typical hard rock ICP-AES run (Table T14) during Leg 206 included (1) a set of five certified rock standards (JA-3, JB-3, JB-2, BHVO-2, and JGb-1) analyzed twice each throughout the sample run; (2) up to 20 unknown samples run in duplicate; (3) a drift-correcting sample, BCR-2; spiked with Ni after Run 2 and P after Run 3, analyzed every fourth sample position and at the beginning and end of each run; (4) blank solutions run near the beginning and end of each run; and (5) a check standard (i.e., standard run as an unknown), typically BAS-148 and BAS-206, although Run 2 consisted primarily of check standards. A 10% HNO<sub>3</sub> wash solution was run for 90 s between each analysis.

Following each sample run, the raw intensities were transferred to a data file and all samples were corrected first for drift and then for the full procedural blank. The drift correction was applied to each element by linear interpolation between drift-monitoring solutions run approximately every fourth analysis. Following drift correction and blank subtraction, calibration curves were constructed based on five certified rock standards (JA-3, JB-3, BHVO-2, JB-2, and JGb-1 for Run 2 onward). Unknown concentrations were then calculated from the calibration line.

Estimates of accuracy and precision for major and trace element analyses were based on replicate analyses of check standards (usually

---

T13. ICP-AES conditions for hard rock, p. 87.

---

---

T14. Example hard rock run sheet, p. 88.

---

BAS-148 and BAS-206), the results of which are presented in Table T15. In general, run-to-run relative precision by ICP-AES was <3.5% for the major elements. Run-to-run relative precision for trace elements was generally <9%. Exceptions typically occurred when the element in question was near background values.

T15. Precision and accuracy of ICP-AES, Leg 206, p. 89.

## BIOSTRATIGRAPHY

Only one microfossil group, calcareous nannofossils, was examined for biostratigraphic purposes during Leg 206. The primary biostratigraphic objective was to date sediments immediately overlying the basement. Our secondary objective was to estimate sedimentation rates.

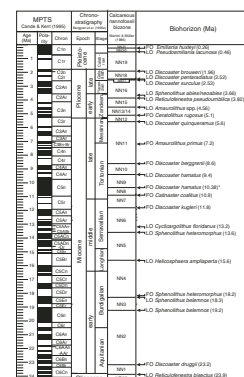
### Timescale

The biostratigraphic zonation of calcareous nannofossils is based primarily upon the studies of Martini and Müller (1986) and Okada and Bukry (1980). The numerical ages for biostratigraphic datums were compiled mainly from Berggren et al. (1995a, 1995b) (Fig. F12) to facilitate easy comparison with other studies. Preliminary ages were assigned to core catcher samples, and these were used to estimate sedimentation rates. Samples from within the cores were examined when a more refined age determination was necessary.

F12. Calcareous nannofossil datums, p. 61.

### Taxonomic Remarks

Several *Reticulofenestra* species have been used as Neogene and Quaternary biostratigraphic markers. They are mainly distinguished by coccolith size and the relative magnitude of the central opening. Some species, however, show a great range of variation in these parameters, causing problems in identification (Backman, 1980; Gallagher, 1989; Young, 1990; Su, 1996). During Leg 206, only one *Reticulofenestra* species, *R. pseudoumbilica*, was used as a stratigraphic marker. This species is identified by specimens having a maximum coccolith length of >7 µm in its uppermost range (the lower Pliocene), which is in accord with the size of the holotype (Gartner, 1967). Identification of other calcareous nannofossils mainly follows the compilation of Perch-Nielsen (1985).



### Methods

Preparation of smear slides followed standard techniques using Norland optical adhesive as a mounting medium. Slides were examined using a Zeiss Axiophot microscope under cross-polarized light, transmitted light, and phase-contrast light at 800×–1250× magnification. Relative abundance of each nannofossil species, overall preservation of the nannofossil assemblage, and the total abundance of nannofossils were recorded for each sample. In all cases, a magnification of 1000× was used to make semiquantitative estimates of abundance of individual species. Five levels of relative abundance of a species were recorded, with the following approximate definitions:

- V = very abundant (>10 specimens per field of view).
- A = abundant (1–10 specimens per field of view).
- C = common (1 specimen per 2–10 fields of view).
- F = few (1 specimen per 11–50 fields of view).



R = rare (1 specimen per 51 or more fields of view).

The total abundance of all calcareous nannofossils for each sample was estimated as follows:

- V = very abundant (>20,000 specimens for 500 fields of view).
- A = abundant (2,001–20,000 specimens for 500 fields of view).
- C = common (51–2,000 specimens for 500 fields of view).
- F = few (11–50 specimens for 500 fields of view).
- R = rare (1–10 specimens for 500 fields of view [~3 traverses]).
- B = barren (none).

The qualitative evaluation of the preservation of calcareous nannofossils was based on the following criteria:

- VG = very good (no evidence of dissolution and/or overgrowth; diagnostic characteristics are perfectly preserved and all specimens can be identified at species level).
- G = good (little or no evidence of dissolution and/or overgrowth; diagnostic characteristics are preserved, and nearly all specimens [~95%] can be identified to species level).
- M = moderate (dissolution and/or overgrowth are evident; besides commonly broken nannofossils, the number of delicate forms is reduced; identification of a significant proportion [up to 10%] of the specimens is impaired and cannot be identified to species level with absolute certainty).
- P = poor (severe dissolution, fragmentation and/or overgrowth have occurred; primary features may have been destroyed and many specimens can be identified only at genera level).

## **PALEOMAGNETISM**

Paleomagnetic investigations during Leg 206 consisted mainly of routine remanent magnetization measurements of (1) archive-half sections and (2) discrete samples from the working-half sections, with both being completed before and after alternating-field (AF) demagnetization. In addition, low-field magnetic susceptibility was measured on whole-core sections using the MST and on archive-half sections using the AMST. To investigate rock magnetic properties, we also conducted thermal demagnetization, anhysteretic remanent magnetization (ARM), and isothermal remanent magnetization (IRM) experiments on some of the discrete samples.

### **Instruments and Measurements**

Measurements of remanent magnetization were made using an automated pass-through cryogenic magnetometer with direct-current superconducting quantum interference devices (DC-SQUIDS) (2-G Enterprises model 760-R). The magnetometer is equipped with an in-line AF demagnetizer (2-G Enterprises model 2G600) capable of producing peak fields of 80 mT with a 200-Hz frequency. The magnetometer is run and data are acquired by a program called LongCore (version 3.3) written by W.G. Mills (ODP) in the LabView programming language. This version of LongCore was last updated during Leg 197. Key parameters used



within the program, including calibration constants for the SQUIDS and coil response functions, are given in Table T16.

The natural remanent magnetization was routinely measured every 2.5 or 5 cm along all sedimentary archive-half sections before demagnetization. Most of these sections were also progressively AF demagnetized up to 30 or 40 mT and measured after each step. Details about the measurement intervals and the demagnetization steps used for the sediments are given in “Paleomagnetism,” p. 29, in “The Sedimentary Overburden (Holes 1256A, 1256B, and 1256C)” in the “Site 1256” chapter.

We decided not to attempt to measure most of the archive-half sections from igneous basement cores because the strong intensities and large volumes of the samples often result in spurious measurements in the long-core magnetometer. Repeated tuning of the magnetometer is necessary, which often entails heating the SQUID coils to release trapped magnetic flux. If not constantly monitored and tuned, the additional magnetometer noise that results from measuring the strong-intensity split-core samples can lead to erratic results. We did, however, experiment with several of the sections that contained continuous pieces that had few or no fractures or gaps over their entire 1.5-m section length. For these sections, the sensor velocity on the magnetometer was set at 10 cm/s in order to avoid saturation of the magnetometer electronics. This saturation is due to high variations of the magnetic flux (flux-jump) induced by the rapid motion of highly magnetized material past the sensor. Details about the sections measured, the measurement interval, and the demagnetization steps used for these basalt sections are given in “Paleomagnetism,” p. 80, in “Basement Formed at Superfast Spreading Rate (Holes 1256C and 1256D)” in the “Site 1256” chapter.

The discrete samples were also measured with the cryogenic magnetometer. Typically, samples were demagnetized in steps of 1 to 5 mT from 0 to 80 mT. One to four samples were placed in the discrete sample tray and run as a batch. Throughout the cruise, we only placed samples in the 20-, 60-, 100-, and 140-cm tray positions to ensure that samples were not influenced by the magnetizations of adjacent samples.

Several basalt samples were progressively demagnetized using a Schonstedt Thermal Demagnetizer (model TSD-1), which demagnetizes the rock specimens by heating them to any specified temperature from room temperature up to 800°C and then cooling them in a low magnetic field environment (<10 nT).

To investigate rock magnetic characteristics of some of the discrete samples, ARM and IRM experiments were conducted and then samples were measured using the cryogenic magnetometer. The DTECH AF demagnetizer was used to impart ARM to discrete samples, using a 100-mT peak alternating field and a 0.05-mT DC field. The ARM was imparted along the  $-z$ -axis of the samples, which is accomplished by placing the samples in the DTECH sample holder with the sample orientation arrow pointing into the instrument and aligned with the biasing and demagnetizing field. We then progressively demagnetized the ARM at 5-mT increments from 0 to 80 mT using the cryogenic magnetometer. IRM was imparted to the discrete samples by a DC field generated in the ASC (Analytical Services Company) Impulse Magnetizer (model IM-10). We typically measured the remanence of the discrete samples after imparting an IRM of 1000 mT along the  $-z$ -axis, which is accomplished by placing the samples in the Impulse Magnetizer sample holder with the sample orientation arrow pointing out of the instrument and

---

T16. Cryogenic magnetometer set-up, p. 91.

---

aligned with the biasing and demagnetizing field. The samples were then stepwise AF demagnetized at 5-mT increments from 0 to 80 mT using the cryogenic magnetometer. Backfield IRM (BIRM) experiments were conducted by imparting (1) an IRM of 1000 mT along the +z-axis, (2) a BIRM of 100 mT along the -z-axis, and (3) a BIRM of 300 mT along the -z-axis. After each step, the remanence was measured. In addition, we conducted IRM acquisition experiments by first demagnetizing the sample at 150 mT in the DTECH AF demagnetizer and measuring the remanence. Then IRM was imparted at 10, 30, 100, 150, 200, 300, 400, 500, 600, 800, 1000, and 1200 mT, with the remanence measured after each step.

### **Susceptibility**

Low-field magnetic susceptibility was measured for all whole-core sections as part of the MST measurements (see “**Multisensor Track Measurements,**” p. 30, in “Physical Properties”). The MST susceptibility meter (a Bartington model MS2 with an MS2C sensor, a coil diameter of 88 mm, and an operating frequency of 0.565 kHz) has a nominal resolution of  $2 \times 10^{-6}$  SI (Blum, 1997). Susceptibility was determined at 2.5-cm intervals using a 1-s integration time for each measurement and with five measurements at each interval. The “units” option was set on SI units, and the values were stored in the ODP Janus database in raw meter units. To convert to true SI volume susceptibilities, meter units should be multiplied by  $10^{-5}$  and then multiplied by a correction factor to take into account the volume of material that passed through the susceptibility coils. Except for measurements near the ends of each section, this factor for a standard ODP core is  $\sim 0.7$  (Blum, 1997). No correction was applied for any figures illustrating magnetic susceptibilities in the “Paleomagnetism” subsections of the “Site 1256” chapter. Hence, the units are given as raw meter values. Magnetic susceptibility of discrete samples obtained from the working half of cores was measured using a Bartington MS2 susceptibility meter with a dual-frequency MS1B sensor. In addition, magnetic susceptibility was measured every 2 cm on the archive half of cores using the point susceptibility probe (Bartington MS2 susceptibility meter with a MS2F sensor) on the AMST.

### **Calibration and Instrument Sensitivity**

Even though results from the shipboard cryogenic magnetometer have been compared with many other laboratories and shown to give consistent results, it is useful to check the calibration of the magnetometer against a known standard at the beginning of each leg. We used a standard purchased from Geofyzika that is an 8-cm<sup>3</sup> cube with an intensity of 7.62 A/m (moment =  $6.096 \times 10^{-5}$  Am<sup>2</sup>). All three axes gave results that differ <2% from this standard. In addition, the automated tray positioning was checked by putting the standard at known positions and measuring the tray. The position indicated by the software was found to be accurate to better than  $\pm 1$  cm, which is reasonable given the stretch in the pulley system used to move the sample boat.

Based on tests conducted during Legs 186 and 200, the background noise level of the magnetometer in the shipboard environment is  $\sim 2 \times 10^{-9}$  Am<sup>2</sup> (Shipboard Scientific Party, 2000, 2003). We repeated tests during Leg 206 for an empty split-core tray (also referred to as the sample boat) and for the tray that holds discrete samples. The results were similar in that the x-, y-, and z-axis moments measured on the sample

boat before cleaning were less than  $\pm 2 \times 10^{-9}$  Am<sup>2</sup> except for two intervals that were only slightly above this (Fig. F13A). After cleaning the sample boat with window cleaner (Windex brand) and demagnetizing it at 80 mT, the moments are all less than  $\pm 1 \times 10^{-9}$  Am<sup>2</sup> (Fig. F13B). These results include the drift correction, which only marginally changes the results (Fig. F13). During Leg 206, we always applied a tray correction to the split-core and discrete samples. The tray-corrected data are the measured magnetic moments for a sample minus those measured at the same position for the empty sample boat. The tray values were updated throughout the cruise by remeasuring the tray. The relative size of these values, however, should always be comparable to those shown in Figure F13 for the clean, empty sample boat. When the tray correction is applied to measurements made on a clean, empty sample boat, the moments drop to less than  $\pm 2 \times 10^{-10}$  Am<sup>2</sup> (Fig. F14).

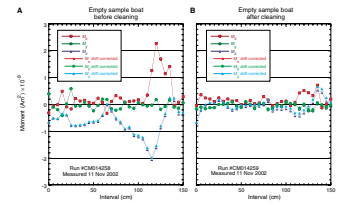
Several discrete sample trays (DSTs) are available for use, but we only used the DST provided by 2-G Enterprises. This one is 150 cm long and has holders for discrete samples every 10 cm. The holders alternate between those capable of holding samples with 2-cm  $\times$  2-cm bases and those capable of holding samples with 2.6-cm  $\times$  2.6-cm bases. We oriented the DST such that the holders with 2-cm  $\times$  2-cm bases were at 20-, 40-, 60-, 80-, 100-, 120-, and 140-cm positions when the DST was in the sample boat.

To test the noise in the DST, it was placed in the sample boat, cleaned with window cleaner, AF demagnetized at 80 mT, and then measured every 5 cm in continuous mode. After the drift correction is made and the effect of the sample boat is subtracted, the noise level associated with the DST is similar to that of the cleaned sample boat (cf. Figs. F13B, F15). When measured in discrete mode and when tray-corrected, where the tray correction accounts for the magnetization of the sample boat and the DST, the four sample positions we used (the 20-, 60-, 100-, and 140-cm tray slots) had magnetic moments of  $< 4 \times 10^{-10}$  Am<sup>2</sup>.

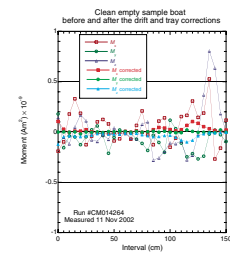
The machine noise level is sufficiently low that it is of minor significance for most samples measured. The practical noise level is, however, higher by about an order of magnitude from the cleaned, drift-corrected, and tray-corrected examples above. As was apparent when the sample boat was not clean, just a little bit of dirt on the tray puts the noise level in the  $10^{-9}$  Am<sup>2</sup> range. Noise related to dirt on the sample boat or the DST and to the magnetization of the plastic core liners for split-core samples and plastic cubes for sediment discrete samples will at least be in that range. Even with diligence, it is difficult to keep the trays clean, given the amount of core material measured during a typical leg. For long-core measurements, it is not practical to clean and re-measure the empty tray before each new sample. Thus, the correction for the tray magnetization may only improve the accuracy of the measurements marginally for the shipboard environment. Moreover, the split-core sections are in a plastic core liner that has been stored in dusty conditions prior to coring and that resides in a metal core barrel just prior to core collection. Therefore, the noise associated with the core liners will likely be several times greater than the noise associated with the sample boat (i.e., several times greater than  $\pm 2 \times 10^{-9}$  Am<sup>2</sup>).

We conclude that under favorable conditions the noise level will be approximately  $\pm 2 \times 10^{-9}$  Am<sup>2</sup>. For a split core, given the large volume of core material within the sensing region of the magnetometer, which is  $\sim 100$  cm<sup>3</sup>, the minimum measurable remanent intensities will be greater than  $\sim 2 \times 10^{-5}$  A/m. For discrete samples, which typically have

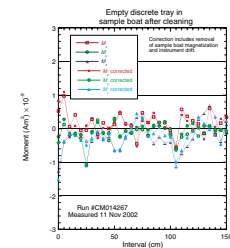
F13. Magnetic moments before and after sample boat cleaning, p. 62.



F14. Magnetic moments before and after tray correction, p. 63.



F15. Magnetic moments for an empty sample tray in a sample boat, p. 64.



volumes of 6–10 cm<sup>3</sup>, the minimum measurable remanent intensities are greater than  $\sim 4 \times 10^{-4}$  A/m.

### Core Orientation

The standard ODP paleomagnetic coordinate system was used. In this system, +x is vertically upward from and perpendicular to the split-core surface of the archive half, +z is downcore, and +y is orthogonal to x and y in a right-hand sense (i.e., it points left along the split-core surface when looking upcore at the archive half) (Fig. F16).

APC Cores 206-1256B-3H through 18H were azimuthally oriented using the Tensor tool. The Tensor tool consists of a three-component fluxgate magnetometer and a three-component accelerometer rigidly attached to the core barrel. The information from both sets of sensors allows the azimuth and dip of the hole to be measured as well as the azimuth of the double-line orientation mark on the core liner. Orientation is not usually attempted for the top two or three cores (~20–30 mbsf) as the bottom-hole assembly (BHA) is insufficiently stabilized by the sediment. The output from the Tensor tool, which contains a variety of angles including the inclination angle of the hole and the magnetic toolface (MTF) angle (Fig. F17) is archived in the Janus database. The inclination angle of the hole is a measure of deviation of the hole from vertical, and the MTF angle gives the angle between the magnetic north and the double-line orientation mark on the core liner. The core liner is always cut such that the double lines are at the bottom of the working half.

Using the ODP coordinate system for the archive and working halves or for samples taken from them, the measured remanent declination can then be corrected to magnetic north by adding the MTF angle and can be further corrected to true north by adding the deviation of magnetic north from true north, the latter of which can be estimated from the International Geomagnetic Reference Field (IGRF) coefficients. The equation is

$$D_T = D_O + A_{MTF} + M_{IGRF}$$

where,

$D_T$  = Tensor tool corrected or true declination.

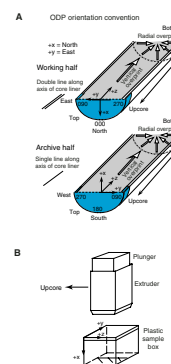
$D_O$  = observed declination output from the cryogenic magnetometer.

$A_{MTF}$  = MTF angle.

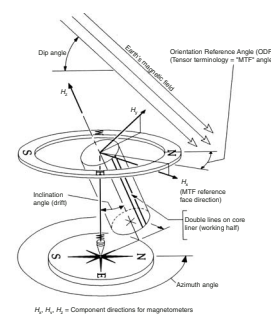
$M_{IGRF}$  = the deviation of magnetic north from true north. At Site 1256, we used 4.9° for the  $M_{IGRF}$  correction.

For hard rocks it is possible to combine images of the exterior of the core with images of the borehole wall from the Formation MicroScanner (FMS) logging tool. To allow for this possibility, the exterior of basalt cores pieces were scanned with the DMT CoreScan, which is a digital camera system that records an image of the whole-core piece as it is rotated (see “Digital Imaging,” p. 34). Postcruise analysis of the FMS and digital images will allow the reorientation of some distinctive pieces of core to true geographical north.

F16. ODP paleomagnetic coordinate system, p. 65.



F17. Tensor tool measurements, p. 66.



## Sampling Methods and Orientations for Discrete Samples

Oriented discrete samples were taken from the working half of selected sections. For sedimentary intervals, one sample per core was typically collected for shipboard analysis using plastic cubes with a 2-cm × 2-cm × 2-cm exterior dimension and an aluminum extruder. The interior volume of a plastic cube is ~7 cm<sup>3</sup>. Each plastic cube has an arrow on the bottom face. The sediment is collected in the extruder with a 2-cm × 2-cm cross-section opening (Fig. F16). Usually a few millimeters of sediment is extruded and removed from the bottom of the extruder with a spatula, leaving a flat surface of sediment and just enough sediment in the extruder to fill the plastic cube. The sediment is then carefully extruded into the plastic cube. An orientation mark on the extruder aids in ensuring the upcore orientation of the sample is maintained, and a mark on the plunger in the extruder aids in ensuring that enough sediment is collected to fill the plastic cube. When measuring a sediment sample, we placed the side with the lid down in the tray with the arrow pointing along the -z-axis, or upcore, direction. This makes the discrete sample orientation the same as that of the archive half, allowing for a more direct comparison of the discrete sample measurements with archive-half measurements.

In lithified intervals, we drew an arrow on the split-core face pointing upcore and used the rock saw to cut the sample. For shipboard samples, we typically cut cubes with ~2-cm-long sides (volume = ~8 cm<sup>3</sup>), although we also collected smaller pieces for analysis of the drilling overprint. When measuring a hard rock sample, we placed the side with the arrow down in the tray with the arrow pointing along the -z-axis, or uphole, direction, which for the hard rock discrete sample makes the orientation the same as that of the archive half.

## Magnetic Overprints

Several types of secondary magnetization were acquired during coring, which sometimes hampered magnetostratigraphic and paleomagnetic interpretation. The most common was a steep downward-pointing overprint attributed to the drill string. For the Leg 206 cores, we also observed a bias for 0° declinations in archive-half sections, which has been observed during many previous cruises and has been interpreted as a radially inward overprint (Fig. F16). Details of these and other magnetic complexities are presented in the “Paleomagnetism” sections in the “Site 1256” chapter.

## Data Reduction and Analysis

In interpreting the data, we avoided using the measurements within 5 cm from the ends of each section, although we saved these values for future studies that might wish to deconvolve the remanence signal. We also remove data from intervals where drilling disturbance, gaps, or other features exist, as these intervals give erroneous results. A table of the intervals removed is presented in the “Paleomagnetism” sections in the “Site 1256” chapter.

The characteristic remanent magnetization (ChRM) was estimated in three ways. When only the highest demagnetization step used was above (or at least nearly above) the field needed to remove the drilling overprint, then the results from the remanence measured after this sin-



gle demagnetization step were interpreted as the best estimate of the ChRM. When multiple demagnetization steps were measured at fields above that needed to remove the drilling overprint, the ChRM was estimated by principal component analysis (PCA) (Kirschvink, 1980) and from a Fisherian average (Fisher, 1953) of three or more of the stable endpoint directions.

The PCA analysis was conducted using a program that iteratively searches for the demagnetization steps that minimized the size of the maximum angular deviation, which is a measure of how well the vector demagnetization data fit a line. Maximum angular deviation values  $<10^\circ$  are typically considered to provide lines that fit the observations well. The program requires that at least three demagnetization steps be used, never uses data from demagnetization steps lower than a user-defined value, and does not require that the best-fit PCA line pass through the origin of the plot (the “free” option of standard PCA). Because the drilling overprint persisted beyond 15-mT demagnetization in most of the intervals, we only used results from 15 mT or higher in the PCA.

For comparison, the program also computes a Fisherian mean of the highest three or four demagnetization steps for each interval. This is referred to as the stable endpoint direction. Typically, only the highest three demagnetization steps are used in the average, unless the mean of these three directions has a precision parameter of  $<200$  (a measure of dispersion), in which case the fourth highest demagnetization step is included. In cases where the precision parameter is  $<200$ , the program will first search for outliers and remove them if they lie  $>10^\circ$  from the mean. Both the PCA and stable endpoint directions for interpreted intervals are given in tables in the “Paleomagnetism” sections in the “Site 1256” chapter.

Comparison of the stable endpoint with the PCA direction can be useful for indicating where unremoved or partially unremoved magnetization components exist or where progressive demagnetization has been ineffective in revealing linear demagnetization paths. To assist with this comparison, we have computed the angular distance between the two directions and included it in the tables in the “Paleomagnetism” sections in the “Site 1256” chapter.

### **Magnetostratigraphy**

Where AF demagnetization successfully isolated the characteristic component of remanence, paleomagnetic directions were used to define polarity zones. Given the shallow inclinations recorded by the Site 1256 sediments, we relied heavily on the declinations for polarity determination. Ages for reversals are from the revised Cenozoic timescale of Cande and Kent (1995) (Fig. F12).

### **MICROBIOLOGY**

The primary microbiology objective for Leg 206 was to determine the types and abundance of microbes in igneous rocks formed in fast-spreading oceanic crust. To do this, water and rock samples were collected to prospect for evidence of extant and fossil microbial activity, to extract and characterize deoxyribonucleic acid (DNA) contained within the samples, and to establish cultures of microorganisms inhabiting these environments. Interpretation of results is complicated by the pos-



sibility of contamination of samples with microbes from the seawater, the drilling fluid, the ship and drilling equipment, and from postcollection processing of samples. A sample handling protocol was established to minimize postcollection contamination, and tracer tests were conducted to determine the extent of microbial contamination during drilling and sample preparation. Methods for tracer tests are detailed in *ODP Technical Note, 28* (Smith et al., 2000).

## **Igneous Rocks**

### **Sampling**

Whole-round cores were collected on the catwalk through the ends of unsplit core liners or in the core-splitting room immediately after the core liner was split. Cores were handled with latex gloves, placed in sterile aluminum foil, taken immediately to the anaerobic chamber (Coy) in the microbiology laboratory, and put on blue ice to maintain core temperature at or below in situ temperature. Samples were in anaerobic conditions within ~30 min of the core arriving on deck, and work was performed quickly to avoid warming.

In the anaerobic chamber, samples were rinsed of unwanted debris with a nitrogen-flushed anaerobic marine salts solution (23.5 g NaCl + 10.8 mg MgCl<sub>2</sub>·6H<sub>2</sub>O per liter). A hydraulic rock trimmer (Ward) was used to split off the outside of the cores. Using sterile techniques, interior pieces of core were crushed by wrapping the rock in sterile aluminum foil and breaking it into several pieces with a sterile chisel and hammer or in a sterile percussion mortar (Rock Labs). Additional interior pieces of core were used as described below, and any unused portions were returned to the core.

A nitrogen atmosphere with 5% CO<sub>2</sub> and >2% H<sub>2</sub> was maintained in the anaerobic chamber, and several hours before each use the chamber was flushed with this gas mixture to ensure anaerobic handling of the core. Hydrogen is present to combine with residual oxygen in a reaction catalyzed by palladium pellets maintained within the chamber. As an additional precaution to minimize oxygen contamination, tools and glassware to be used for manipulation and storage of samples for strict anaerobic work were stored within the chamber.

### **Scanning Electron Microscopy, Thin Sections, and Chemical Analysis**

Samples were collected for shore-based examination by scanning electron microscopy (SEM) and in thin section for evidence of extant and fossil microbial activity. Some of the samples were subsamples of those collected for other microbial studies. Additional samples for thin sections were collected during regular shipboard sampling parties, particularly in intervals of interest to others. The samples for SEM analysis were placed in 10- or 50-mL sterile Falcon tubes, depending on sample size. They were then fixed in 2% glutaraldehyde for 4–24 hr before being washed twice and stored in 0.25% glutaraldehyde at 4°C. Samples for shore-based chemical analysis were placed in sterile sample bags, immediately frozen, and stored at –80°C.

## **DNA Extraction and In Situ Hybridization**

Whole-rock pieces and crushed rock split from the interior of cores were preserved for shore-based DNA extraction and in situ hybridization. For DNA extraction, samples were immediately stored in sterile 2-mL Eppendorf tubes and frozen at  $-80^{\circ}\text{C}$  for future genetic analyses. Samples for in situ hybridization were fixed in 4% paraformaldehyde in sterile Falcon tubes for 4–24 hr. The samples were then washed twice and stored in a carefully blended 1:1 mixture of phosphate buffered saline/100% ethanol at  $-20^{\circ}\text{C}$ .

## **Cultivation of Microorganisms**

To enrich microorganisms, culturing media, which were prepared prior to the cruise, were inoculated with 0.25 mL of a slurry from a sub-sample set aside for culturing work. The slurry was prepared by first crushing the rock fragment into very small pieces ( $<2$  mm) with a hammer or with a percussion mortar. Next, the finely crushed pieces were placed into sterile beakers with anoxic minimal salts solution used for initial rinsing of the core. The beakers were shaken and vortexed to remove microorganisms attached to the rock fragments. Sterile syringes flushed with nitrogen were used to transfer the slurry into capped 5-mL serum vials or into gradient tubes. A sterile needle was used each time to inoculate the various media. Inoculated media and gradient tubes were stored at  $4^{\circ}\text{C}$ .

## **Contamination Tests**

Two types of tracer tests were conducted to check for the potential intrusion of drill water and confirm the suitability of the core material for microbiological research: perfluorocarbon tracer (PFT) and 0.5- $\mu\text{m}$  fluorescent microspheres. The presence or absence of these two tracers also acts as a quality assurance check on core handling methods. Detailed methods for these tests are described in *ODP Technical Note, 28* (Smith et al., 2000). Samples of the drilling fluids were also collected upon core retrieval to determine the “background contamination.”

## **Perfluorocarbon Tracer**

PFT was continuously fed to the drill water at a concentration close to the limit of solubility (1  $\mu\text{g/g}$ ) and well above the detection limit for gas chromatographic analysis (1  $\text{pg/g}$ ). Samples for PFT analysis were taken from three cores in Hole 1256C as a test for drill water intrusion and possible contamination. To verify delivery of the PFT, a sterile cotton ball was used to wipe the interior of the liner and then placed in a headspace vial and sealed with a Teflon septum. After processing in the anaerobic chamber, a small rock fragment was taken from the interior of the core (to monitor tracer intrusion) and stored in a similar fashion as the cotton ball. Air samples were occasionally taken in sealed headspace vials on the catwalk and in the core laboratory to monitor the background (blank) levels of PFT. Samples were analyzed by gas chromatography.

### Particulate Tracer

Latex fluorescent microspheres (Polysciences, Inc., Warrington, Pennsylvania; 0.5- $\mu\text{m}$  diameter; YG) were used as a particulate tracer complementary to the volatile PFT. Two milliliters of microsphere stock (2.69% solids) was diluted with 40 mL distilled water, sonicated for 2 min, and heat-sealed into a 4-oz Whirl-Pak bag. The bag was then attached with thread to the core catcher, a slight modification from procedures as described in Smith et al. (2000). The bag was positioned to rupture upon impact of the core barrel with the core, where the microspheres mixed with the drill fluid and coated the outside of the core as it was pushed into the liner.

To monitor the successful deployment of the microspheres, samples of the core exterior were taken by washing the core sample with sterile nitrogen-flushed marine salts solution and collecting the fluid in Falcon tubes. Interior core samples were crushed with a steel percussion mortar, mixed with the marine salts solution, and collected in Falcon tubes. The fluid samples were vortexed and allowed ~5 min each for settling of the larger particulates. A 5-mL aliquot was taken from each sample and filtered onto black polycarbonate filters (0.2- $\mu\text{m}$  pore size; Millipore), and the filter was mounted on a clean slide with nonfluorescent immersion oil for microscopic examination.

The usable filter area was  $\sim 1.98 \times 10^8 \mu\text{m}^2$  as determined by the inner diameter of the filtration tower (15.64 mm). Microspheres in slide preparations were counted using a Zeiss Axioplan fluorescence microscope equipped with the Zeiss number 9 filter set (BP 450-490; LP 520), and the number of spheres observed was used to quantify contamination in spheres per milliliter of sample. The 100 $\times$  objective was used for detecting microspheres, where the area for one entire field of view was  $\sim 3.14 \times 10^4 \mu\text{m}^2$  (diameter for one field of view = 200  $\mu\text{m}$ ). A total of 20 fields of view were analyzed for each sample. Comparison of microsphere numbers between paired samples from inner and outer core layers provides a relative measure of fluid intrusion and contamination. A sample with many spheres in outer layers and few or none within may be considered "higher quality" than one with very few spheres in the outer layers and few or none within.

## PHYSICAL PROPERTIES

Shipboard measurements of physical properties provide preliminary information on variations in the recovered core material, which can be used to characterize lithologic units, correlate with downhole geophysical logging data, and interpret seismic reflection data. After the cores had equilibrated to ambient room temperature, physical properties were measured on whole-round sections, undisturbed parts of split cores, and discrete samples.

Nondestructive measurements of wet bulk density, magnetic susceptibility, transverse compressional wave (*P*-wave) velocity, and NGR were made on whole-round sections using the MST. The MST has a gamma ray attenuation (GRA) bulk densitometer, a *P*-wave logger (PWL), a magnetic susceptibility meter, and an NGR sensor. Thermal conductivity measurements were also made on sediment whole cores and hard rock split cores. *P*-wave velocity measurements were made on sediment and hard rock cores and on discrete sample cubes (minicubes) of hard rock. Bulk properties of discrete samples were determined by moisture

and density (MAD) analysis, which included measurements of wet bulk density, dry bulk density, grain density, water content, and porosity. A comprehensive discussion of all methodologies and calculations used in the *JOIDES Resolution* Physical Properties laboratory can be found in Blum (1997).

Visible and near-infrared spectroscopy (VNIS) analyses were performed on all MAD sediment samples as well as an additional sample per section to determine semiquantitative mineralogy. On hard rock core, VNIS analyses were performed directly on the archive split-core half. VNIS analysis was conducted for the determination of alteration and physical property variations and the effect of crustal age and extrusive style on alteration.

### **Multisensor Track Measurements**

The MST consists of four physical property sensors on an automated track that measures magnetic susceptibility, bulk density, compressional wave velocity, and NGR emissions on whole-round core sections. During Leg 206, MS, GRA bulk density, and NGR were measured on both soft-sediment cores and hard rock cores; compressional wave velocities were measured using the PWL on APC cores only.

The measurement of wet bulk density by the GRA system is based on the principle that the attenuation, mainly by Compton scattering, of a collimated beam of gamma rays produced by a  $^{137}\text{Ce}$  source passing through a known volume of sediment is related to material density (Evans, 1965). Calibration of the GRA system was completed using known seawater/aluminum density standards. GRA bulk density data are of highest quality when determined on APC cores because the liner is generally completely filled with sediment. In XCB and RCB cores, GRA measurements are of lower quality and typically cannot be used to reliably determine bulk density on their own. The measurement width of the GRA sensor is ~5 mm, with sample spacing generally set at 2.5 cm for Leg 206 cores. The minimum integration time for a statistically significant GRA measurement is 1 s, and routine Leg 206 GRA measurements used either a 3- or 5-s integration time. A freshwater control standard was run with each section to measure instrument drift.

Whole-core magnetic susceptibility was measured with the MST using a Bartington MS2 meter coupled to a MS2C sensor coil with a diameter of 8.8 cm operating at 565 Hz. The measurement resolution of the MS2C sensor is 4 cm, with a minimum statistically significant count time of 1 s. During Leg 206, MST magnetic susceptibility was routinely measured every 2.5 cm, with five data acquisitions at each interval. Magnetic susceptibility data were archived as raw instrument units (SI) and not corrected for changes in volume, although a correction was made for instrument drift. The raw susceptibility measurements can be converted to SI volume units as described in "**Susceptibility**," p. 22, in "Instruments and Measurements" in "Paleomagnetism" (see also Blum, 1997).

Transverse *P*-wave velocity was measured on the MST with the PWL for all APC cores. The use of the PWL on XCB and RCB cores was limited by poor acoustic coupling between the sediment and the core liner. The PWL transmits a 500-kHz compressional wave pulse through the core every 1 ms. The transmitting and receiving transducers are aligned perpendicular to the core axis, and a pair of displacement transducers monitors the separation between the compressional wave transducers. Variations in the outer diameter of the liner do not degrade the accu-

racy of the velocities, but the unconsolidated sediment or rock core must completely fill the liner for the PWL to provide acoustic coupling. Calibration of the displacement transducer and measurement of electronic delay within the PWL circuitry were conducted using a series of acrylic blocks of known thickness and *P*-wave traveltime. Repeated measurement of *P*-wave velocity through a core liner filled with distilled water was used to check calibration validity. The measurement width of the PWL sensor is ~1 mm, with sample spacing routinely set at 5 cm for Leg 206 APC cores.

NGR emissions of sediments are a function of the random and discrete decay of radioactive isotopes, predominantly those of uranium, thorium, and potassium, and are measured through scintillation detectors arranged at 90° to each other and perpendicular to the core. The installation and operating principles of the NGR system used on the *JOIDES Resolution* are discussed in Hoppie et al. (1994). Data from 256 energy channels were collected and archived. For presentation purposes, the counts were summed over the range of 200–3000 keV, so as to be comparable with data collected during previous legs. This integration range also allows direct comparison with downhole logging data, which are collected over a similar integration range (Hoppie et al., 1994). Over the 200- to 3000-keV integration range, background counts, measured using a core liner filled with distilled water, averaged 30 during a 1-hr measurement period. Before taking measurements, each of the four NGR amplifiers were adjusted so that the thorium peak was at the highest resolution possible when the other three amplifiers were disabled. The multichannel analyzer was then calibrated by assigning certain channels to the characteristic energies of <sup>40</sup>K and the main peak of <sup>232</sup>Th (Blum, 1997). The measurement width of the NGR is ~15 cm, with a statistically significant count time of at least 5 s, depending on lithology. The sample spacing of the NGR measurements was set at 5 cm for 6 s on the sediment cores and 5 cm for 20 s on the hard rock cores. No corrections were made to NGR data obtained from XCB and RCB cores to account for incomplete filling of the core liner.

### Thermal Conductivity

The thermal conductivity was measured with the TK04 (Teka Bolin) system, using the needle-probe method in full-space configuration for soft sediments (von Herzen and Maxwell, 1959). The needle probe contains a heater wire and calibrated thermistor. It is assumed to be a perfect conductor because it is much more conductive than unconsolidated sediments. With this assumption, the temperature of the superconductive probe has a linear relationship with the natural logarithm of the time after the initiation of the heat:

$$T(t) = (q/4k) \ln(t) + C,$$

where,

- $T$  = temperature.
- $q$  = heat input per unit length per unit time.
- $k$  = thermal conductivity.
- $t$  = time after the initiation of the heat.
- $C$  = a constant.

Thermal conductivity was measured on unconsolidated sediment and rock samples using the TK04 system as described by Blum (1997). These measurements are used, along with in situ temperature measurements, to estimate heat flow. The system uses a single-needle probe (Von Herzen and Maxwell, 1959) heated continuously in full-space mode for soft sediments and in half-space configuration for hard rock samples (Vacquier, 1985). A self-test, including a drift study, was conducted at the beginning of each cycle. Once the samples were thermally equilibrated, the heater circuit was closed and the temperature rise in the probes was recorded. Thermal conductivities were calculated from the rate of temperature rise while the heater current was flowing. Temperatures measured during the first 150 s of the heating cycle were fitted to an approximate solution of a constantly heated line source (for details see Kristiansen, 1982; Blum, 1997). For full-core soft-sediment sections, a hole was drilled in the outer core liner and a 2-mm-diameter temperature probe was inserted into the working half of the core section. For hard rock samples, a half-space needle probe was strapped onto ~5-cm-long split-core sections that had been immersed in a water bath for at least 15 min. The thermal conductivity measurement for each sample was the average of three repeated measurements for the full-space method and of four repeated measurements for the half-space method. All results are in units of watts per meter degree Kelvin. Thermal conductivity measurements were taken with a frequency of one per core except for instances when downhole temperature measurements were taken, in which case thermal conductivity was taken three times per core.

### **Moisture and Density Properties**

Samples of ~10 cm<sup>3</sup> for sediments and <10 cm<sup>3</sup> for hard rock were collected at a frequency one per section for sediment cores and one every other section or one per section for the hard rock cores (depending on the variability) to allow for determination of moisture and density. Samples were taken from undisturbed parts of the core where possible. Wet sediment mass was measured immediately after the samples were collected. Dry mass and volume were measured after samples were heated in an oven at 105°C ± 5°C for 24 hr and allowed to cool in a desiccator. Hard rock samples were soaked in seawater for 24 hr, and then moisture and density properties were measured using the same procedure as for the sediment sections.

Sample mass was determined to a precision of 0.01 g using two Scientech 202 electronic balances and a computer averaging system to compensate for the ship's motion. Sample volumes were determined using a Quantachrome penta-pycnometer, a helium-displacement pycnometer with a precision of 0.02 cm<sup>3</sup>. Volume measurements were repeated five times. All cells were calibrated after three sample runs to check for instrument drift and systematic error. A purge time of 3–5 min was used before each run. The procedures for the determination of these properties comply with the American Society for Testing and Materials (ASTM) designation (D) 2216 (ASTM, 1990). Blum (1997) discusses the fundamental phase relations and assumptions for the calculations of all relevant phase relationships, summarized below.

### **Mass and Volume Calculation**

Wet mass ( $M_{\text{wet}}$ ), dry mass ( $M_{\text{dry}}$ ), and dry volume ( $V_{\text{dry}}$ ) are measured in the laboratory. Salt precipitated in sediment pores during the drying



process is included in the dry mass and dry volume values. The mass of the evaporated water ( $M_{\text{water}}$ ) and the salt ( $M_{\text{salt}}$ ) in the sample are given by

$$M_{\text{water}} = M_{\text{wet}} - M_{\text{dry}} \text{ and}$$

$$M_{\text{salt}} = M_{\text{water}} [s/(1 - s)],$$

where  $s$  = assumed saltwater salinity (0.035) corresponding to a pore water density ( $\rho_{\text{pw}}$ ) of 1.024 g/cm<sup>3</sup> and a salt density ( $\rho_{\text{salt}}$ ) of 2.257 g/cm<sup>3</sup>. The corrected mass of pore water ( $M_{\text{pw}}$ ), volume of pore water ( $V_{\text{pw}}$ ), mass of solids excluding salt ( $M_{\text{solid}}$ ), volume of salt ( $V_{\text{salt}}$ ), volume of solids excluding salt ( $V_{\text{solid}}$ ), and wet volume ( $V_{\text{wet}}$ ) are, respectively,

$$M_{\text{pw}} = M_{\text{water}} + M_{\text{salt}} = M_{\text{water}}/(1-s),$$

$$V_{\text{pw}} = M_{\text{pw}}/\rho_{\text{pw}},$$

$$M_{\text{solid}} = M_{\text{dry}} - M_{\text{salt}},$$

$$V_{\text{salt}} = M_{\text{salt}}/\rho_{\text{salt}},$$

$$V_{\text{solid}} = V_{\text{dry}} - V_{\text{salt}} = V_{\text{dry}} - M_{\text{salt}}/\rho_{\text{salt}}, \text{ and}$$

$$V_{\text{wet}} = V_{\text{solid}} + V_{\text{pw}}.$$

### Calculation of Bulk Properties

For all sediment samples, water content ( $w$ ) is expressed as the ratio of the mass of pore water to the wet sediment (total) mass:

$$w = M_{\text{pw}}/M_{\text{wet}}.$$

Wet-bulk density ( $\rho_{\text{wet}}$ ), dry-bulk density ( $\rho_{\text{dry}}$ ), sediment grain (solid) density ( $\rho_{\text{solid}}$ ), and porosity ( $\phi$ ) are calculated from, respectively,

$$\rho_{\text{wet}} = M_{\text{wet}}/V_{\text{wet}},$$

$$\rho_{\text{dry}} = M_{\text{solid}}/V_{\text{wet}},$$

$$\rho_{\text{solid}} = M_{\text{solid}}/V_{\text{solid}}, \text{ and}$$

$$\phi = V_{\text{pw}}/V_{\text{wet}}.$$

### Visible and Near-Infrared Spectroscopy

For the sediment cores, VNIS studies were conducted on the MAD sample powdered samples as well as an additional sample per section. The ~10-cm<sup>3</sup> samples were heated in an oven at 105° ± 5°C for 24 hr and allowed to cool in a desiccator. Samples need to be dry or water will completely dominate the spectral signature. Samples were then crushed to reduce the variability in repeat total reflectance measurements. Light reflectance, at a bandwidth of 350 to 2500 nm, was found for each sample using the FieldSpec Pro FR portable spectroradiometer. Semiquanti-

tative mineral concentrations were then calculated from the collected spectra, assuming a three-component system: calcite, opal, and smectite. For a complete description of the VNIS technique and calibration methods, refer to Vanden Berg and Jarrard (2002).

### Velocity

For sediment sections, velocity determinations were made using the Hamilton Frame PWS3 contact probe system. Using this system, *P*-wave velocities were measured at a frequency of one per section on all cores. For hard rock samples, *x*-, *y*-, and *z*- directional velocities were measured on the 2-cm × 2-cm × 2-cm minicubes that were also used for shipboard paleomagnetic measurements. The compressional wave velocity calculation is based on the accurate measurement of the delay time of a 500-kHz square wave signal traveling between a pair of piezoelectric transducers. The transducer pair for PWS3 is adjusted to the thickness of the core half or discrete sample. The separation between the fixed lower PWS3 transducer and the movable upper transducer is measured by a linear voltage displacement transducer. Deionized water was added to the contact between the transducers and sample to improve acoustic coupling.

The core temperature was recorded at the time velocity was measured; however, the velocity data stored in the Janus database are uncorrected for in situ temperature and pressure. These corrections can be made using the relationships outlined in Wyllie et al. (1956), Wilson (1960), and Mackenzie (1981).

### DIGITAL IMAGING

During Leg 206 the external surfaces of whole-round basalt cores were scanned using the DMT Digital Color CoreScan system after they had been run through the MST but prior to splitting. In addition, all split archive-half cores were imaged in slabbed mode with the Geotek camera system. Core imaging during this leg had four main objectives:

1. To provide a comprehensive suite of digital core images, including both unrolled 360° and slabbed images, to aid petrological interpretation;
2. To identify and measure planar features on unrolled images for comparison with core structural analysis and integration with structures measured on geographically oriented FMS and Ultrasonic Borehole Imager (UBI) images (see “**High-Resolution Electrical Images,**” p. 40, and “**Ultrasonic Borehole Images,**” p. 40, both in “Tool String Configurations and Geophysical Measurements” in “Downhole Measurements”);
3. To correlate between core images and FMS and UBI images of the borehole wall derived from downhole log measurements to determine true core depth as opposed to curated depth in intervals with <100% recovery; and
4. To match structures observed on core and FMS and UBI images and reorient core pieces and associated structural data to magnetic north obtained from the General Purpose Inclinerometer Tool (GPIT) on the FMS and UBI tool strings and to geographic north from the GBR borehole magnetometer tool (see “**BGR Oriented Borehole Magnetometer,**” p. 41, in “Tool String Config-

urations and Geophysical Measurements” in “Downhole Measurements”).

Core orientation is particularly important for Leg 206 because Site 1256 has a low paleolatitude, which means the paleomagnetic inclination will be nearly horizontal and the magnetic polarity will be indeterminate from azimuthally unoriented cores. Similarly, without a known polarity, the paleomagnetic declination cannot be used to orient the core for structural analyses or for the determination of anisotropy of physical properties. The drill Site 1256 is sufficiently close (<10 km) to the Anomaly 5Bn/5Br boundary that the polarity cannot simply be assumed. In order to determine the source of marine magnetic anomalies, which is one of the leg objectives, estimating the true rather than the relative paleomagnetic direction is critical and can only be accomplished if the core is oriented.

### DMT CoreScan System

The DMT Color CoreScan system (Fig. F18), developed by Deutsche Montan Technologie (DMT), is a portable core imaging device that was previously used on board the *JOIDES Resolution* during Leg 173 (Whitmarsh, Beslier, Wallace, et al., 1998), Leg 176 (Dick, Natland, Miller, et al., 1999), and Leg 197 (Tarduno, Duncan, Scholl, et al., 2002). Images are recorded on whole-round outer core surfaces using a 24-bit, three-color (red, green, and blue) charge-coupled device line-scan camera that has a resolution of 5184 pixels/m (131 pixels/in) and a spectral response of between 400 and 700 nm (DMT, 1996, 2000).

The whole-round core is rotated 360° around its cylindrical axis with the line-scan camera positioned parallel to the axis of rotation. The unrolled images, up to 1 m long, are recorded in 33-cm sections that are integrated and light calibrated using the DigiCore software provided with the DMT CoreScan System. Whole-round cores are scanned in the unrolled mode at a rate of ~1.2 min/m, creating a ~14-MB bitmap file (DMT, 1996).

### Methodology

During Leg 206, all core pieces that could be rotated cleanly through 360° were scanned in unrolled mode. The conventional ODP core piece numbers, associated curated depths, and piece lengths were entered into a spreadsheet (see “[Digital Imaging](#),” p. 90, in “Basement Formed at Superfast Spreading Rate (Holes 1256C and 1256C)” and Table T45, p. 395, both in the “Site 1256” chapter). Pieces that were not fully cylindrical or intervals of unoriented drilling rubble were not imaged, but the lengths of these intervals were measured and recorded in the spreadsheet so that allowance could be made for them when integrated into core barrel lengths using the DMT CoreLog software (DMT, 1996, 2000). The vertical line marked on the core with a red grease pencil allows an initial reorientation of the core images back to the ODP reference frame. When the cores images are unrolled, nonhorizontal planar structures (e.g., veins, faults, or fractures) produce sinusoidal-shaped curves. These can be matched to similar shaped features imaged along the borehole wall by the four pads of the FMS logging tool or by the Ultrasonic Borehole Imager (UBI) (see “[Ultrasonic Borehole Images](#),” p. 40, in “Tool String Configurations and Geophysical Measurements” in “Downhole Measurements”). Other distinct petrological features or

F18. DMT CoreScan system, p. 67.



structures that are imaged on the outer surface of the core and the borehole wall can be similarly matched to determine the depth of the core in the borehole and reorient the core azimuth (Haggas et al., 2001). Initial comparisons with FMS and UBI images and structural analyses were performed onboard, but detailed structural analysis, core-log integration, and core reorientation work will be done postcruise.

## DOWNHOLE MEASUREMENTS

Downhole wireline logs are spatially continuous records of the in situ physical, chemical, and structural properties of the formation penetrated by a borehole. They provide information on a scale that is intermediate between laboratory measurements on core samples and geophysical surveys. The logs are recorded rapidly using a variety of probes or sondes combined into tool strings. These tool strings are lowered downhole on a heave-compensated electrical wireline and raised at a constant speed (typically 250–300 m/hr) to provide continuous simultaneous measurements of the various properties as a function of depth. The vertical sampling interval ranges from 2.5 mm to 15 cm.

Logs can be used to interpret the stratigraphy, magnetic stratigraphy, lithology, mineralogy, and geochemical composition of the penetrated formation. Where core recovery is incomplete or disturbed, log data may provide the only means to characterize the borehole section. Where core recovery is good, log and core data complement one another and may be interpreted jointly.

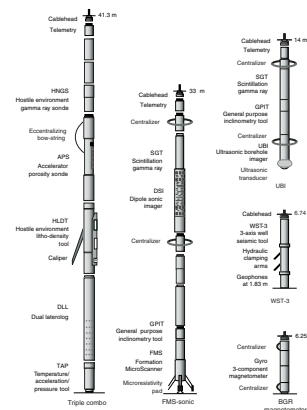
### Tool String Configurations and Geophysical Measurements

During ODP Leg 206, five different tool strings were deployed (Fig. F19; Tables T17, T18):

1. The triple combination (triple combo) tool string, which consists of the Hostile Environment Spectral Gamma Ray Sonde (HNGS), the Dual LateroLog (DLL) tool, the Hostile Environment Litho-Density Tool (HLDT), and the Accelerator Porosity Sonde (APS) (the Lamont-Doherty Earth Observatory [LDEO] high-resolution Temperature/Acceleration/Pressure [TAP] tool is attached at the bottom of this tool string);
2. The FMS-sonic tool string, which consists of the FMS, the GPIT, the Scintillation Gamma Ray Tool (SGT), and the Dipole Shear Sonic Imager (DSI) tool;
3. The UBI tool string, which also includes the GPIT and the SGT;
4. The Well Seismic Tool (WST); and
5. The Bundesanstalt für Geowissenschaften und Rohstoffe (BGR) magnetometer.

Explanations of tool name acronyms and their measurement units are summarized in Table T17. The parameters measured by each tool, the sample intervals used, and the vertical resolution are summarized in Tables T18 and T19. More detailed descriptions of individual logging tools and their geological applications can be found in Ellis (1987), Goldberg (1997), Rider (1996), Schlumberger (1989, 1994), Serra (1984, 1986, 1989), Bosum (1992), and the LDEO-Borehole Research Group (LDEO-BRG) Wireline Logging Services Guide (1994).

F19. Tool strings deployed during Leg 206, p. 68.



T17. Wireline logging tool acronyms, p. 92.

T18. Specifications of the BGR, p. 93.

T19. Wireline tool string measurements, p. 94.

## Natural Gamma Radiation

Two gamma ray tools were used to measure and characterize natural radioactivity in the formation: the HNGS and the SGT. The HNGS measures the natural gamma radiation from isotopes of potassium, thorium, and uranium using five-window spectroscopy to determine concentrations of radioactive potassium (in weight percent), thorium (in parts per million), and uranium (in parts per million). The HNGS uses two bismuth germanate scintillation detectors for gamma ray detection with full spectral processing. The spectral analysis filters out gamma ray energies below 500 keV, eliminating sensitivity to bentonite or KCl in the drilling mud and improving measurement accuracy. Corrections to the HNGS log account for variability in borehole size and borehole potassium concentrations. All of these effects are corrected for during processing of HNGS data at LDEO-BRG. The HNGS also provides a measure of the total gamma ray emission (in American Petroleum Institute [gAPI] units) and the uranium-free or computed gamma ray (in gAPI units).

The SGT uses a sodium iodide (NaI) scintillation detector to measure the total natural gamma ray emission, combining the spectral contributions of potassium, uranium, and thorium concentrations in the formation. The SGT is not a spectral tool but provides high-resolution total gamma ray data for depth correlation between logging strings. It is included in the FMS-sonic and UBI tool strings to provide a reference log to correlate depth between different logging runs.

## Density

Density is measured with the HLDT, which consists of a radioactive cesium ( $^{137}\text{Cs}$ ) gamma ray source (622 keV) and far and near gamma ray detectors mounted on a shielded skid, which is pressed against the borehole wall by a hydraulically activated eccentricizing arm (Fig. F19). Gamma rays emitted by the source experience both Compton scattering and photoelectric absorption. Compton scattering involves the transfer of energy from gamma rays to the electrons in the formation via elastic collision. The number of scattered gamma rays that reach the detectors is directly related to the number of electrons in the formation, which is a function of the bulk density.

The HLDT measures the photoelectric effect factor (PEF) caused by absorption of low-energy gamma rays. Photoelectric absorption occurs when gamma ray energies drop to <150 keV after being repeatedly scattered by electrons in the formation. As the PEF depends on the atomic number of the elements in the formation, it is essentially independent of porosity. Thus, the PEF varies according to the chemical composition of the sediment. Some examples of PEF values are pure calcite = 5.08 b/e<sup>-</sup>, pyrite = 16.97 b/e<sup>-</sup>, quartz = 1.81 b/e<sup>-</sup>, illite = 3.03 b/e<sup>-</sup>, and kaolinite = 1.49 b/e<sup>-</sup>. The PEF values can be used in combination with HNGS curves to identify different types of clay minerals. Coupling between the tool and borehole wall is essential for good HLDS logs. Poor contact results in underestimation of density values. Both density correction and caliper measurement of the hole are used to check the contact quality.

## Neutron Porosity

The APS consists of a minitron neutron generator that produces fast neutrons (14.4 MeV) and five neutron detectors (four epithermal and one thermal) positioned at different spacings along the tool. The tool is pressed against the borehole wall by an eccentricizing bow-spring. Emitted high-energy (fast) neutrons are slowed by collisions with atoms, and the amount of energy lost per collision depends on the relative mass of the nucleus with which the neutron collides. Significant energy loss occurs when the neutron strikes a hydrogen nucleus of equal mass, which is mainly present in pore water. Degrading to thermal energies (0.025 eV), the neutrons are captured by the nuclei of silicon, chlorine, boron, and other elements, resulting in a gamma ray emission. The neutron detectors record both the numbers of neutrons arriving at various distances from the source and the neutron arrival times, which act as a measure of formation porosity. Hydrogen bound in minerals such as clays or in hydrocarbons, however, also contributes to the measurement, and so the raw porosity value is often an overestimate. In sediments, hydrogen is mainly present in pore water, so the neutron log is essentially a measure of porosity, assuming pore fluid saturation. In igneous and hydrothermally altered rocks, hydrogen may also be present in alteration minerals such as clays; therefore, neutron logs may not give accurate estimates of porosity in these rocks.

The pulsing of the neutron source provides the measurement of the thermal neutron cross section ( $\Sigma$ ) in capture units (cu). This is a useful indicator for the presence of elements of high thermal neutron capture cross section such as boron, chloride, and rare earth elements.

## Electrical Resistivity

The DLL tool provides two resistivity measurements with different depths of investigation: deep and shallow. In both devices, a 61-cm-thick current beam is forced horizontally into the formation by using focusing (also called bucking) currents. Two monitoring electrodes are part of the loop that adjusts the focusing currents so that there is no current flow in the borehole between the two electrodes. For the deep laterolog (LLD) measurement, both measuring and focusing currents return to a remote electrode on the surface; this configuration greatly improves the depth of investigations and reduces the effect of borehole and adjacent formation conductivity. In the shallow laterolog (LLS) measurement, the return electrodes that measure the focusing currents are located on the sonde, and therefore the current sheet retains focus over a shorter distance than the LLD. Because of high resistivity expected in an igneous environment, the DLL is recommended over the Dual Induction Tool (DIT), as the DLL tool response ranges from 0.2 to 40,000  $\Omega\text{m}$ , whereas the DIT response range is 0.2–2,000  $\Omega\text{m}$ .

Fracture porosity can be estimated from the separation between the LLD and LLS measurements, based on the observation that the former is sensitive to the presence of horizontal conductive fractures only, whereas the latter responds to both horizontal and vertical conductive structures. Because the solid constituents of rocks are essentially infinitely resistive relative to the pore fluids, resistivity is controlled mainly by the nature of the pore fluids, porosity, and permeability. In most rocks, electrical conduction occurs primarily by ion transport through pore fluids and is strongly dependent on porosity.



### Temperature/Acceleration/Pressure

The TAP tool is deployed in low-resolution memory mode with the data being stored in the tool and then downloaded after the logging run is completed. Temperatures determined using the TAP tool are not necessarily the in situ formation temperatures because water circulation during drilling will have disturbed temperature conditions in the borehole. From the spatial temperature gradient, however, abrupt temperature changes can be identified that may represent localized fluid flow into the borehole, indicating fluid pathways, fracturing, and/or changes in permeability at lithologic boundaries.

### Acoustic Velocities

The DSI tool employs a combination of monopole and dipole transducers to make accurate measurements of sonic wave propagation in a wide variety of formations. In addition to a robust and high-quality measurement of compressional wave velocity, the DSI excites a flexural mode in the borehole that can be used to estimate shear wave velocity even in highly unconsolidated formations. When the formation shear velocity is less than the borehole fluid velocity, particularly in unconsolidated sediments, the flexural wave travels at the shear wave velocity and is the most reliable way to estimate a shear velocity log. The omnidirectional source generates compressional, shear, and Stoneley waves in hard formations. The configuration of the DSI tool also allows recording of both in-line and cross-line dipole waveforms. In hard rocks, the dipole sources can result in a better or equivalent estimate of shear wave velocity to that from a monopole source. These combined modes can be used to estimate shear wave splitting caused by preferred mineral and/or structural orientation in consolidated formations. A low-frequency (80 Hz) source enables Stoneley waveforms to be acquired as well. The DSI tool measures the transit times between sonic transmitters and an array of eight receiver groups with 15-cm spacing, each consisting of four orthogonal elements that are aligned with the dipole transmitters. During acquisition, the output from these 32 individual elements are differenced or summed appropriately to produce in-line and cross-line dipole signals or monopole-equivalent (compressional and Stoneley) waveforms, depending on the operation modes.

Preliminary processing of DSI data estimates monopole and dipole mode velocities using waveform correlation of the digital signals recorded at each receiver. In most instances, the shear wave data should be reprocessed postcruise to correct for dispersion, which is caused by the variation of sound velocity with frequency. Processing techniques must be applied to account for a dispersive model without assumptions or to compute a bias correction to minimize any frequency effects on the velocity. In addition, information such as mode amplitudes, shear wave polarization, and Poisson's ratio can be extracted postcruise to provide information about lithology, porosity, and anisotropy. Amplitude processing and stacking of Stoneley wave reflections may also be used to identify fractures, fracture permeability, and aperture in the vicinity of the borehole. The DSI tool is particularly important for determining shear wave velocities for the upper parts of the basalt flow units. The  $V_p/V_s$  ratio in basalts is typically 1.8–2.0. Thus, the part of the lava flow with  $V_p < 3.0$  km/s will have a  $V_s < 1.5$  km/s, which cannot be determined without using the dipole source of the DSI tool.

## High-Resolution Electrical Images

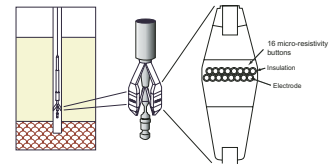
The FMS provides high-resolution electrical resistivity-based images of borehole walls (Fig. F20). The tool has four orthogonal arms (pads), each containing 16 microelectrodes, or “buttons,” which are pressed against the borehole wall during recording. The electrodes are arranged in two diagonally offset rows of eight electrodes each and are spaced ~2.5 mm apart. A focused current is emitted from the four pads into the formation, with a return electrode near the top of the tool. Array buttons on each of the pads measure the current intensity variations. The FMS image is sensitive to structure within ~25 cm of the borehole wall and has a vertical resolution of 5 mm with a coverage of 22% of the borehole wall on a given pass. FMS logging commonly includes two passes, the images of which are merged to improve borehole wall coverage. The pads must be firmly pressed against the borehole wall to produce reliable FMS images. In holes with a diameter >38 cm (>15 in), the pad contact will be inconsistent and the FMS images can be blurred. The maximum borehole deviation where good data can be recorded with this tool is 10° from vertical. Irregular borehole walls will also adversely affect the images, as contact with the wall is poor. FMS images are oriented to magnetic north using the GPIT (see “Magnetic Field,” p. 41). Processing transforms these measurements of the microresistivity variations of the formation into continuous, spatially oriented, and high-resolution images that mimic geologic structures behind the borehole walls. This allows the dip and azimuth of geological features intersecting the hole to be measured from the processed FMS image. FMS images can be used to visually compare logs with core to ascertain the orientations of bedding, fracture patterns, and sedimentary structures. FMS images have proved to be particularly valuable in the interpretation of volcanic stratigraphy during previous ODP legs (Ayadi et al., 1998; Lovell et al., 1998; Brewer et al., 1999; Haggas et al., 2001). Detailed interpretation of FMS images in combination with other log data and core imaging will be carried out postcruise.

## Ultrasonic Borehole Images

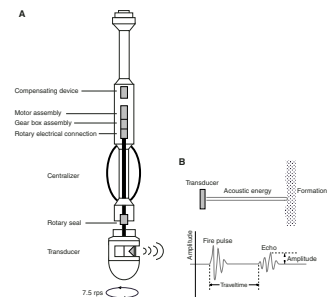
The UBI features a high-resolution transducer that provides acoustic images of the borehole wall. The transducer emits ultrasonic pulses at a frequency of 400 kHz, which are reflected at the borehole wall and then received by the same transducer. The amplitude and traveltime of the reflected signal are determined (Fig. F21). A continuous rotation of the transducer and the upward motion of the tool produce a complete map of the borehole wall.

The amplitude depends on the reflection coefficient of the borehole fluid/rock interface, the position of the UBI tool in the borehole, the shape of the borehole, and the roughness of the borehole wall. Changes in the borehole wall roughness (e.g., at fractures intersecting the borehole) are responsible for the modulation of the reflected signal; therefore, fractures or other variations in the character of the drilled rocks can easily be recognized in the amplitude image. The recorded traveltime image gives detailed information about the shape of the borehole, which allows calculation of one caliper value of the borehole from each recorded traveltime. Amplitude and traveltime are recorded together with a reference to magnetic north by means of a magnetometer, permitting the orientation of images. If features (e.g., fractures) recognized in the core are observed in the UBI images, orientation of the core is

F20. Formation MicroScanner pad, p. 69.



F21. Ultrasonic Borehole Imager, p. 70.



possible. The UBI orientated images can also be used to measure stress in the borehole through identification of borehole breakouts and slip along fault surfaces penetrated by the borehole (i.e., Paillet and Kim, 1987). In an isotropic, linearly elastic rock subjected to an anisotropic stress field, drilling a subvertical borehole causes breakouts in the direction of the minimum principal horizontal stress (Bell and Gough, 1983).

**Magnetic Field**

Downhole magnetic field measurements are made with the GPIT. The GPIT is used in combination with the FMS and the UBI. This sonde incorporates a three-component accelerometer and a three-component magnetometer, and its primary purpose is to determine the acceleration and orientation of the FMS and UBI tool strings. The acceleration data allow more precise determination of log depths than is possible on the basis of cable length alone, as the wireline is subject to both stretching and ship heave.

**BGR Oriented Borehole Magnetometer**

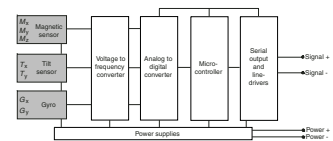
BGR (Germany) has developed three-component borehole magnetometers with gyro orientation since the 1980s. These tools were originally built for mineral exploration purposes (Bosum et al., 1988). The current tool (Fig. F22) has been designed for super-deep boreholes like the German KTB borehole and can withstand pressures as high as 800 bar and temperatures up to 230°C (Bosum, 1992). Modified versions of the BGR magnetometer have been deployed during previous ODP legs: Leg 102, Hole 418A (Bosum and Scott, 1988), Leg 109, Hole 395A (Bosum and Kopietz, 1990) and Leg 148, Holes 504B and 896A (Worm et al., 1996).

The tool consists of three fluxgate sensors in the lower part of the instrument that log the horizontal (x- and y-) and the vertical (z-) components of the magnetic flux density. Attached to the same mount are two tiltmeters, which record the tilt angle in the x- and y-axis, respectively. The upper part of the tool is equipped with an angular rate sensor (gyro) monitoring the tool’s rotation around its z-axis. The tool connects to a Gearhart-Owen GO 7 cable head. The use of centralizers is highly recommended since they reduce rotation and motion in regular halt phases, which are necessary for offset and drift correction of the gyro data. The housing is made of nonmagnetic titanium. Specifications are listed in Table T18. Since rotation angles around x-, y-, and z-axes are measured, the recorded magnetic flux density vector can be unrotated for all axes using principal axes rotation matrices. The processed magnetic data is referenced to the ship’s heading (northing) at the start and end of the logging run.

**Well Seismic Tool**

The WST is used to produce a zero-offset vertical seismic profile and/or checkshots in the borehole. The WST consists of a single geophone used to record the full waveform of acoustic waves generated by a seismic source positioned just below the sea surface. During Leg 206, an 80-in<sup>3</sup> generator-injector air gun, positioned at a water depth of ~7 m with a borehole offset of 50 m on the port side of the *JOIDES Resolution*, was used as the seismic source. The WST was clamped against the borehole

F22. BGR magnetometer, p. 71.



wall at 30- to 50-m intervals, and the air gun was typically fired between 5 and 15 times at each station. The recorded waveforms were stacked, and a one-way traveltime was determined from the median of the first breaks for each station, thus providing checkshots for calibration of the integrated transit time calculated from sonic logs. Checkshot calibration is required for the core-seismic correlation because *P*-wave velocities derived from the sonic log may differ significantly from true formation velocity because of (1) frequency dispersion (the sonic tool operates at 10–20 kHz, but seismic data are in the 50- to 200-Hz range), (2) difference in travel paths between well seismic and surface seismic surveys, and (3) borehole effects caused by formation alterations (Schlumberger, 1989). In addition, sonic logs cannot be measured through pipe, so the traveltime down to the uppermost logging point has to be estimated by other means.

### **In Situ Temperature Measurements**

Temperature measurements were taken during coring in Hole 1256B to determine the in situ temperatures within the sediment column for the purpose of measuring heat flow. The discrete in situ measurements were made with the Advanced Piston Coring Temperature (APCT) tool, formerly Adara), which is located in an annulus in the coring shoe of the APC during piston coring operations. The components of the tool include a platinum temperature sensor and a battery-powered data logger. The platinum resistance-temperature device is calibrated for temperatures ranging from  $-20^{\circ}$  to  $100^{\circ}\text{C}$ , with a resolution of  $0.01^{\circ}\text{C}$ . During operation, the adapted coring shoe is mounted on a regular APC core barrel and lowered down the pipe by wireline. The tool is typically held for 5–10 min at the mudline to equilibrate with bottom-water temperatures and then is lowered to the bottom of the drill string. Standard APC coring techniques are used, with the core barrel being fired out through the drill bit using hydraulic pressure. The APCT tool (and the APC corer) remains in the sediment for 10–15 min to obtain a temperature record. This provides a sufficiently long transient record for reliable extrapolation back to the steady-state temperature. The nominal accuracy of the temperature measurement is  $\pm 0.1^{\circ}\text{C}$ .

Data reduction for the APCT tool estimates the steady-state bottom-hole temperature by forward-modeling the recorded transient temperature curve as a function of time. The shape of the transient temperature curve is determined by the response function of the tool and the thermal properties of the bottom-hole sediment (Bullard, 1954; Horai and von Herzen, 1985). A synthetic curve is constructed based on the tool geometry, sampling interval, and the properties of the tool and surrounding sediments. It is difficult to obtain a perfect match between the synthetic curves and the data because (1) the probe never reaches thermal equilibrium during the penetration period; (2) contrary to theory, the frictional pulse upon insertion is never instantaneous; and (3) temperature data are sampled at discrete intervals, meaning that the exact time of penetration is always uncertain. As a result, both the effective penetration time and equilibrium temperature must be estimated by applying a fitting procedure, which involves shifting the synthetic curves in time to obtain a match with the recorded data.

## **Logging Operations**

In preparation for logging, a borehole is usually flushed of debris by circulating a “pill” of viscous drilling fluid (sepiolite mud mixed with seawater; approximate weight = 8.8 lb/gal or 1.11 g/cm<sup>3</sup>) through the drill pipe to the bottom of the hole. The BHA is pulled up to a depth of between 50 and 100 mbsf then run down to the bottom of the hole again to ream borehole irregularities. The hole is subsequently filled with more sepiolite mud, and the pipe is raised to ~50–80 mbsf and kept there to prevent hole collapse during logging. The tool strings are then lowered downhole during sequential runs. The tool strings are pulled uphole at constant speed to provide continuous measurements as a function of depth of several properties simultaneously. After the logs are acquired, the data are transferred to the downhole measurements laboratory (DHML) and also to LDEO-BRG for processing using a high-speed satellite data link.

Each tool string also contains a telemetry cartridge, facilitating communication from the tools along a double-armored seven-conductor wireline cable to the Schlumberger Minimum Configuration Maxis (MCM) computer van on the drill ship. The 9000-m-long logging cable connects the MCM to the tool string through the logging winch and LDEO-BRG wireline heave compensator (WHC). The WHC is employed to minimize the effect of ship’s heave on the tool position in the borehole. The logging winch is located aft of the pipe racker. The 160-m-long logging cable fairlead runs from the winch forward to the drill floor, through a sheave back to the heave compensator located alongside the logging winch, then forward to another sheave on the rig floor, up to the crown block on the top of the derrick, and then down into the drill string. As the ship heaves in the swell, an accelerometer located near the ship’s center of gravity measures the movement and feeds the data, in real time, to the WHC. The WHC responds to the ship’s heave by hydraulically moving the compensator sheave to decouple the movement of the ship from the desired movement of the tool string in the borehole.

## **Wireline Log Data Quality**

Logging data quality may be seriously degraded by changes in the hole diameter and in sections where the borehole diameter greatly decreases or is washed out. Deep-investigation measurements such as resistivity and sonic velocity are less sensitive to borehole conditions. Nuclear measurements (density and neutron porosity) are more sensitive because of their shallower depth of investigation and the effect of drilling fluid volume on neutron and gamma ray attenuation. Corrections can be applied to the original data in order to reduce these effects. Very large washouts, however, cannot be corrected for. HNGS and SGT data provide a depth correlation between logging runs, but logs from different tool strings may still have minor depth mismatches caused by either cable stretch or ship heave during recording. Ship heave is minimized by the WHC, designed to adjust for rig motion during logging operations.

## **Logging Data Flow and Processing**

Data for each wireline logging run are recorded and stored digitally and monitored in real time using the Schlumberger MCM system. After



logging is completed in each hole, data are transferred to the shipboard DHML for preliminary processing and interpretation. FMS image data are interpreted using Schlumberger's Geoframe version 4.0.2 software package. Well seismic, sonic, and density data are used for calculation of synthetic seismograms with GeoQuest's IESX software package in order to relate specific seismic reflectors to depths in the borehole.

Log data are transmitted to LDEO-BRG using a FFASTEST satellite high-speed data link for processing soon after each hole is logged. Data processing at LDEO-BRG consists of (1) depth-shifting all logs relative to a common datum (i.e., mbsf), (2) corrections specific to individual tools, and (3) quality control and rejection of unrealistic or spurious values. Once processed at LDEO-BRG, log data are transmitted back to the ship, providing near real-time data processing. Log curves of LDEO-BRG-processed data are then replotted on board (see "Downhole Measurements," p. 49, in "The Sedimentary Overburden (Holes 1256A, 1256B, and 1256C)" in the "Site 1256" chapter). Further postcruise processing of the log data from the FMS is performed at LDEO-BRG. Postcruise-processed acoustic, caliper, density, gamma ray, neutron porosity, resistivity, and temperature data in ASCII are available directly from the LDEO-BRG Internet Web site at [www.ldeo.columbia.edu/BRG/ODP/DATABASE/](http://www.ldeo.columbia.edu/BRG/ODP/DATABASE/). A summary of "logging highlights" is posted on the LDEO-BRG Web site at the end of each leg.

Downhole logging aboard the *JOIDES Resolution* is provided by LDEO-BRG in conjunction with Leicester University Borehole Research, the Laboratoire de Geophysique et d'Hydrodynamique en Forage Montpellier, University of Aachen, University of Tokyo, and Schlumberger Well Logging Services.

## UNDERWAY GEOPHYSICS

While transiting between Panama and Site 1256, we collected 3.5-kHz echo sounder and magnetometer data. Because the exact location of Site 1256 had been chosen based on analysis of site survey data prior to Leg 206, no additional surveys were conducted.

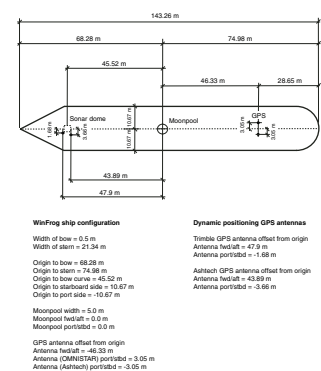
Navigation data were acquired throughout the leg on an Ashtech GG24 Global Positioning System (GPS) receiver. The antenna was mounted on the starboard stack 46.33 m aft of the moonpool (Fig. F23). The datum is the moonpool. GPS fixes were recorded by WinFrog navigation software every 60 s. Generic Mapping Tools software (Wessel and Smith, 1995) on Sun Sparc 10 Unix workstations was used to process and display the navigation data.

The time datum for all underway geophysics activities is Universal Time Coordinated (UTC) (similar to Greenwich Mean Time) as provided from the Ashtech receivers. If communication between the Ashtech receiver and the satellite is interrupted, the receiver uses its own internal clock to maintain the time base. The WinFrog navigation system displays the UTC time many times per second, but the internal clock is not synchronized to UTC.

The magnetic data were acquired with an EG&G Geometrics Marine Proton Magnetometer (model G-886) towed 500 m behind the ship. Values of total field intensity were acquired every 60 s using the WinFrog navigation software on a Windows PC.

The underway 3.5-kHz echo sounder data were acquired using an EDO Model 515A-250 transceiver mounted in a sonar dome located 45.52 m forward of the moonpool. The data were processed in real time

F23. Navigation antenna positions, p. 72.





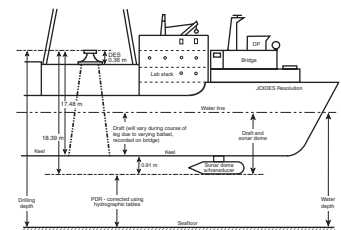
using a Raytheon CESP III (Correlator Echo Sounder Processor). The underway echo sounder data were not digitized but were recorded on an EPC 9802 analog line-scan thermal paper recorder. The ship's speed, heading, and position were annotated on the EPC recorders and were logged each minute on WinFrog. The paper recorder was set to a 1-sweep, and uncorrected depths were logged at 5-min intervals by hand.

Uncorrected depths convert traveltime to nominal depth assuming a velocity of 1500 m/s. A corrected depth (using Matthews' tables to allow for the varying sound speed with depth and location in the ocean [Carter, 1980]) was computed by hand upon arrival at the site.

The transducer elements are 0.9 m below the keel of the ship and 18.4 m below the dual elevator stool (the reference datum for drilling activities). Water depth relative to sea level was obtained by adding 0.9 m and the mean draft (typically  $6.5 \pm 0.6$  m) to the corrected echo sounder depth. Figure F24 is a schematic of the ship that summarizes some of the key dimensions used in computing depth to various datums. The shipboard 12-kHz system had poor signal-to-noise characteristics and was not used during this leg.

A program called "U/W Watch" was developed by ODP to configure the acquisition sequences for the echo sounder and the magnetometer and to display and annotate the echo sounder output on the EPC graphic recorders. This program is written in the National Instruments LabView language and runs on a Compaq Deskpro Workstation.

F24. Water depth, drilling depth, and sonar depth, p. 73.



## REFERENCES

- ASTM, 1990. Standard method for laboratory determination of water (moisture) content of soil and rock. *Annual Book of ASTM Standards* (Vol. 04.08): Philadelphia (Am. Soc. Testing and Mater.), D 2216-90 (revision of 2216-63, 2216-80).
- Ayadi, M., Pezard, P.A., Laverne, C., and Bronner, G., 1998. Multi-scalar structure at DSDP/ODP Site 504, Costa Rica Rift, I: stratigraphy of eruptive products and accretion processes. In Harvey, P.K., and Lovell, M.A. (Eds.), *Core-Log Integration: Spec. Publ.—Geol. Soc. London*, 136:297-310.
- Bach, W., Erzinger, J., Alt, J.C., and Teagle, D.A.H., 1996. Chemistry of the lower sheeted dike complex, Hole 504B (Leg 148): influence of magmatic differentiation and hydrothermal alteration. In Alt, J.C., Kinoshita, H., Stokking, L.B., and Michael, P.J. (Eds.), *Proc. ODP, Sci. Results*, 148: College Station, TX (Ocean Drilling Program), 39-55.
- Backman, J., 1980. Miocene-Pliocene nannofossils and sedimentation rates in the Hatton-Rockall Basin, NE Atlantic Ocean. *Stockholm Contrib. Geol.*, 36:1-91.
- Bell, J.S., and Gough, D.I., 1983. The use of borehole breakouts in the study of crustal stress. In Zoback, M.D., and Haimson, B.C. (Eds.), *Hydraulic Fracturing Stress Measurements: Washington* (National Academy Press), 201-209.
- Berggren, W.A., Hilgen, F.J., Langereis, C.G., Kent, D.V., Obradovich, J.D., Raffi, I., Raymo, M.E., and Shackleton, N.J., 1995a. Late Neogene chronology: new perspectives in high-resolution stratigraphy. *Geol. Soc. Am. Bull.*, 107:1272-1287.
- Berggren, W.A., Kent, D.V., Swisher, C.C. III, and Aubry, M.-P., 1995b. A revised Cenozoic geochronology and chronostratigraphy. In Berggren, W.A., Kent, D.V., Aubry, M.-P., and Hardenbol, J. (Eds.), *Geochronology, Time Scales and Global Stratigraphic Correlation*. Spec. Publ.—Soc. Econ. Paleontol. Mineral., 54:129-212.
- Blum, P., 1997. Physical properties handbook: a guide to the shipboard measurement of physical properties of deep-sea cores. *ODP Tech. Note*, 26 [Online]. Available from World Wide Web: <<http://www-odp.tamu.edu/publications/tnotes/tn26/INDEX.HTM>>. [Cited 2001-09-02]
- Bosum, W., 1992. Magnetic field measurements in the KTB-Oberpfalz VB using a three-axis borehole magnetometer. *Sci. Drill.*, 3:49-62.
- Bosum, W., Eberle, D., and Rehli, H.-J., 1988. A gyro-oriented three-component borehole magnetometer for mineral prospecting, with examples of its application. *Geophys. Prosp.*, 36:933-961.
- Bosum, W., and Kopietz, J., 1990. BGR magnetometer logging in Hole 395A, Leg 109. In Detrick, R., Honnorez, J., Bryan, W.B., Juteau, T., et al. *Proc. ODP, Sci. Results*, 106/109: College Station, TX (Ocean Drilling Program), 309-313.
- Bosum, W., and Scott, J.H., 1988. Interpretation of magnetic logs in basalt, Hole 418A. In Salisbury, M.H., Scott, J.H., et al., *Proc. ODP, Sci. Results*, 102: College Station, TX (Ocean Drilling Program), 77-95.
- Brewer, T.S., Harvey, P.K., Lovell, M.A., Haggas, S., Pezard, P.A., and Goldberg, D., 1999. Borehole images of the ocean crust: case histories from the Ocean Drilling Program. In Lovell, M.A., Williamson, and Harvey, P.K. (Eds.), *Borehole Images: Application and Case Histories: Spec. Publ.—Geol. Soc. London*, 159:283-294.
- Bullard, E.C., 1954. The flow of heat through the floor of the Atlantic Ocean. *Proc. R. Soc. London A*, 222:408-429.
- Cande, S.C., and Kent, D.V., 1995. Revised calibration of the geomagnetic polarity timescale for the Late Cretaceous and Cenozoic. *J. Geophys. Res.*, 100:6093-6095.
- Carter, D.J.T., 1980. *Echo-Sounding Correction Tables (Formerly Matthews' Tables)*: Taunton, Somerset, UK (Hydrographic Dept., Min. of Defence).
- Dick, H.J.B., Natland, J.H., Miller, D.J., et al., 1999. *Proc. ODP, Init. Repts.*, 176 [CD-ROM]. Available from: Ocean Drilling Program, Texas A&M University, College Station, TX 77845-9547, U.S.A.

- DMT GmbH, 2000. *DMT CoreScan Colour Acquisition Software Digicore and Hardware Information*.
- DMT-GeoTec/Geo-Engineering, 1996. *DMT Color CoreScan Users Manual. Acquisition and Evaluation Software*.
- Droser, M.L., and Bottjer, D.J., 1986. A semiquantitative field classification of ichnofabric. *J. Sediment. Petrol.*, 56:558–559.
- Ellis, D.V., 1987. *Well Logging for Earth Scientists*: New York (Elsevier).
- Evans, H.B., 1965. GRAPE—a device for continuous determination of material density and porosity. *Trans. SPWLA 6th Ann. Logging Symp.*: Dallas, 2:B1–B25.
- Fisher, R.A., 1953. Dispersion on a sphere. *Proc. R. Soc. London A*, 217:295–305.
- Gallagher, L., 1989. *Reticulofenestra*: a critical review of taxonomy, structure and evolution. In Crux, J.A., and van Heck, S.E. (Eds.), *Nannofossils and Their Applications*: Chichester (Ellis Horwood), 41–75.
- Gartner, S., 1967. Calcareous nannofossils from Neogene of Trinidad, Jamaica, and Gulf of Mexico. *Univ. Kansas Paleontol. Contrib.*, 29:1–7.
- Gieskes, J.M., Gamo, T., and Brumsack, H., 1991. Chemical methods for interstitial water analysis aboard *JOIDES Resolution*. *ODP Tech. Note*, 15.
- Goldberg, D., 1997. The role of downhole measurements in marine geology and geophysics. *Rev. Geophys.*, 35:315–342.
- Govindaraju, K., 1994. 1994 compilation of working values and sample description for 383 geostandards. *Geostand. Newsl.*, 18 (spec. iss.).
- Haggas, S., Brewer, T.S., Harvey, P.K., and Iturrino, G., 2001. Relocating and orienting cores by the integration of electrical and optical images: a case study from Ocean Drilling Program Hole 735B, *J. Geol. Soc. London*, 158:615–623.
- Hoppie, B.W., Blum, P., and the Shipboard Scientific Party, 1994. Natural gamma-ray measurements on ODP cores: introduction to procedures with examples from Leg 150. In Mountain, G.S., Miller, K.G., Blum, P., et al., *Proc. ODP, Init. Repts.*, 150: College Station, TX (Ocean Drilling Program), 51–59.
- Horai, K., and Von Herzen, R.P., 1985. Measurement of heat flow on Leg 86 of the Deep Sea Drilling Project. In Heath, G.R., Burckle, L.H., et al., *Init. Repts. DSDP*, 86: Washington (U.S. Govt. Printing Office), 759–777.
- Keene, J.B., 1975. Cherts and porcellanites from the North Pacific DSDP, Leg 32. In Larson, R.L., Moberly, R., et al. *Init. Repts. DSDP*, 32: Washington (U.S. Govt. Printing Office), 429–507.
- Kirschvink, J.L., 1980. The least-squares line and plane and the analysis of palaeomagnetic data. *Geophys. J. R. Astron. Soc.*, 62:699–718.
- Kristiansen, J.I., 1982. The transient cylindrical probe method for determination of thermal parameters of earth materials [Ph.D. dissert.]. Aarhus Univ.
- Lamont-Doherty Earth Observatory-Borehole Research Group (LDEO-BRG), 1994. *Wireline Logging Services Guide*. Available from the World Wide Web: <http://www.ldeo.columbia.edu/BRG/ODP/DATABASE/>. [Cited 2002-10-30]
- Lovell, M.A., Harvey, P.K., Brewer, T.S., Williams, C., Jackson, P.D., and Williamson, G., 1998. Application of FMS images in the Ocean Drilling Program: an overview. In Cramp, A., MacLeod, C.J., Lee, S.V., and Jones, E.J.W. (Eds.), *Geological Evolution of Ocean Basins: Results from the Ocean Drilling Program*. Spec. Publ.—Geol. Soc. London, 131:287–303.
- Mackenzie, K.V., 1981. Nine-term equation for sound speed in the oceans. *J. Acoust. Soc. Am.*, 70:807–812.
- Manheim, F.T., and Sayles, F.L., 1974. Composition and origin of interstitial waters of marine sediments, based on deep sea drill cores. In Goldberg, E.D. (Ed.), *The Sea* (Vol. 5): *Marine Chemistry: The Sedimentary Cycle*: New York (Wiley), 527–568.
- Martini, E., and Müller, C., 1986. Current Tertiary and Quaternary calcareous nannoplankton stratigraphy and correlations. *Newsl. Stratigr.*, 16:99–112.
- Mazzullo, J.M., Meyer, A., and Kidd, R.B., 1988. New sediment classification scheme for the Ocean Drilling Program. In Mazzullo, J., and Graham, A.G. (Eds.), *Handbook for Shipboard Sedimentologists*. *ODP Tech. Note*, 8:45–67.

- Murray, R.W., Miller, D.J., and Kryc, K.A., 2000. Analysis of major and trace elements in rocks, sediments, and interstitial waters by inductively coupled plasma-atomic emission spectrometry (ICP-AES). *ODP Tech. Note, 29* [Online]. Available from World Wide Web: <<http://www-odp.tamu.edu/publications/tnotes/tn29/INDEX.HTM>>. [Cited 2003-03-16]
- Okada, H., and Bukry, D., 1980. Supplementary modification and introduction of code numbers to the low-latitude coccolith biostratigraphic zonation (Bukry, 1973; 1975). *Mar. Micropaleontol.*, 5:321–325.
- Paillet, F.L., and Kim, K., 1987. Character and distribution of borehole breakouts and their relationship to in situ stresses in deep Columbia River Basalts. *J. Geophys. Res.*, 92:6223–6234.
- Passchier, C.W., and Trouw, R.A.J., 1996. *Microtectonics*: Berlin (Springer-Verlag).
- Perch-Nielsen, K., 1985. Cenozoic calcareous nannofossils. In Bolli, H.M., Saunders, J.B., and Perch-Nielsen, K. (Eds.), *Plankton Stratigraphy*: Cambridge (Cambridge Univ. Press), 427–554.
- Ramsay, J.G., and Huber, M.I., 1987. *The Techniques of Modern Structural Geology* (Vol. 2): *Folds and Fractures*: New York (Academic Press).
- Rider, M.H., 1996. *The Geological Interpretation of Well Logs* (2nd ed.): Houston (Gulf Publishing Co.).
- Rock-Color Chart Committee, 1991. *Rock Color Charts*. Geol. Soc. Am.
- Schlumberger, 1989. *Log Interpretation Principles/Applications*: Houston (Schlumberger Educ. Services), SMP-7017.
- Schlumberger, 1994. *Log Interpretation Charts*: Sugar Land (Schlumberger), SMP-7006.
- Serra, O., 1984. *Fundamentals of Well-Log Interpretation* (Vol. 1): *The Acquisition of Logging Data*: Dev. Pet. Sci., 15A.
- , 1986. *Fundamentals of Well-Log Interpretation* (Vol. 2): *The Interpretation of Logging Data*. Dev. Pet. Sci., 15B.
- , 1989. *Formation MicroScanner Image Interpretation*: Houston (Schlumberger Educ. Services), SMP-7028.
- Shipboard Scientific Party, 1989. Introduction and explanatory notes. In Robinson, P.T., Von Herzen, R., et al., *Proc. ODP, Init. Repts.*, 118: College Station, TX (Ocean Drilling Program), 3–24.
- , 1991. Explanatory notes. In Taira, A., Hill, I., Firth, J.V., et al., *Proc. ODP, Init. Repts.*, 131: College Station, TX (Ocean Drilling Program), 25–60.
- , 1992a. Explanatory notes. In Behrmann, J.H., Lewis, S.D., Musgrave, R.J., et al., *Proc. ODP, Init. Repts.*, 141: College Station, TX (Ocean Drilling Program), 37–71.
- , 1992b. Explanatory notes. In Dick, H.J.B., Erzinger, J., Stokking, L.B., et al., *Proc. ODP, Init. Repts.*, 140: College Station, TX (Ocean Drilling Program), 5–33.
- , 1992c. Explanatory notes. In Parson, L., Hawkins, J., Allan, J., et al., *Proc. ODP, Init. Repts.*, 135: College Station, TX (Ocean Drilling Program), 49–79.
- , 1993a. Explanatory notes. In Alt, J.C., Kinoshita, H., Stokking, L.B., et al., *Proc. ODP, Init. Repts.*, 148: College Station, TX (Ocean Drilling Program)], 5–24.
- , 1993b. Explanatory notes. In Gillis, K., Mével, C., Allan, J., et al., *Proc. ODP, Init. Repts.*, 147: College Station, TX (Ocean Drilling Program), 15–42.
- , 1995. Explanatory notes. In Cannat, M., Karson, J.A., Miller, D.J., et al., *Proc. ODP, Init. Repts.*, 153: College Station, TX (Ocean Drilling Program), 15–42.
- , 1999. Explanatory notes. In Dick, H.J.B., Natland, J.H., Miller, D.J., et al., *Proc. ODP, Init. Repts.*, 176, 1–42 [CD-ROM]. Available from: Ocean Drilling Program, Texas A&M University, College Station, TX 77845-9547, U.S.A.
- , 2000. Explanatory notes. In Sacks, I.S., Suyehiro, K., Acton, G.D., et al., *Proc. ODP, Init. Repts.*, 186, 1–51 [CD-ROM]. Available from: Ocean Drilling Program, Texas A&M University, College Station TX 77845-9547, USA.
- , 2002. Explanatory notes. In Salisbury, M.H., Shinohara, M., Richter, C., et al., *Proc. ODP, Init. Repts.*, 195 [Online]. Available from World Wide Web: <http://>

- www-odp.tamu.edu/publications/195\_IR/chap\_02/ chap\_02.htm. [Cited 2002-10-30]
- , 2003. Explanatory Notes. In Stephen, R.A., Kashara, J., Acton, G.D., et al., *Proc. ODP, Init. Repts.*, 200, 1–66 [CD-ROM]. Available from: Ocean Drilling Program, Texas A&M University, College Station TX 77845-9547, USA.
- Smith, D.C., Spivack, A.J., Fisk, M.R., Haveman, S.A., Staudigel, H., and ODP Leg 185 Shipboard Scientific Party, 2000. Methods for quantifying potential microbial contamination during deep ocean coring. *ODP Tech. Note*, 28 [Online]. Available from the World Wide Web: <<http://www-odp.tamu.edu/publications/tnotes/tn28/INDEX.HTM>>. [Cited 2002-10-30]
- Sparks, J.W., and Zuleger, E., 1995. Data report: Chemical analyses of the Leg 140 reference sample. In Erzinger, J., Becker, K., Dick, H.J.B., Stokking, L.B. (Eds.), *Proc. ODP, Sci. Results*, 137/140: College Station, TX (Ocean Drilling Program), 353–355.
- Su, X., 1996. Development of Late Tertiary and Quaternary coccolith assemblages in the Northeast Atlantic. *GEOMAR Rep.*, 48.
- Tarduno, J.A., Duncan, R.A., Scholl, D.W., et al., 2002. *Proc. ODP, Init. Repts.*, 197 [CD-ROM]. Available from: Ocean Drilling Program, Texas A&M University, College Station TX 77845-9547, USA.
- Twiss, R.J., and Moores, E.M., 1992. *Structural Geology*: New York (Freeman).
- Vacquier, V., 1985. The measurement of thermal conductivity of solids with a transient linear heat source on the plane surface of a poorly conducting body. *Earth Planet. Sci. Lett.*, 74:275–279.
- Vanden Berg, M., and Jarrard, R., 2002. Determination of equatorial Pacific mineralogy using light absorption spectroscopy. In Lyle, M.W., Wilson, P.A., Janecek, T.R., et al., *Proc. ODP, Init. Repts.*, 199, 1–20 [CD-ROM]. Available from: Ocean Drilling Program, Texas A&M University, College Station TX 77845-9547, USA.
- Vearncombe, J.R., 1993. Quartz vein morphology and implications for formation depth and classification of Archaean gold-vein deposits. *Ore Geol. Rev.*, 8:407–424.
- Von Herzen, R.P., and Maxwell, A.E., 1959. The measurement of thermal conductivity of deep-sea sediments by a needle-probe method. *J. Geophys. Res.*, 64:1557–1563.
- Wentworth, C.K., 1922. A scale of grade and class terms of clastic sediments. *J. Geol.*, 30:377–392.
- Wessel, P., and Smith, W.H.F., 1995. New version of the Generic Mapping Tools released. *Eos, Trans. Am. Geophys. Union*, 76:329.
- Whitmarsh, R.B., Beslier, M.O., Wallace, P.J., et al., 1998. *Proc. ODP, Init. Repts.*, 173 [CD-ROM]. Available from: Ocean Drilling Program, Texas A&M University, College Station, TX 77845-9547, U.S.A.
- Wilson, W.D., 1960. Speed of sound in seawater as a function of temperature, pressure and salinity. *J. Acoust. Soc. Am.*, 32:641–644.
- Worm, H.-U., Böhm, V., and Bosum, W., 1996. Implications for the sources of marine magnetic anomalies derived from magnetic logging in Holes 504B and 896A. In Alt, J.C., Kinoshita, H., Stokking, L.B., and Michael, P.J. (Eds.), *Proc. ODP, Sci. Results*, 148: College Station, TX (Ocean Drilling Program), 331–338.
- Wyllie, M.R.J., Gregory, A.R., and Gardner, L.W., 1956. Elastic wave velocities in heterogeneous and porous media. *Geophysics*, 21:41–70.
- Young, J.R., 1990. Size variation of Neogene *Reticulofenestra* coccoliths from Indian Ocean DSDP cores. *J. Micropaleontol.*, 9:71–85.

Figure F1. Cartoon illustrating ODP labeling scheme used for holes, cores, and sections. RCB = rotary core barrel.

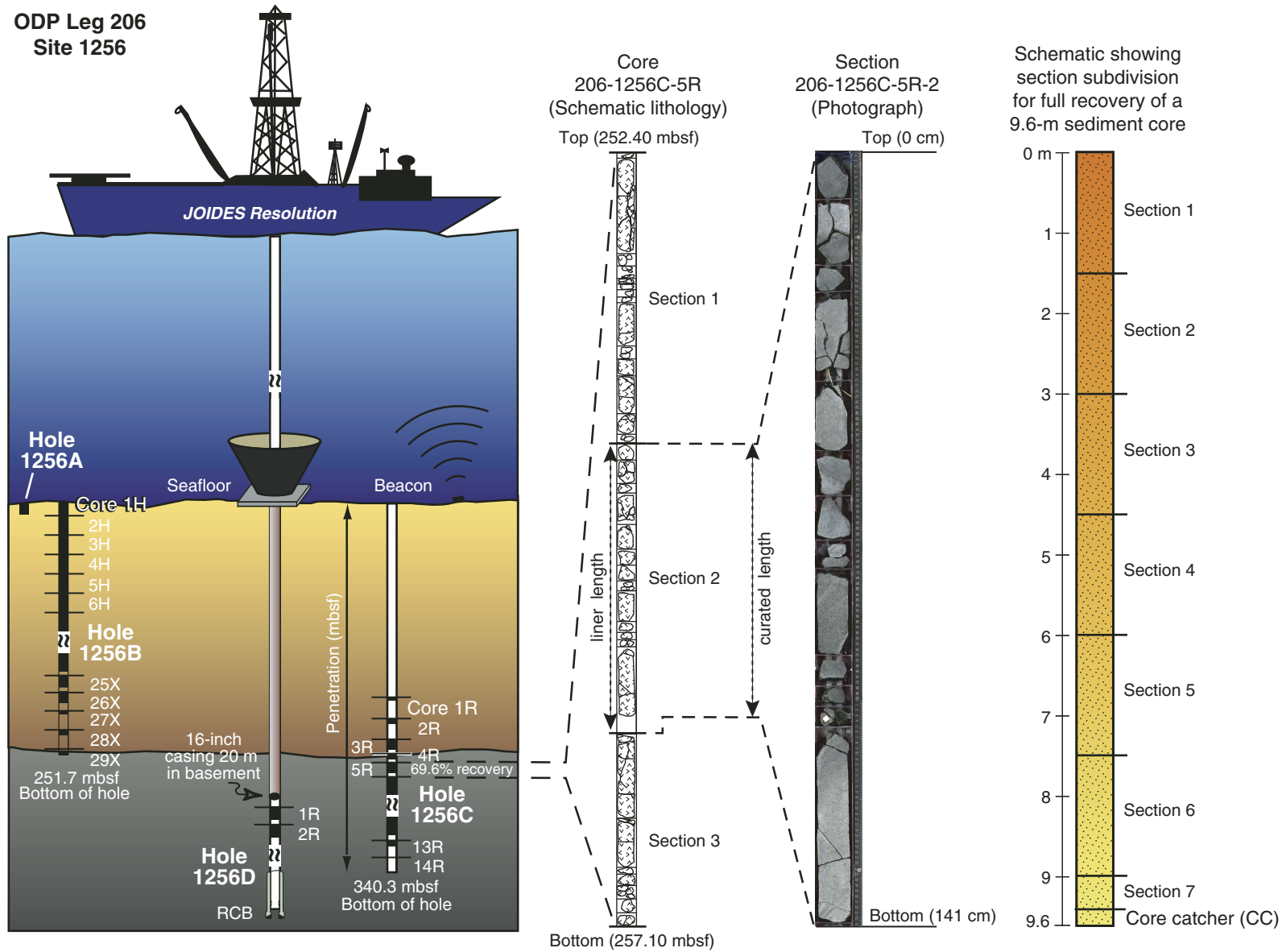
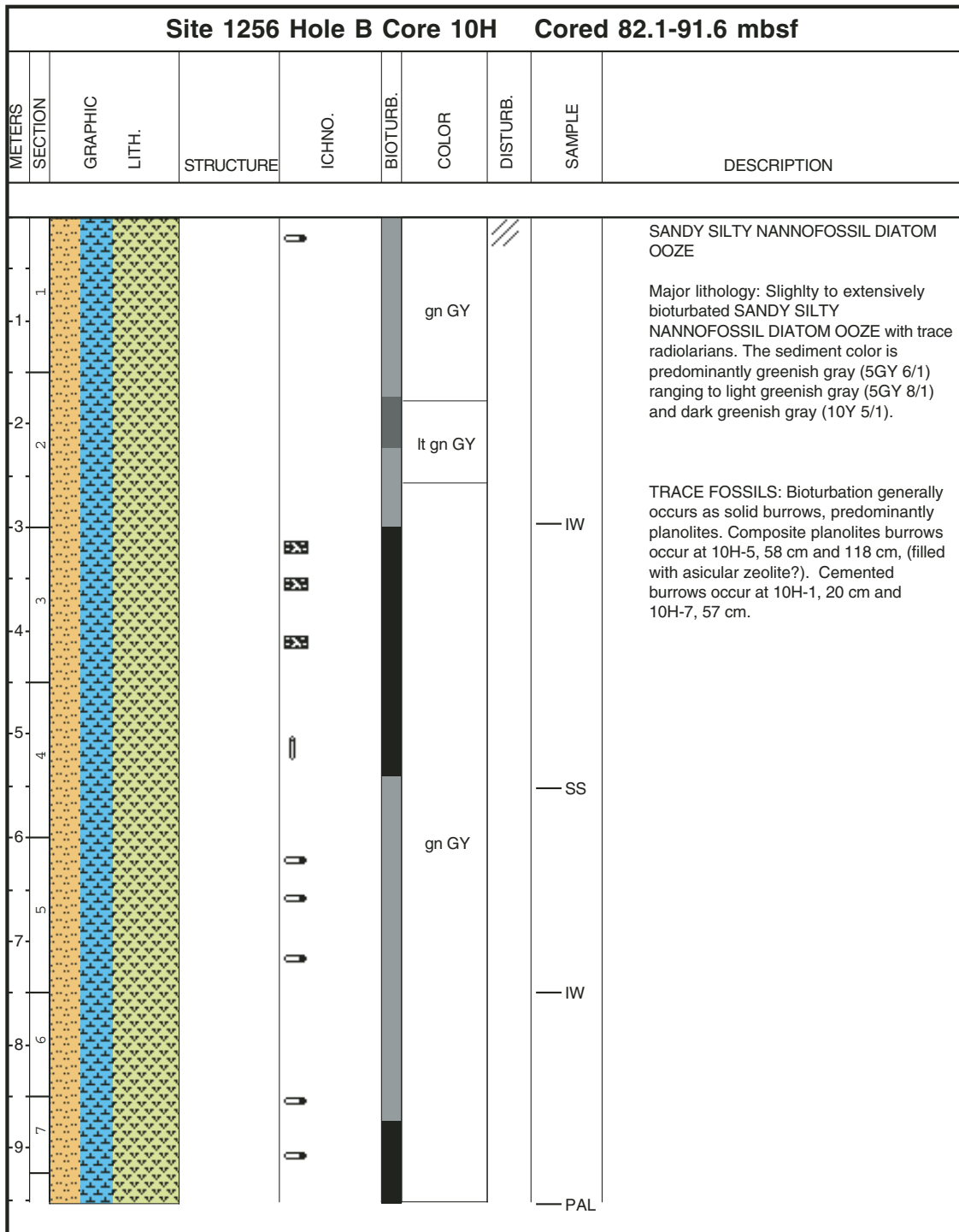




Figure F2. Example of a computer-generated visual core description barrel sheet.



**Figure F3.** Key to symbols used in the graphic lithology column log on the computer-generated core description forms.

**Pelagic Sediment**

-  Chert
-  Diatomite
-  Diatom Ooze
-  Nannofossil Ooze

**Siliciclastic Sediments**

-  Basalt
-  Clay or Claystone
-  Sand or Sandstone
-  Sandy Silt
-  Silt or Siltstone
-  Silty Clay
-  Volcanic Ash or Tuff

**Additional Symbols**










-  Void
-  Lost Core






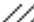
Figure F4. Key to symbols used for contacts, physical structures, lithologic accessories, ichnofossils, fossils, core disturbance, and bioturbation on the computer-generated core description forms.

Physical structures	
	Planar lamination

---

Ichnofossils					
	- <i>Planolites</i>		- <i>Skolithos</i>		- <i>Arenicolites</i>
	- <i>Chondrites</i>		- <i>Zoophycos</i>		- <i>Ophiomorpha</i>

---

Core disturbance					
	- Disturbed		- Deformed		- Biscuit
	- Soupy		- Flow-In		- Fractured

---






Bioturbation		Sample log	
	Abundant	SS	Smear slides
	Common	IW	Interstitial waters
	Moderate	PAL	Micropaleontology
	Rare		
	Barren		

Figure F5. Grain-size divisions for sedimentary rocks (adapted from Wentworth, 1922).

Millimeters (mm)	Micrometers ( $\mu\text{m}$ )	Phi ( $\phi$ )	Wentworth size class	Rock type
4096		-12.0	Boulder	Conglomerate/ Breccia
256		-8.0	Cobble	
64		-6.0	Pebble	
4		-2.0	Granule	
2.00		-1.0		
1.00		0.0	Very coarse sand	Sandstone
1/2	0.50	1.0	Coarse sand	
1/4	0.25	2.0	Medium sand	
1/8	0.125	3.0	Fine sand	
1/16	0.0625	4.0	Very fine sand	
1/32	0.031	5.0	Coarse silt	Siltstone
1/64	0.0156	6.0	Medium silt	
1/128	0.0078	7.0	Fine silt	
1/256	0.0039	8.0	Very fine silt	
0.00006	0.06	14.0	Clay	Claystone

Figure F6. Example VCD.

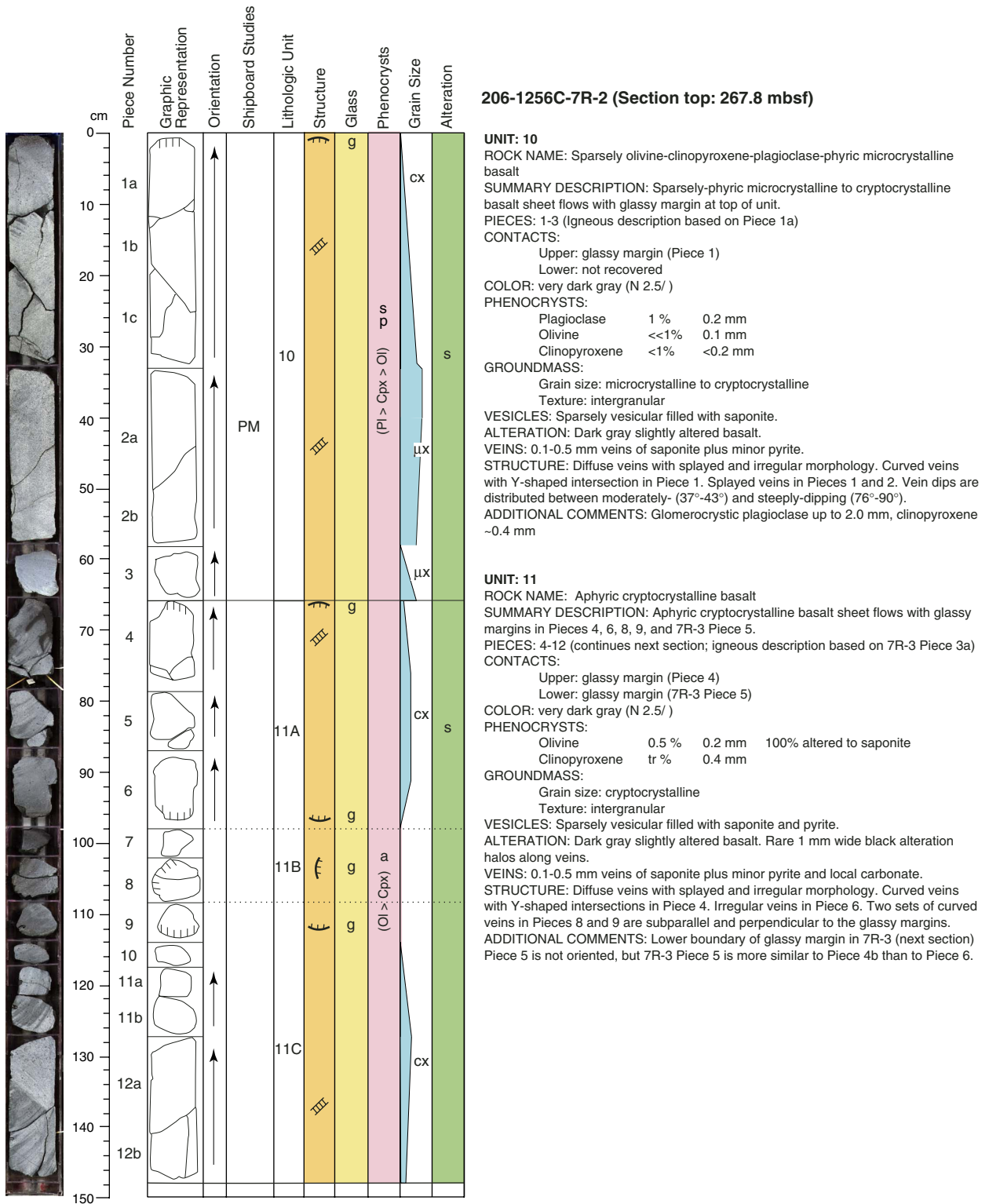


Figure F7. Key for VCD sheets.

Leg 206 Igneous texture/structure-definitions and abbreviations

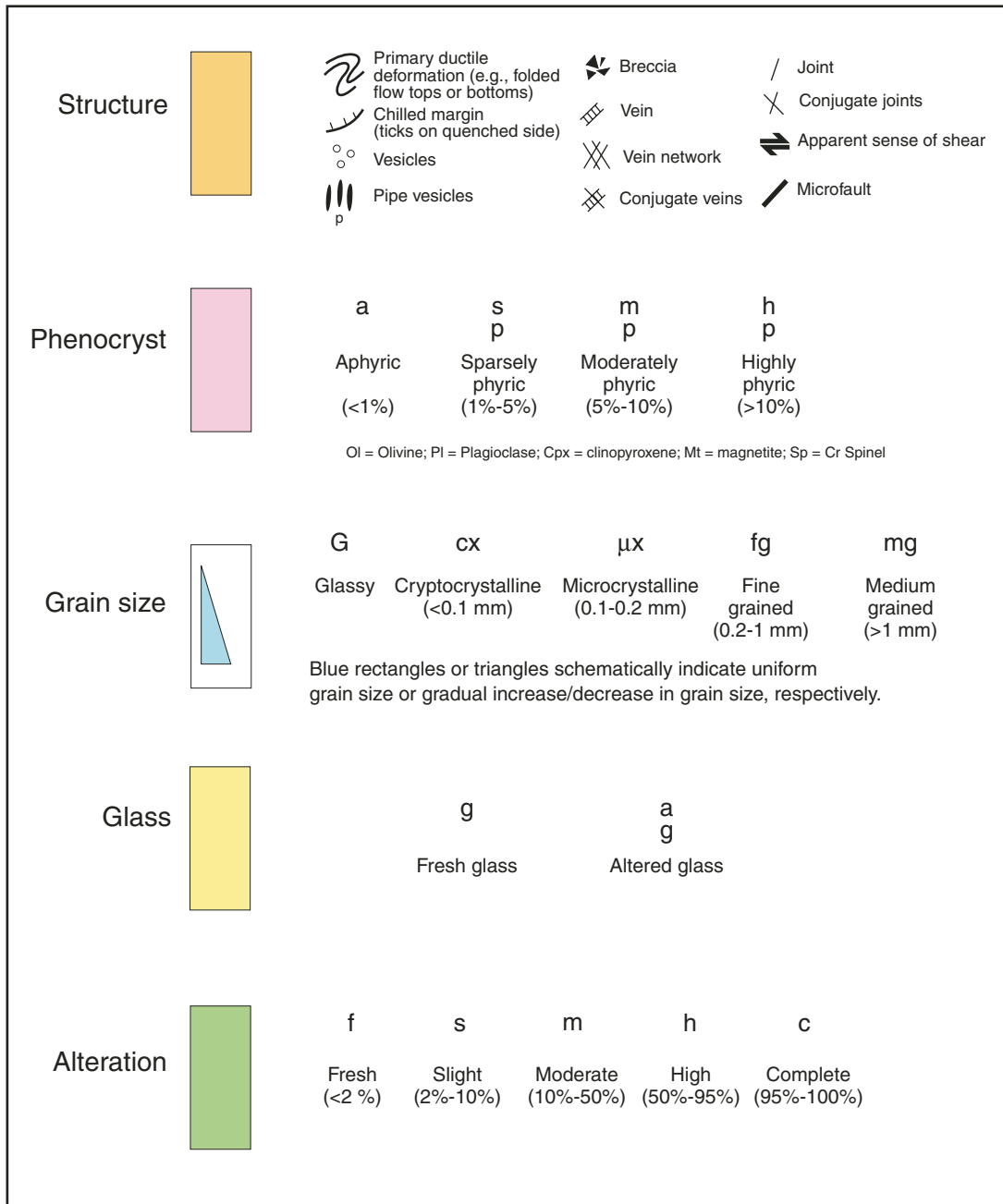




Figure F8. Example thin section form.

<b>THIN SECTION:</b>		206-1256C-5R1, 4-6 cm		<b>Piece No.:</b> 2		<b>Unit:</b> 1		<b>ODP TS#:</b> 3	
<b>ROCK NAME:</b>		Moderately ol-pl-phyric cryptocrystalline basalt							
<b>WHERE SAMPLED:</b>									
<b>GRAIN SIZE:</b>		0.04 mm							
<b>TEXTURE:</b>		Intergranular							
PRIMARY MINERALOGY	PERCENT PRESENT	PERCENT ORIGINAL	SIZE (mm)			MORPHOLOGY	COMMENTS		
			min.	max.	av.				
<b>PHENOCRYSTS</b>									
ol	0.00	0.90	0.10	0.20	0.15	Equant, euhedral	Replaced by clay minerals.		
pl	2.00	2.00	0.10	0.20	0.15	Platy, euhedral-subhedral			
<b>GROUNDMASS</b>									
cpx						Prismatic euhedral			
pl						Laths, euhedral			
Fe-Ti ox						Skeletal-equant polyhedral			
SECONDARY MINERALOGY	PERCENT		SIZE (mm)			REPLACING / FILLING	COMMENTS		
			min.	max.	av.				
saponite	1.50					olivine/pores	veinlets in plagioclase		
pyrite	<1					replacing olivine	small veinlet		
<b>STRUCTURES:</b>									
<b>COMMENTS :</b> Ol + pl + cpx forming glomerocrysts. Apparent coarsening of groundmass minerals downward. 50- $\mu$ m vein of saponite + pyrite.									



Figure F10. Schematic illustration of vein morphology and fiber growth commonly found during Leg 206. Partially redrawn from Ramsay and Huber (1987) and Vearncombe (1993).

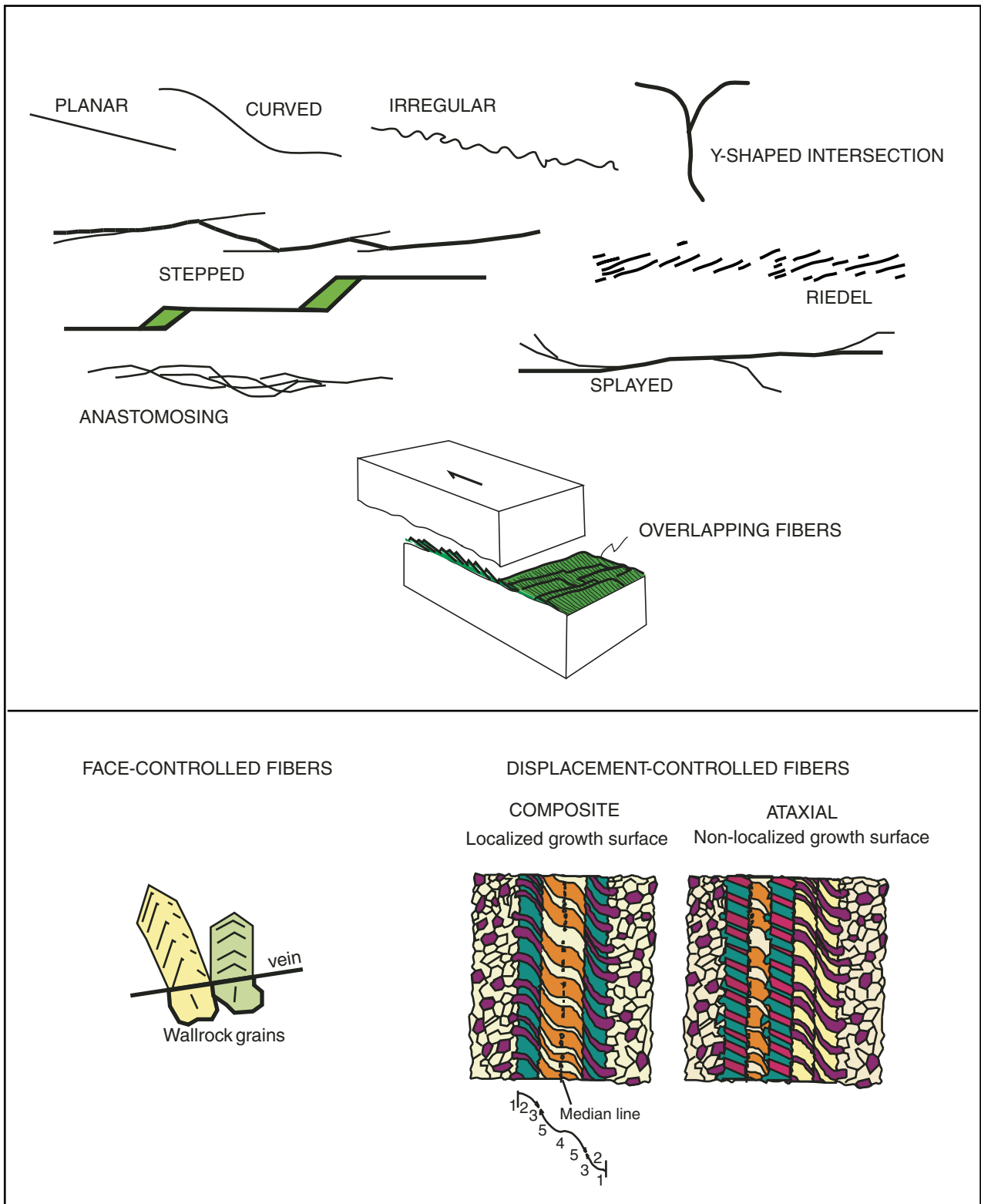
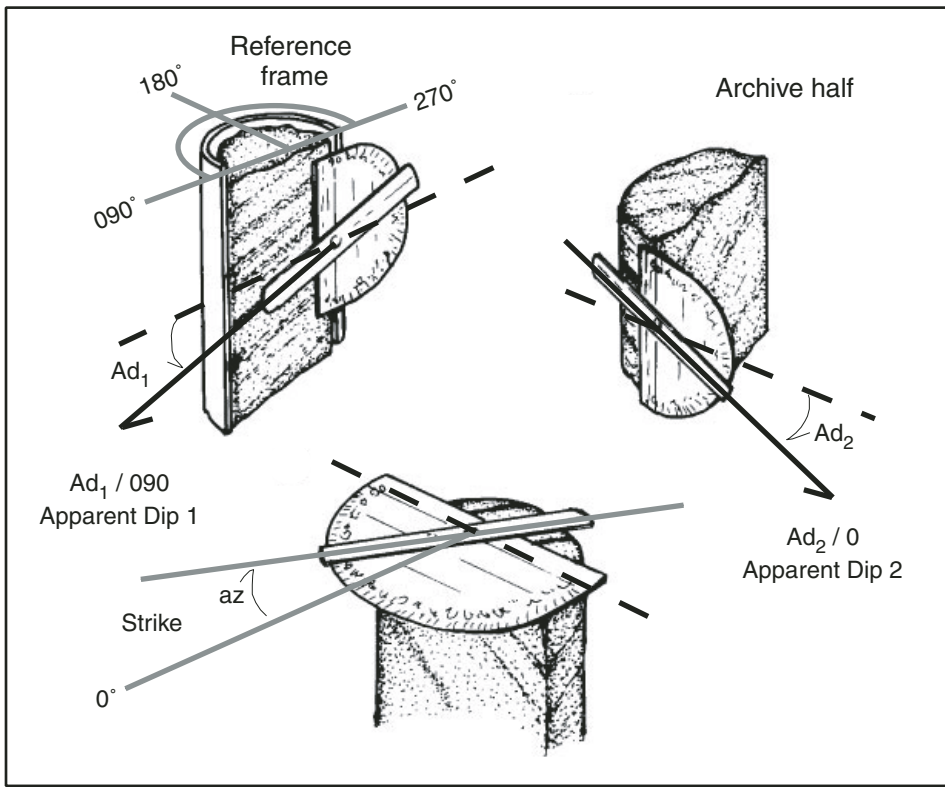
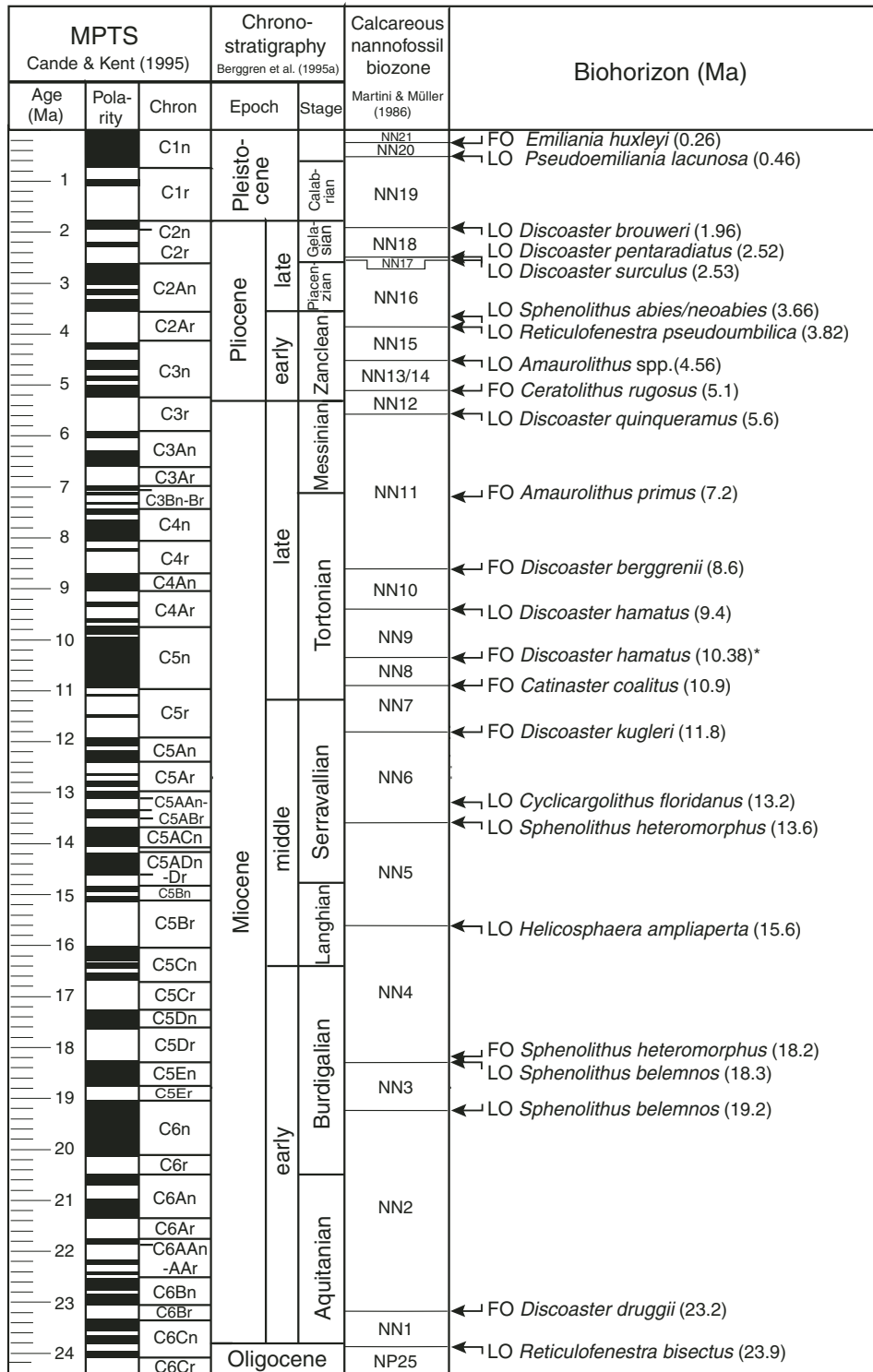


Figure F11. Sketch of the archive half of the core showing the conventions used for measuring orientation of structural features. Examples of orientation measurements with the protractor-based device are shown.



**Figure F12.** Leg 206 timescale and primary calcareous nannofossil datums for the Cenozoic (after Shipboard Scientific Party, 2002). The datums are after Berggren et al. (1995b); datum marked with an asterisk is after Berggren et al. (1995a). MPTS = magnetic polarity timescale, FO = first occurrence, LO = last occurrence. Polarity bands: black = normal, and white = reversed polarity.



**Figure F13.** Magnetic moments for the x-, y-, and z-axes measured for an empty sample boat at the beginning of Leg 206, (A) prior to cleaning the sample boat and (B) after the sample boat was cleaned with window cleaner and AF demagnetized at 80 mT.

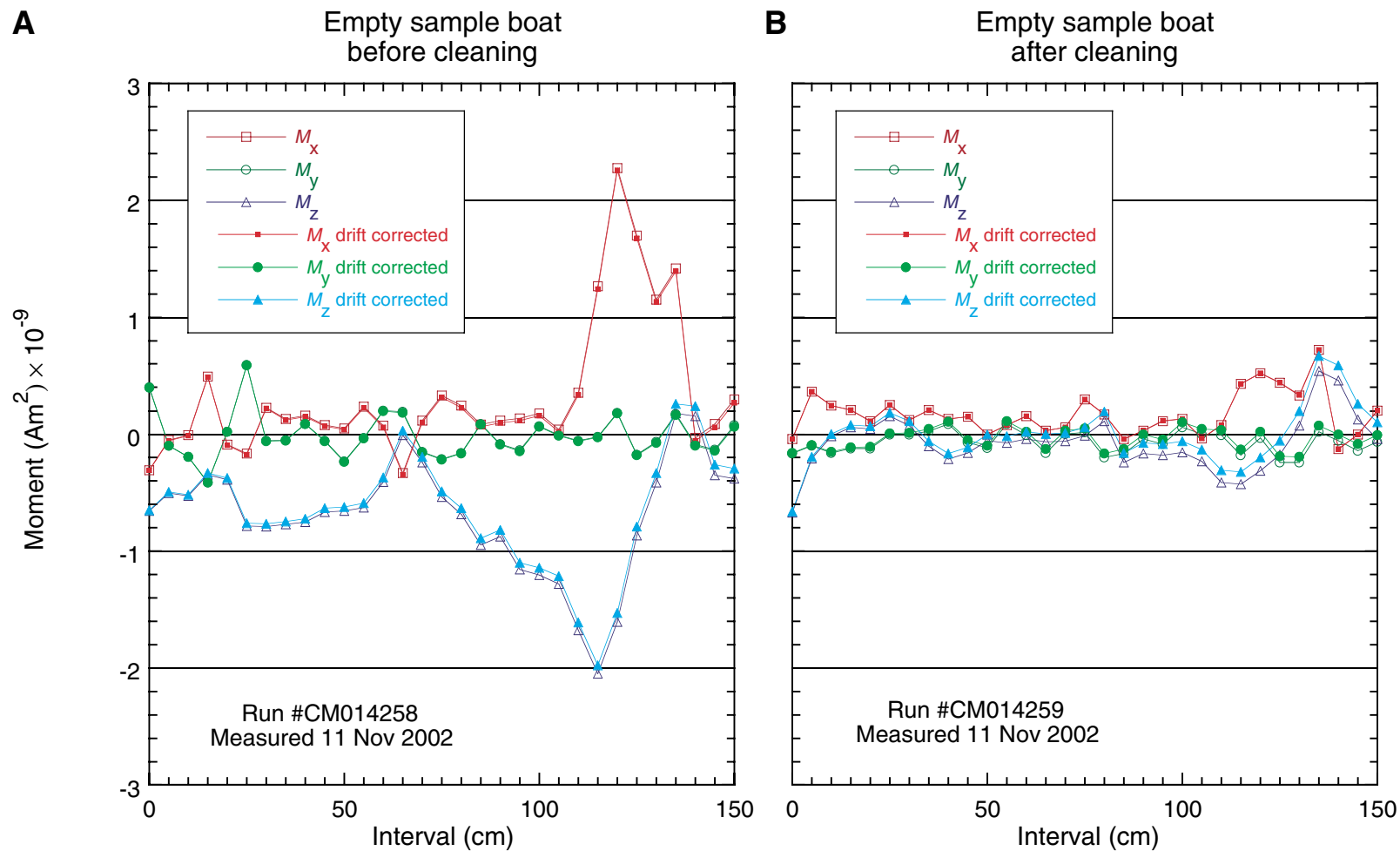




Figure F14. Magnetic moments for the x-, y-, and z-axes measured for a clean empty sample boat before and after applying the tray correction.

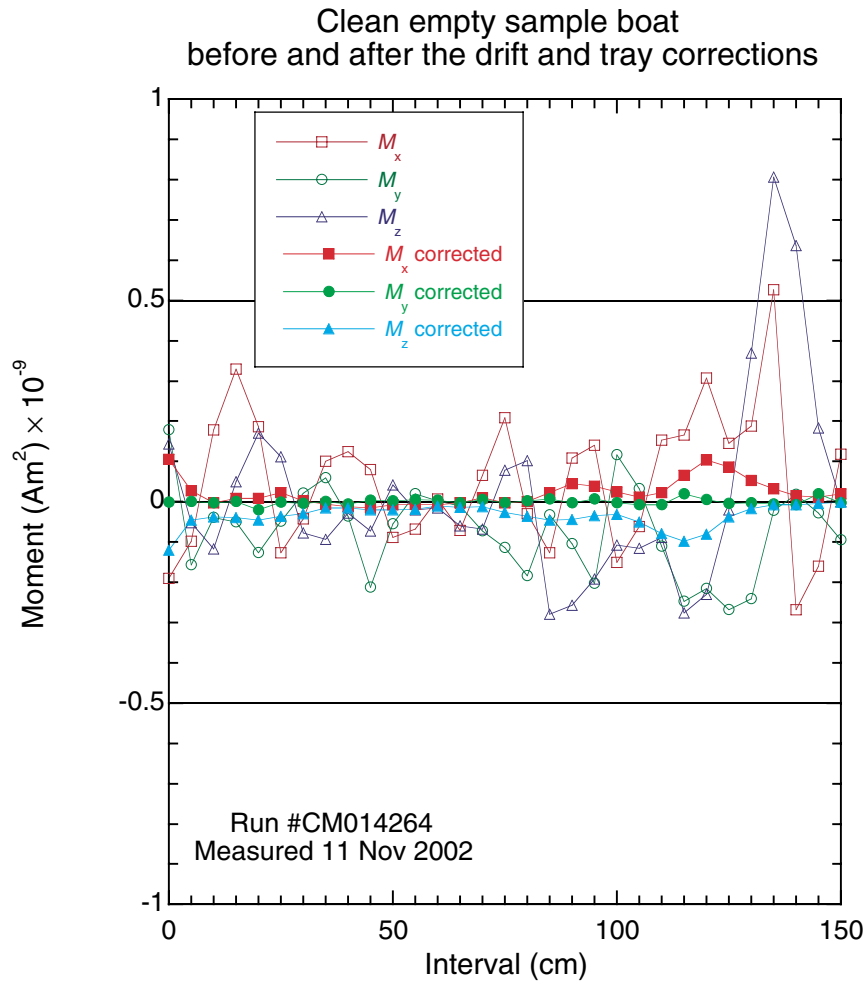
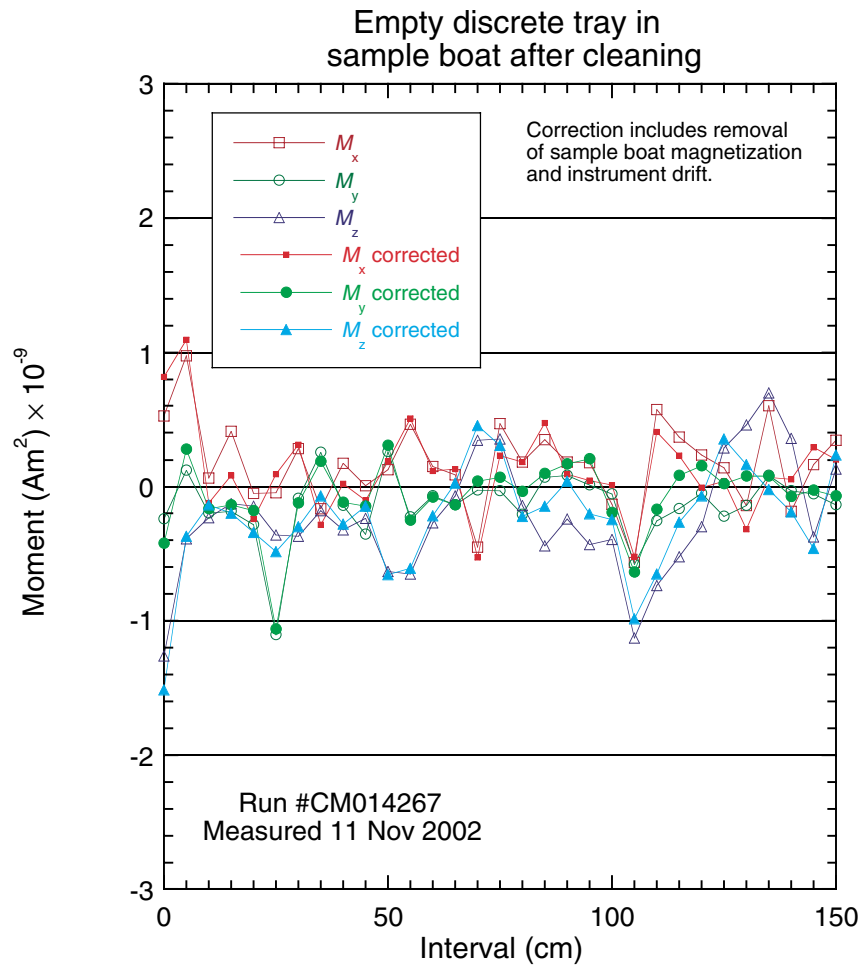


Figure F15. Magnetic moments for the x-, y-, and z-axes measured for an empty discrete sample tray sitting within the sample boat. The moment was measured after the tray was cleaned with window cleaner and AF demagnetized at 80 mT. The drift correction as well as a tray correction that removes the magnetization related to the sample boat, but not that related to the discrete sample tray, have been applied.



**Figure F16.** A. ODP paleomagnetic coordinate system for archive and working halves with radial and vertical overprints shown. B. Coordinate system for discrete samples collected with the extruder from the working half.

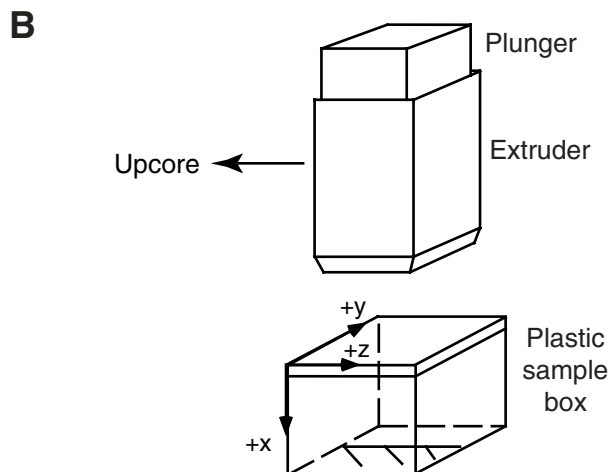
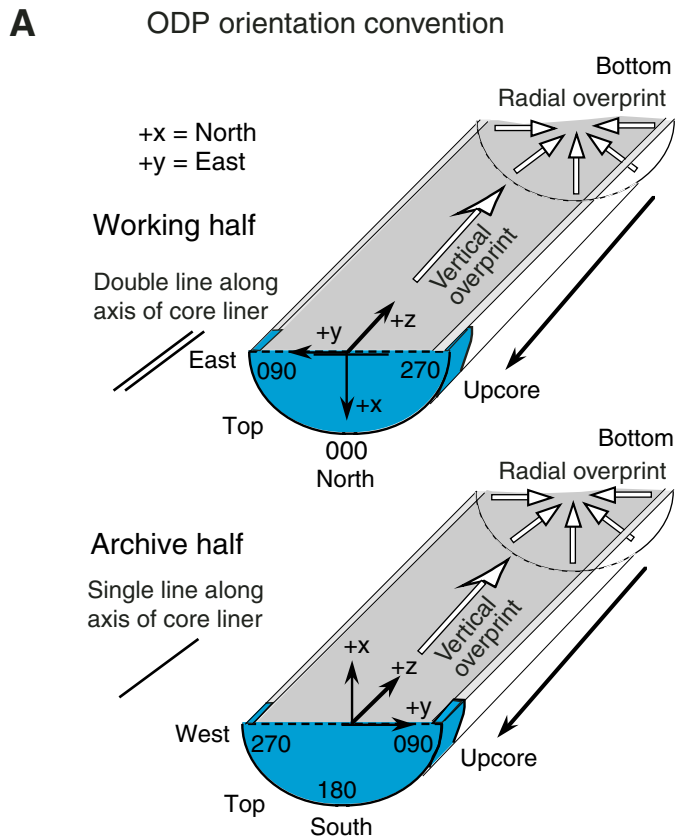
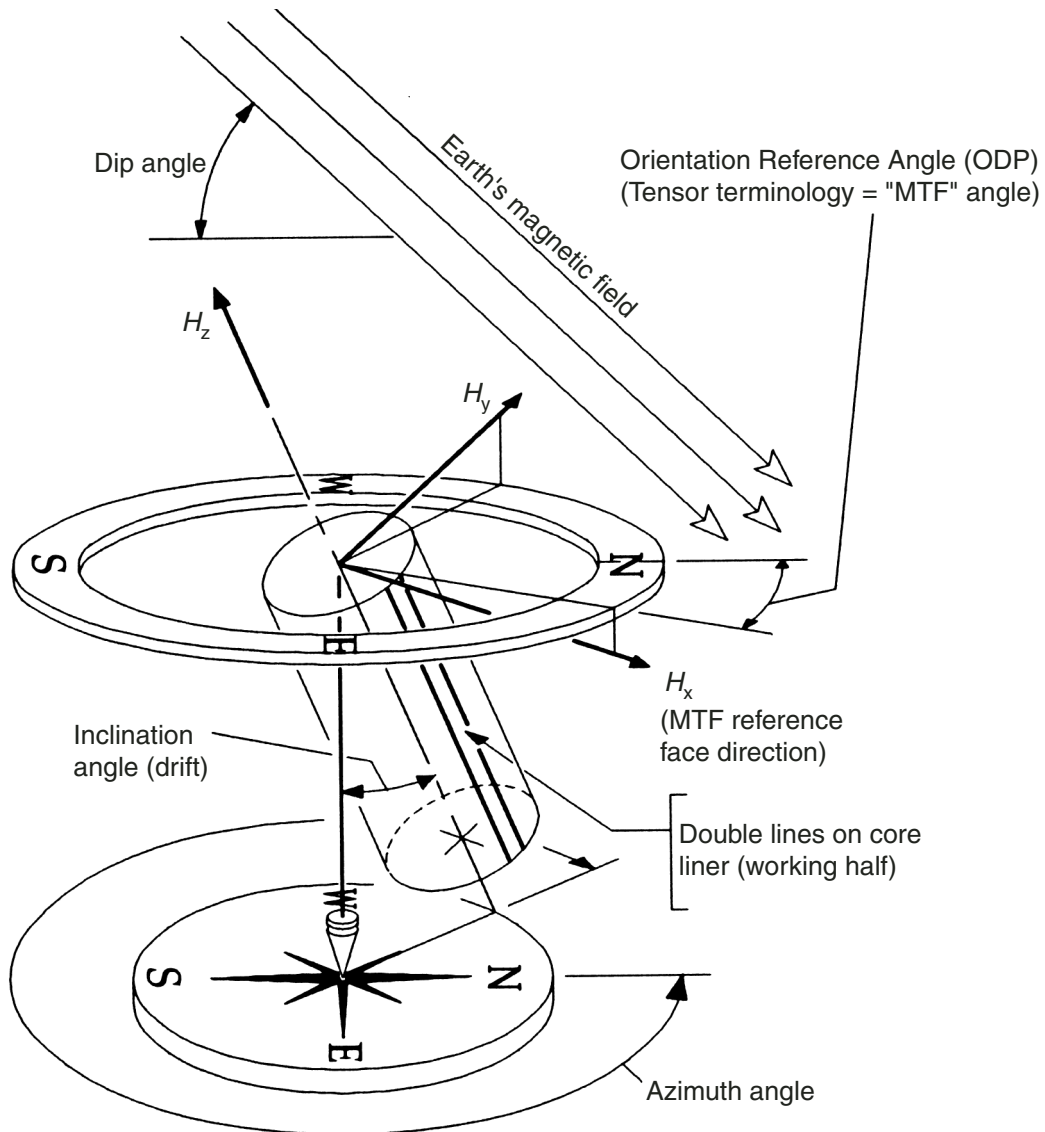


Figure F17. The orientation system and angles measured by the Tensor tool. MTF = magnetic toolface.



$H_x, H_y, H_z$  = Component directions for magnetometers

Figure F18. Photograph of the DMT Digital Color CoreScan system used during Leg 206.



Figure F19. Schematic presentation of the five tool strings deployed during Leg 206.

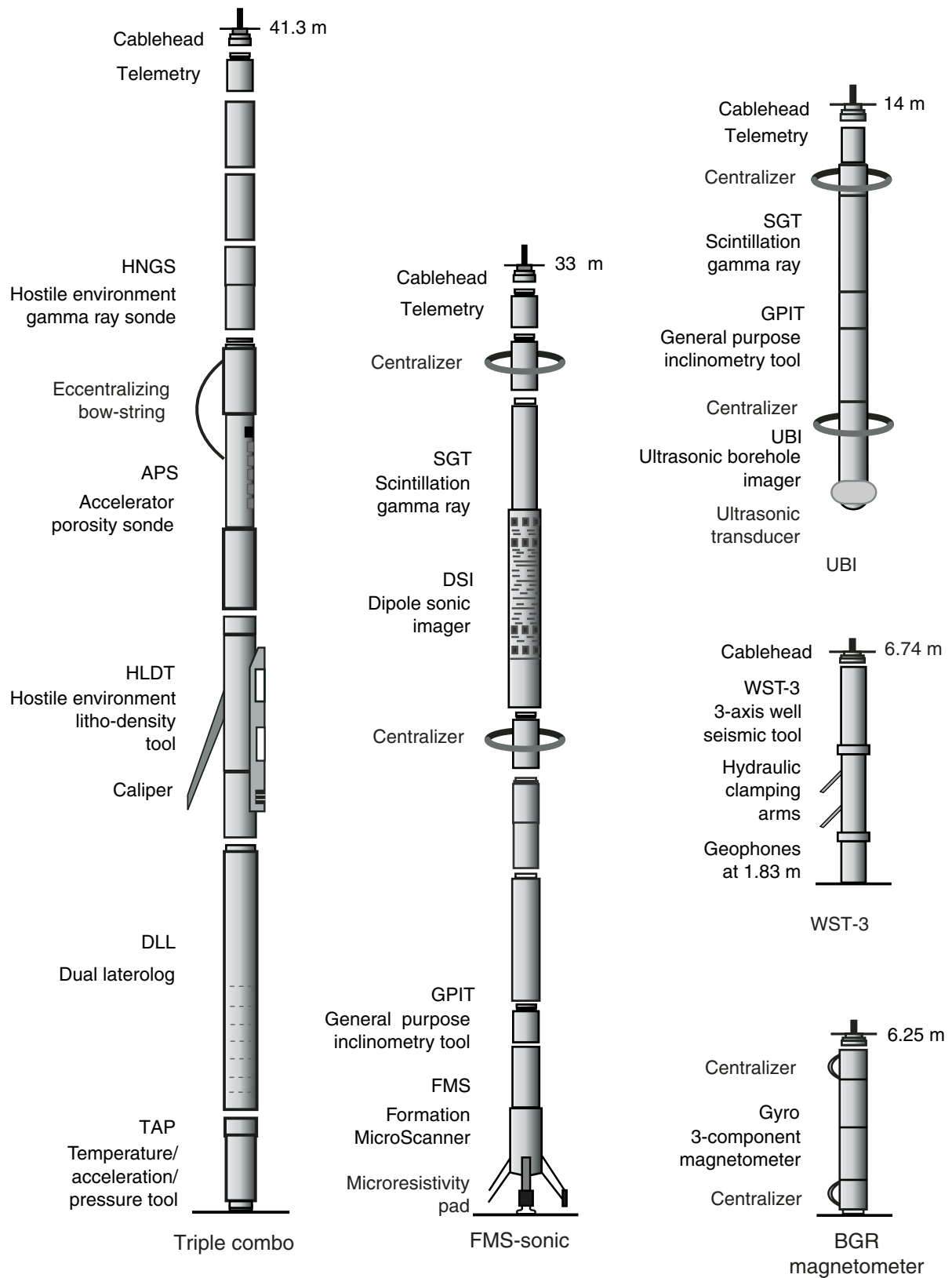




Figure F20. Schematic diagram of the Formation MicroScanner pad.

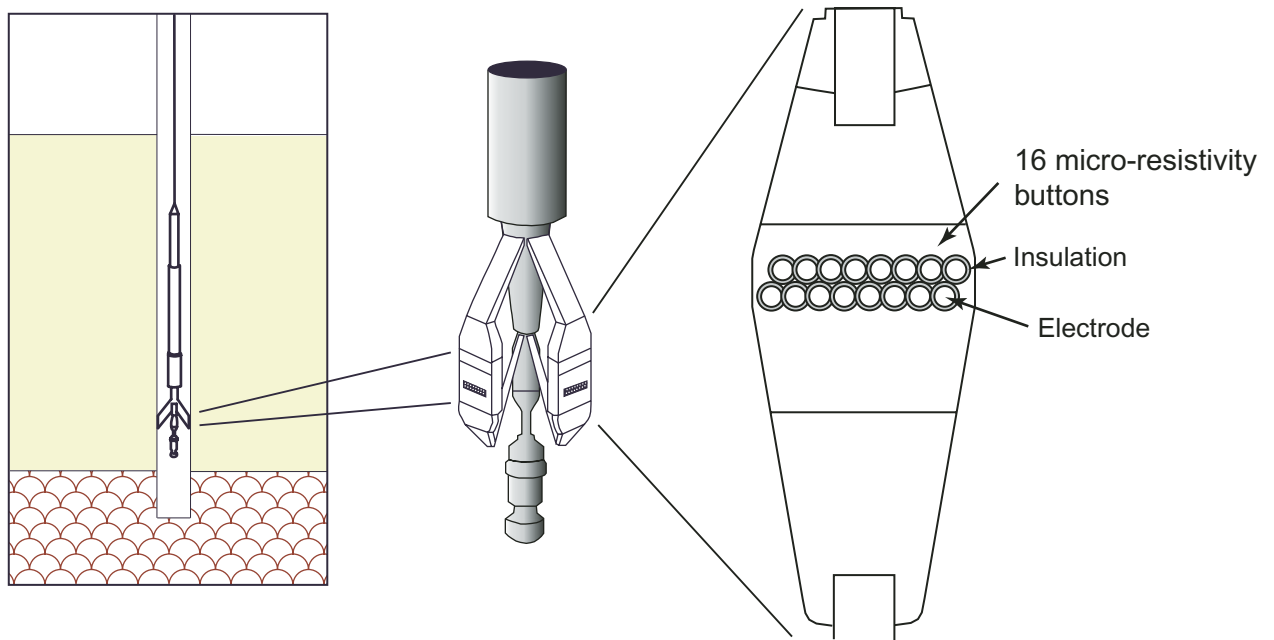


Figure F21. A, B. Schematic diagram of the Ultrasonic Borehole Imager.

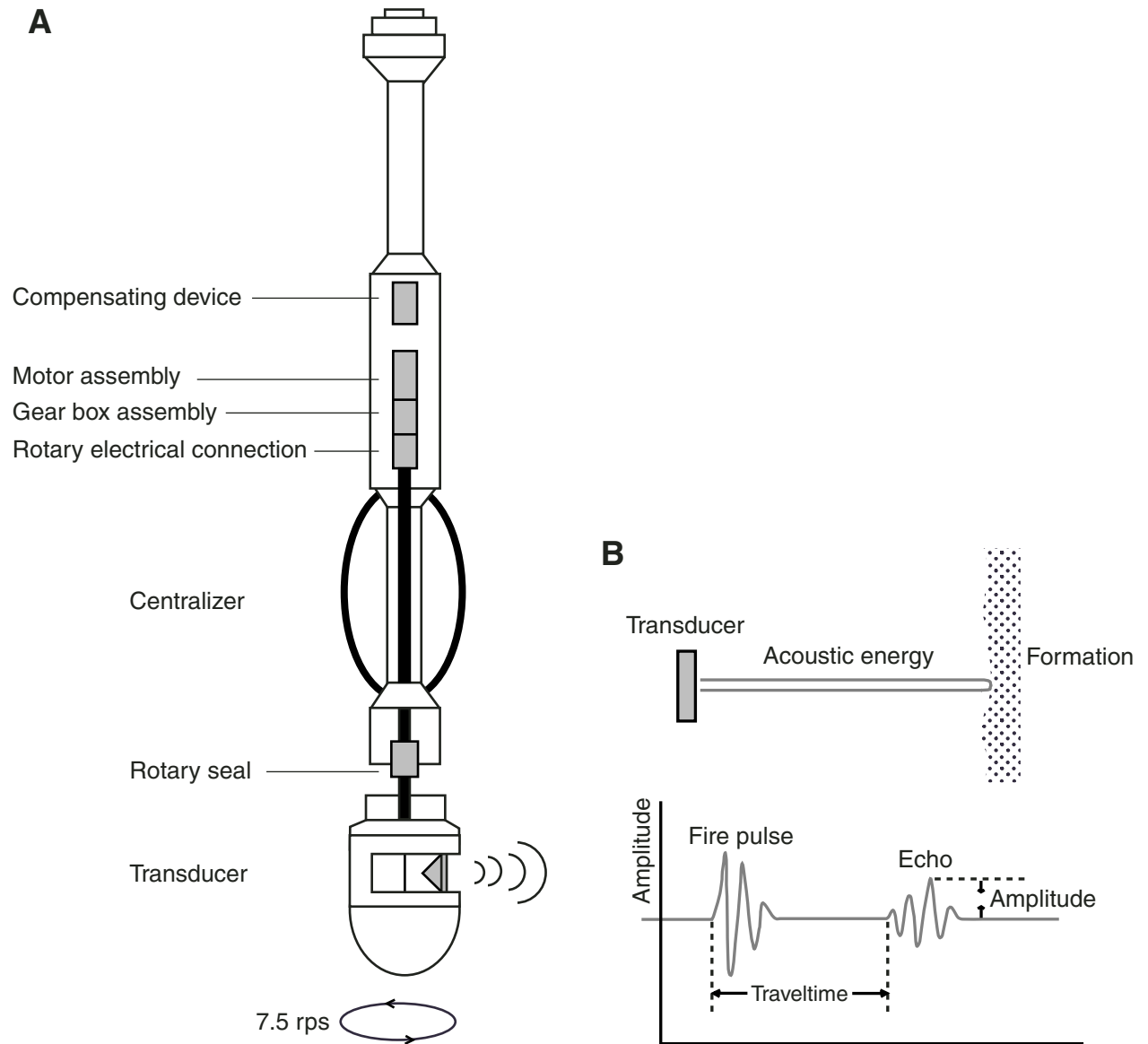
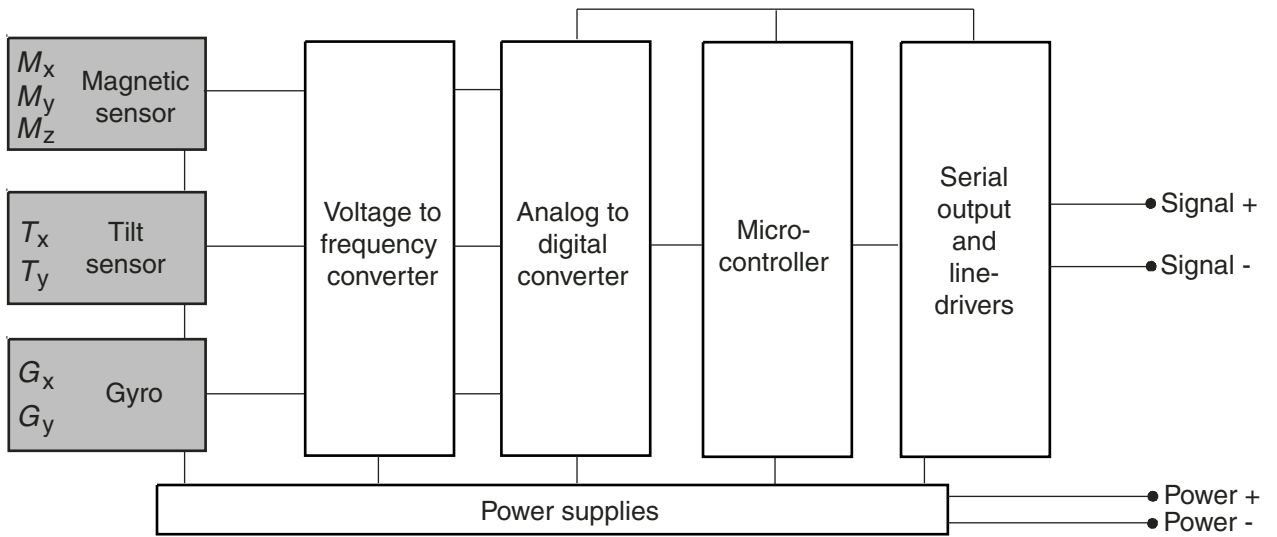
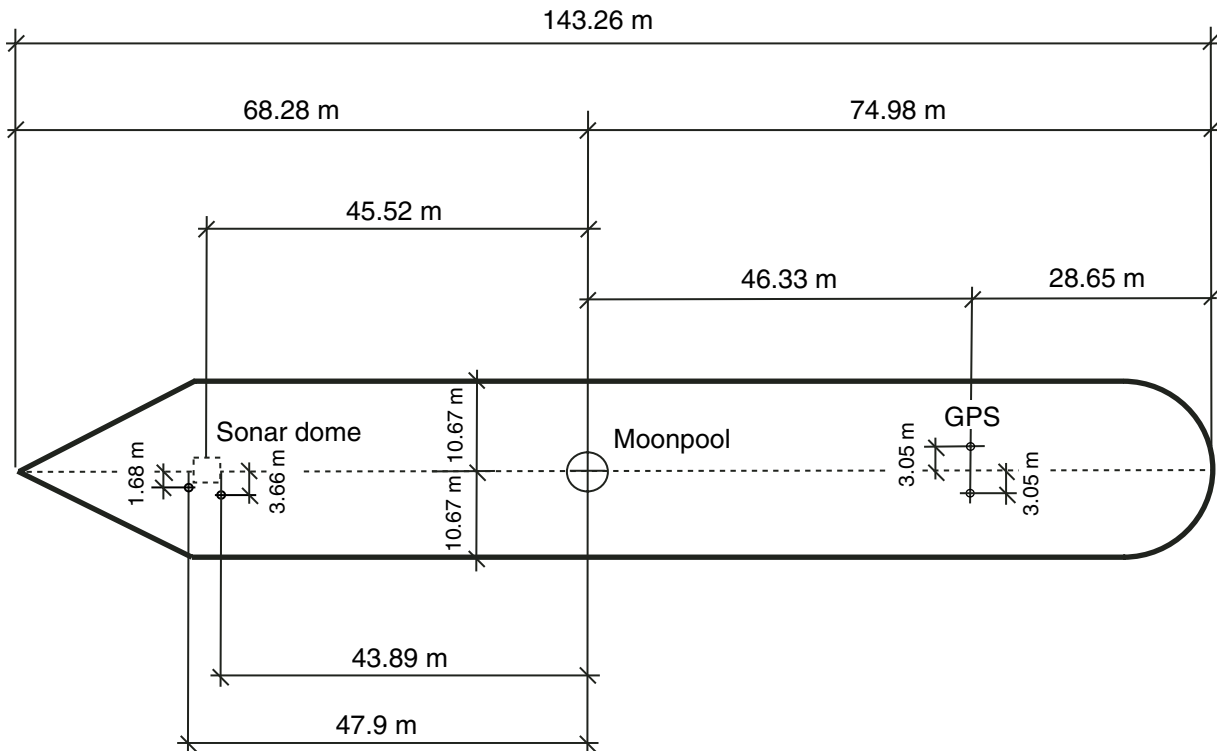


Figure F22. Schematic diagram of BGR three-component magnetometer tool.



**Figure F23.** Schematic diagram showing positions of navigation antennas relative to the moonpool datum.  
 GPS = Global Positioning System.



**WinFrog ship configuration**

Width of bow = 0.5 m  
 Width of stern = 21.34 m  
  
 Origin to bow = 68.28 m  
 Origin to stern = 74.98 m  
 Origin to bow curve = 45.52 m  
 Origin to starboard side = 10.67 m  
 Origin to port side = -10.67 m

Moonpool width = 5.0 m  
 Moonpool fwd/aft = 0.0 m  
 Moonpool port/stbd = 0.0 m

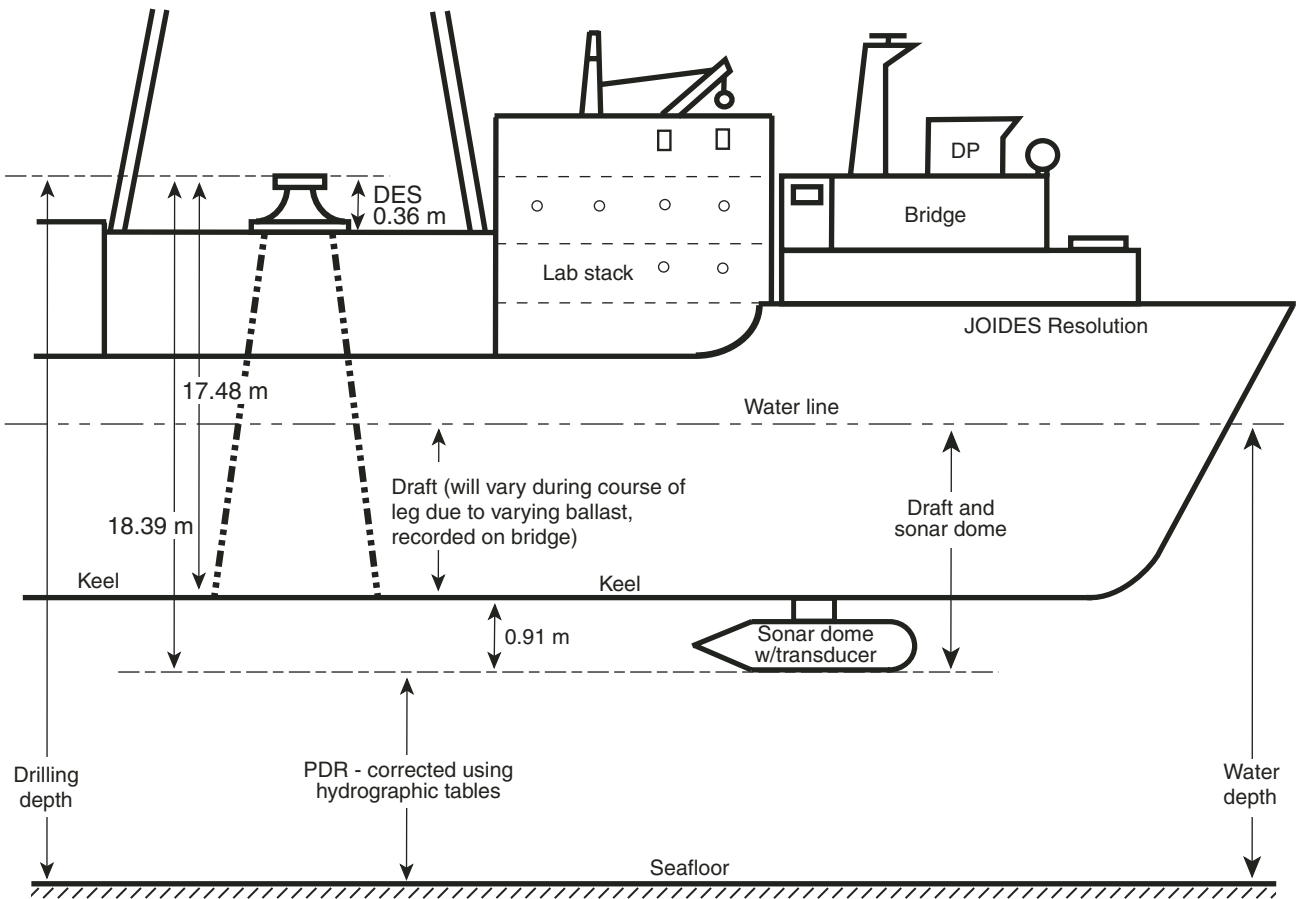
GPS antenna offset from origin  
 Antenna fwd/aft = -46.33 m  
 Antenna (OMNISTAR) port/stbd = 3.05 m  
 Antenna (Ashtech) port/stbd = -3.05 m

**Dynamic positioning GPS antennas**

Trimble GPS antenna offset from origin  
 Antenna fwd/aft = 47.9 m  
 Antenna port/stbd = -1.68 m

Ashtech GPS antenna offset from origin  
 Antenna fwd/aft = 43.89 m  
 Antenna port/stbd = -3.66 m

Figure F24. Schematic diagram showing the relations between water depth, drilling depth, and sonar depth. DES = dual elevator stool, DP = dynamic positioning, PDR = precision depth recorder (sonar).



**Table T1.** Acronyms used in the “Color” column of the AppleCORE core description sheets.

Term	Acronym
<b>Intensity</b>	
very light	vlt
light	lt
medium light	mlt
moderate/medium	med
medium dark	mdk
dark	dk
very dark	vdk
very pale	vpl
pale	pl
dusky	dsk
very dusky	vds
brilliant	bri
vivid	viv
strong	str
deep	dp
very deep	vdp
<b>Modifier</b>	
bluish	bl
brownish	br
creamy	cr
grayish	gy
greenish	gn
orange	or
olive	ol
pinkish	pk
purplish	pu
reddish	rd
whitish	wh
yellowish	ye
mottled	mo
spotty	sp
Blue	BL
Brown	BR
Cream	CR
Gray	GY
Green	GN
Orange	OR
Olive	OL
Pink	PK
Purple	PU
Red	RD
White	WH
Yellow	YE
Buff	BF



Table T2. Example piece log.

CURATORIAL DATA SHEET/PIECE LENGTH							
Hole	Core	Section	Piece	Top (cm)	Bottom (cm)	Length (cm)	Groundmass grain size
1256C	4R	1	2	6	11	5	Chert
1256C	4R	1	3	12	21	9	Chert
1256C	4R	1	4	21	23	2	Chert
1256C	4R	1	5	24	29	5	2
1256C	4R	1	6	29	35	6	2
1256C	4R	1	7	36	38	2	2
1256C	4R	1	8	40	57	17	2
1256C	5R	1	1	0	3	3	Chert
1256C	5R	1	2	4	51	47	3
1256C	5R	1	3	53	58	5	2
1256C	5R	1	4	60	65	5	2
1256C	5R	1	5	65	68	3	3
1256C	5R	1	6	68	71	3	3
1256C	5R	1	7	71	74	3	2
1256C	5R	1	8	75	78	3	2
1256C	5R	1	9	78	99	21	3
1256C	5R	1	10	100	106	6	2
1256C	5R	1	11	107	115	8	2
1256C	5R	1	12	115	135	20	2
1256C	5R	1	13	135	145	10	2
1256C	5R	1	14	145	149	4	2

Notes: Grain size: 1 = glassy, 2 = cryptocrystalline, 3 = microcrystalline, 4 = fine grained. Only a portion of this table appears here. The entire table is available in [ASCII](#).

Table T3. Example igneous unit and contacts log.

Unit/Subunit	Upper contact				Type	Minimum thickness (m)	Rock type
	Core	Section	Piece	Depth (mbsf)			
S1	4R	1	1	245.025	nr	0.16	Chert
1	4R	2	5	245.185	nr	3.8	Sheet flows
S2	5R	1	1	252.415	nr	0.03	Chert
2	5R	3	5	255.93	nr	0.35	Sheet flows
3	6R	1	4	257.26	nr	0.29	Sheet flows
4	6R	1	7	257.55	C	0.28	Sheet flows
S3	6R	1	12	257.83	nr	0.17	Sediment
5	6R	1	15	347.1	nr	1.17	Sheet flows
6	6R	2	11	259.17	C	3.44	Sheet flows
7	6R	5	2	262.61	nr	1.01	Sheet flows
8	7R	1	2	266.4	nr	0.5	Sheet flows
9	7R	1	11	266.9	C	0.76	Sheet flows
10	10R	2	1	267.66	C	0.63	Sheet flows
11a	7R	2	4	268.29	C	0.28	Sheet flows
11b	7R	2	7	268.57	C	0.1	Sheet flows
11c	7R	2	11	268.67	C	1.35	Sheet flows
11 (total)						1.73	
12	7R	3	6	270.02	nr	0.39	Sheet flows
13	7R	4	3	270.41	C	0.2	Sheet flows
14	7R	5	1	270.61	C	1.21	Sheet flows
15	7R	5	2	271.82	nr	2.63	Sheet flows
16	8R	2	3	277.75	C	0.97	Sheet flows
17	8R	3	9	278.72	nr	1.55	Sheet flows

Notes: nr = not recovered. C = chilled margin. Only a portion of this table appears here. The entire table is available in [ASCII](#).

**Table T4.** Key to rock data recorded in the logs and thin section descriptions.

Code	Description	Size (mm)
Grain size:		
G	Glassy	
cx	Cryptocrystalline	<0.1
μx	Microcrystalline	0.1–0.2
fg	Fine	0.2–1
mg	Medium	1–5
c	Coarse	5–30
p	Pegmatitic	>30
	ND	Not determined
Contact type:		
nr	Not recovered	
C	Chilled margin—lava surface	
I	Chilled margin—intrusive	
T	Tectonic	
GS	Gradational change in grain size	
Mineral name:		
ol	Olivine	
pl	Plagioclase	
cpx	Clinopyroxene	
opx	Orthopyroxene	
di	Diopside	
aug	Augite	
pig	Pigeonite	
hyp	Hypersthene	
sp	Spinel	
ox	Fe-Ti oxide	
py	Pyrite	
Contact form:		
P	Planar	
C	Curved	
I	Irregular	
S	Sheared	
Rock type:		
	Pillow basalt	
	Flow margins	
	Sheet flows	
	Massive flow	
	Dike	
	Breccia	
	Pillow breccia	
	Hyaloclastite	

**Table T5.** Example alteration log.

Hole	Core	Section	Piece	Top (cm)	Base (cm)	Length (cm)	Core-top depth (mbsf)	Rock color/alteration type (%)						Glass (%)		Vesicles		Comments
								Dark gray	Brown	Black halo	Light gray	Mixed halo	Dark patch	Blue green	gl	alt glass	(%)	
1256B	29X	1	3	7	12	5	250.7	100						3	50	2	sap, py, cc	
1256C	4R	1	5	24	29	5	245.0	100						0		1	sap, py	
1256C	4R	1	6	29	35	6	245.0	100						0		1	sap, py	
1256C	4R	1	7	36	38	2	245.0	100						0		1	sap, py	
1256C	4R	1	8	40	57	17	245.0	100						0		1	sap, py	
1256C	5R	1	1	0	3	3	252.4	100										
1256C	5R	1	2	4	51	47	252.4	100										
1256C	5R	1	3	53	58	5	252.4	100										
1256C	5R	1	4	60	65	5	252.4	100										
1256C	5R	1	5	65	68	3	252.4	100										
1256C	5R	1	6	68	71	3	252.4	100										
1256C	5R	1	7	71	74	3	252.4	100										
1256C	5R	1	8	75	78	3	252.4	100										
1256C	5R	1	9	78	99	21	252.4	100										

Notes: gl = glass, alt glass = altered glass. sap = saponite, py = pyrite, cc = calcium carbonate. Only a portion of this table appears here. The entire table is available in [ASCII](#).

Table T6. Example vein log.

Hole	Core	Section	Piece	Top (cm)	Base (cm)	Width (mm)	Vertical?	Breccia, vein net, int. sed...		Secondary minerals in vein (%)							Halo		Comments	
								Type	Secondary (%)	Sap	Cel	CO <sub>3</sub>	Py	FeOx	SiO <sub>2</sub>	Qz/Ab	Zeo	Width (mm)		Type
1256B	29X	1	3	7	12	0.1	v			98			2					0.5	py	
1256B	29X	1	3	8	10	0.1				98			2							
1256C	4R	1	5	24	28															Rubble
1256C	4R	1	6	29	35	0.5	v			99			1							
1256C	4R	1	6	33	33	0.3				99			1							
1256C	4R	1	7	37	39															Rubble
1256C	4R	1	8	41	41	0.2				100										
1256C	4R	1	8	46	51	0.2				80			20							
1256C	4R	1	8	47	49	0.2				80			20							
1256C	4R	1	8	53	56	0.1				95			5							
1256C	5R	1	2	10	10	0.1				100										
1256C	5R	1	2	16	22	0.2	v			90			10							
1256C	5R	1	2	23	23	0.2				90			10							
1256C	5R	1	2	16	52	2	v			68			2			30				
1256C	5R	1	2	23	31	1				8			2			90				
1256C	5R	1	2	31	39	1				90		8	2							
1256C	5R	1	2	42	45	0.2				98			2							
1256C	5R	1	3	52	58	0.1				80			20							
1256C	5R	1	4	59	62				RU	2			98							
1256C	5R	1	5	65	68				RU	4			98							
1256C	5R	1	6	68	68	0.1							98							
1256C	5R	1	6	70	70	0.1							98							
1256C	5R	1	8	74	75				RU	2			99							
1256C	5R	1	9	92	94	0.1				70			30							Mc rosette
1256C	5R	1	9	96	96	0.1				100										
1256C	5R	1	10	100	105	0.2				100										
1256C	5R	1	11	106	107	0.5				100										
1256C	5R	1	12	115	120	0.1				98			2							
1256C	5R	1	12	125	126	0.1				100										

Notes: v = vertical. RU = rubble, not logged. Sap = saponite, Cel = celadonite, Py = pyrite, Qz = quartz, Ab = albite, Zeo = zeolite. Mc = marcasite. Only a portion of this table appears here. The complete table is available in [ASCII](#).

Table T7. Example Structural Log 1 table. (Continued on next page.)

Core	Section	Piece	Oriented?	Features				Veins				Joints			Faults			
				Identifier	Distance from top of section to top of feature (cm)	Distance from top of section bottom of feature (cm)	Color of the filling minerals	Average width (mm)	Morphology	Fabric	Comments	Basement unit	Morphology	Wallrock alteration	Comments	Apparent offset (mm)	Apparent sense of shear	Wallrock alteration
2R	1	1C	Y	V10	34	56	dg + w	2.5	St	Late magmatic (?)/dg with white halo/cuts V11, V12, V14, V15	1a							
2R	1	1C	Y	V11	40	41	dg	0.2	Spl	Cut by V10/apparent offset = 3.3 mm	1a							
2R	1	1C	Y	V12	42.5	44	dg	0.2	Pl	Irregular	1a							
2R	1	1C	Y	V13	44.5	44.5	lg + w	1.4	Pl	Splay of V10/white halo; half width = 1 mm	1a							
2R	1	1C	Y	V14	53	53.5	dg + lg	0.5	Pl	Cut by V10/apparent offset = 3.2 mm	1a							
2R	1	1C	Y	V15	47	47.5	dg	<0.1	Pl		1a							
2R	1	1C	Y	V16	54	54	dg	<0.1	Pl	Cut by V10	1a							
2R	1	1C	Y	V17	57.5	58.2	dg + lg		Pl/St	Irregular, open	1a							
2R	1	1D	Y	V18	64	65	lg + dg	0.8		Irregular with halo	1a							
2R	1	1E	Y	V20	75	76	dg	0.2	Pl	Cut by V21	1a							
2R	1	1E	Y	V21	75	76	lg	<0.1	Pl		1a							
2R	1	1F	Y	V19	73.5	79	lg + dg	0.8	Pl	Sulfide; halo (half width = 0.8 mm)	1a							
2R	1	1F	Y	V22	99	102	lg + dg	0.6	Pl/St	Sulfide	1a							
2R	1	1G	Y	V23	105	111	lg + dg	0.5	Pl		1a							
2R	1	1G	Y	V24	110.5	111.5	lg + dg	0.3	Pl		1a							
2R	1	1G	Y	V25	119.5	120.5	lg + dg	0.5	Cv	Hairline; average measurement	1a							
2R	1	1G	Y	V26	128	129	lg + dg	1.2	Pl/St		1a							
3R	1	2	Y	V1	18	19	dg	0.3	Pl	Irregular	1a							
3R	1	3	Y	V1	19	28	lg + dg	0.2	Pl	Irregular; sulfide	1a							
3R	1	4	Y	V1	29.5	34	dg + lg	0.2	Cv	Irregular	1a							
3R	1	4	Y	V3	34	36.5	dg + lg		Pl	Irregular; sulfide	1a							
3R	1	5	Y	V1	37	37	dg + lg		Pl	On exposed surface; sulfide	1a							
3R	1	5	Y	V2	44	44.5	dg	<0.1	Pl	Sulfide	1a							
3R	1	5	Y	V3	42	46	dg + lg	0.2	Cv	Irregular; average measurement	1a							

Notes: Identifier: V = vein, SV = shear vein, F = fault, J = joint. Color: dg = dark green, w = white, lg = light green. Morphology: Pl = planar, Cv = curved, An = anastomosing, Y = Y-shaped, Spl = splayed, Rd = Riedel, St = stepped. Fabric: Fb = fibrous, Bl = blocky. Apparent sense of shear: dx = dextral, sx = sinistral, n = normal, r = reverse. Only a portion of this table appears here. The complete table is available in [ASCII](#).



Table T7 (continued).

Core	Section	Piece	Oriented?	Structural measurements (°)									
				Real			Calculated						
				Strike	Dip	Dip direction	Apparent dip 1	Dip direction 1	Apparent dip 2	Dip direction 2	Strike	Dip	Dip direction
2R	1	1C	Y	176			76	90			356	76	E
2R	1	1C	Y				11	270	4	180	160	12	W
2R	1	1C	Y				10	270	10	180	135	14	W
2R	1	1C	Y	-	0						-	0	
2R	1	1C	Y				8	90	10	00	309	13	E
2R	1	1C	Y				10	270	18	00	242	20	W
2R	1	1C	Y	270	8	0					270	8	N
2R	1	1C	Y				5	270	3	180	149	6	W
2R	1	1D	Y	177			7	270			177	7	W
2R	1	1E	Y	40			10	90			40	13	E
2R	1	1E	Y				40	270	38	00	223	49	W
2R	1	1F	Y				36	270	36	00	225	46	W
2R	1	1F	Y				28	270	34	180	128	41	W
2R	1	1G	Y	200			58	90			20	60	E
2R	1	1G	Y	180	5	270					180	5	W
2R	1	1G	Y				13	90	15	180	49	19	E
2R	1	1G	Y										
3R	1	2	Y				17	90	14	180	39	22	E
3R	1	3	Y	187	90						187	90	
3R	1	4	Y	0	90						0	90	
3R	1	4	Y	178			70	270			178	70	W
3R	1	5	Y	90	3	180					90	3	S
3R	1	5	Y				10	270	2	180	169	10	W
3R	1	5	Y	180			74	270			180	74	W

Table T8. Example Breccia Log.

Core	Section	Piece	Oriented?	Clasts							Matrix				Cement		Comments	
				Volume (%)	Size range (min-max) (mm)	Shape	Composition	Internal structure	Alteration	Sorting	Volume (%)	Grain size	Composition	Structure	Alteration	Volume (%)		Composition
20R	1	6	Y	60	2-30	A-sA	P		Y	pS	40	Fg	sap ± glass	Ve				P = basalt and glass; shear vein in matrix
20R	1	7	Y	60	2-30	A-sA	P		Y	pS	40	Fg	sap ± glass	Ve				P = more basaltic than glassy clasts
21R	1	16	Y	80	<1-5	sA-sR	P		Y	wS	20	Fg	sap + white min.					Hyaloclastite
21R	1	17	Y	80	<1-5	sA-sR	P		Y	wS	20	Fg	sap + white min.					Hyaloclastite
21R	1	18	Y	80	<1-5	sA	P	Ve	Y	pS	20	Fg	sap + white min.					Concretionary alteration mineral replacing glass shards
21R	1	19	Y	90	<1-5	sA	P			pS	20	Fg	sap ± glass					
21R	1	20	Y	90	<1-5	sA	P	Ve	Y	pS	10	Fg	sap ± glass					
21R	1	22	Y	60	<10	A	P			pS	40	Fg	sap ± glass					P = glassy shards, some lithic basalt clasts
21R	2	1	Y	80	1-10	sR	P	Ve	Y	pS	20	Fg	sap + white min.					

Note: Shape: A = angular, sA = subangular, R = rounded, sR = subrounded. Composition: M = monomictic, P = polymictic. Internal structure: Cr = crushing, Ve = veining, Fr = fracturing, Sh = shearing, Po = preferred orientation. Alteration: Y = yes, N = no. Sorting: wS = well sorted, mS = moderately sorted, pS = poorly sorted. Grain size: Cg = coarse grained (>5 mm), Mg = medium grained (1-5 mm), Fg = fine grained (<1 mm). Composition: M = monomictic, P = polymictic. Only a portion of this table appears here. The complete table is available in [ASCII](#).

**Table T9.** Structural geology checklist for descriptions.

Term	Explanation	Term	Explanation
<b>Veins</b>		<b>Breccia</b>	
Depth of veins		Clast features	
Morphology		Volume % = % clasts vs. bulk rock	
Pl	Planar	Size range = max-min average size	
Cv	Curved	Shape	
An	Anastomosing	Angular	
Y	Y-shaped	Subangular	
Spl	Splayed	Subrounded	
Rd	Riedel	Rounded	
St	Stepped	Composition = lithology and/or mineralogy of clasts	
Fabric and color of the filling minerals		Monomictic	
Fb	Fibrous	Polymictic	
Bl	Blocky	Structure	
Average width		Internal crushing	
Vein mineralogy		Veining	
Occurrence of alteration halo		Fracturing	
Crosscutting relationships		Preferred orientation	
Veins array (conjugate, network, en echelon)		Alteration = alteration halos in the clasts	
Slickenfibers, overlapping fiber, slickenlines		Sorting	
Orientation of veins		Well sorted	
Apparent sense of shear		Moderately sorted	
Fracturing and/or shearing of veins		Poorly sorted	
<b>Joints</b>		Matrix features	
Depth of joints		Volume % = % matrix vs. bulk rock	
Morphology		Grain size	
Pl	Planar	Coarse	
Cv	Curved	Medium	
An	Anastomosing	Fine	
Y	Y-shaped	Composition = lithology and/or mineralogy compared with the clast ones	
Spl	Splayed	Structure	
Rd	Riedel	Veining	
St	Stepped	Fracturing	
Occurrence of wall-rock alteration		Preferred orientation	
Crosscutting relationships		Shearing	
Joints array (conjugate, network, en echelon)		Alteration = alteration in the matrix	
Joints density		<b>Cement features</b>	
Orientation of joints		Volume % = % cement/bulk rock	
Plumose structures		Composition = mineralogy (? Hydrothermal)	
<b>Faults</b>		Type of breccia, if evident	
Depth of faults		Hyaloclastite	
Amount of the apparent offset		Jigsaw-puzzle	
Apparent sense of shear*		Fault rock**	
dx	Dextral	Occurrence of veins network associated with breccia	
sx	Sinistral	Occurrence of contact with the host rock and its orientation	
r	Reversal	Crosscutting relationships of veins/fractures with respect to matrix and clasts	
n	Normal		
Average thickness of the fault zone			
Occurrence of wall-rock alteration			
Occurrence and type of fault rocks			
Slickensides and slickenlines			

Notes: \* = with respect to the reference frame (archive half). \*\* = e.g., crush breccia, cataclastite, ultraclastite, according to Sibson (1977).

**Table T10.** Interstitial water analyses and corresponding re-  
 producibility.

Parameter	Method	IAPSO value		Analytical uncertainty	
		Accepted	Measured	1 $\sigma$ (%)	<i>n</i>
Alkalinity	Gran titration	2.33	2.34	2.2	10
Cl (mM)	Titration with AgCl	559	544	0.7	12
H <sub>4</sub> SiO <sub>4</sub> ( $\mu$ M)	Spectrophotometry			0.8	5
NH <sub>4</sub> ( $\mu$ M)	Spectrophotometry				
PO <sub>4</sub> ( $\mu$ M)	Spectrophotometry			BDL	
SO <sub>4</sub> (mM)	Ion chromatography	28.9	28.9	0.3	6
Mg (mM)	ICP-AES	10.55	10.63	2.1	6
Ca (mM)	ICP-AES	54.0	51.64	2.2	6
K (mM)	ICP-AES	10.44	10.26	4.6	6
Na (mM)	ICP-AES		465	0.4	6
Sr ( $\mu$ M)	ICP-AES	87	90	5.8	6
Ba ( $\mu$ M)	ICP-AES		70	0.6	6
B ( $\mu$ M)	ICP-AES	416	546	2.9	6
Li ( $\mu$ M)	ICP-AES	27	21	5.4	6
Mn ( $\mu$ M)	ICP-AES	0	0.6	2.6	6
Fe ( $\mu$ M)	ICP-AES	0	BDL	BDL	
DOC (mM)	Gas chromatography			9.6	3

Notes: IAPSO = International Association for the Physical Sciences of the Ocean, standard seawater. BDL = below detection limit. DOC = dissolved organic carbon. ICP-AES = inductively coupled plasma–atomic emission spectroscopy. *n* = number of replicate analyses. This table is also available in [ASCII](#).

**Table T11.** Sediment chemistry analyses and corresponding reproducibility.

Parameter	Method	SCO-1 value		Analytical uncertainty	
		Accepted	Measured	1 $\sigma$ (%)	<i>n</i>
Nitrogen	Gas chromatography			5.8	6
Carbon	Gas chromatography			1.5	6
Hydrogen	Gas chromatography			5.3	6
Sulfur	Gas chromatography			BDL	
%CaCO <sub>3</sub>	Coulometry			1.1	5
SiO <sub>2</sub>	ICP-AES	62.78 ± 0.66	64.68	3.4	6
Al <sub>2</sub> O <sub>3</sub>	ICP-AES	13.67 ± 0.21	13.58	5.0	6
TiO <sub>2</sub>	ICP-AES	0.63 ± 0.06	0.61	5.8	6
Fe <sub>2</sub> O <sub>3</sub> T	ICP-AES	5.13 ± 0.18	5.03	7.1	6
MnO	ICP-AES	0.05 ± 0.003	0.05	2.9	6
CaO	ICP-AES	2.62 ± 0.20	2.52	1.5	6
MgO	ICP-AES	2.72 ± 0.18	2.73	3.9	6
Na <sub>2</sub> O	ICP-AES	0.90 ± 0.06	0.92	>20	6
K <sub>2</sub> O	ICP-AES	2.77 ± 0.08	2.76	>20	6
Sr	ICP-AES	170 ± 16	168	2.7	6
Ba	ICP-AES	570 ± 30	578	6.9	6
Cr	ICP-AES	68 ± 5	65	>20	6
Ni	ICP-AES	27 ± 4	25	13.1	6
V	ICP-AES	131	129	10.2	6
Y	ICP-AES	26 ± 4	29	8.5	6

Note: Major element oxides are reported as weight percent and trace elements as parts per million. SCO-1 = Cody Shale, a silty shale sediment standard. BDL = below detection limit. ICP-AES = inductively coupled plasma-atomic emission spectroscopy. *n* = number of analyses. This table is also available in [ASCII](#).

**Table T12.** Analyses of grinding contamination and background blank.

Element	Grinding error ( <i>n</i> = 3)	Background blank ( <i>n</i> = 4)
SiO <sub>2</sub>	0	0.10
Al <sub>2</sub> O <sub>3</sub>	BDL	0.01
TiO <sub>2</sub>	BDL	0.01
Fe <sub>2</sub> O <sub>3</sub>	BDL	0.01
MgO	BDL	0.01
MnO	BDL	BDL
CaO	BDL	0.10
Na <sub>2</sub> O	BDL	BDL
K <sub>2</sub> O	0.01	0.01
P <sub>2</sub> O <sub>3</sub>	BDL	0.02
Cr	4.3	19.3
Ni	3.9	3.7
V	BDL	1.7
Sc	BDL	0.9
Ba	BDL	22.2
Sr	BDL	5.8
Y	BDL	1.6
Zr	BDL	9.2
Nb	BDL	BDL

Notes: Major element oxides are reported as weight percent and trace elements as parts per million. Note that SiO<sub>2</sub> has been subtracted from the grinding error, since pure SiO<sub>2</sub> was used to determine grinding contamination. The background blank was determined from drift-corrected intensities and has been subtracted from standard and sample analyses. BDL = below detection limit. *n* = number of analyses. This table is also available in [ASCII](#).

**Table T13.** Analytical conditions for hard rock inductively coupled plasma–atomic emission spectroscopy runs.

Element	Wavelength (nm)	Integration time per calculation point (s)	Voltage (V)	Mode	Increment between points (nm)*	N
Al	396.152	1.0	570	Gauss	0.003	5
Ba	455.403	4.0	610	Max	0.003	1
Ca	393.366	1.0	390	Gauss	0.003	5
Cr	267.716	4.0	820	Max	0.003	1
Fe	259.940	1.0	570	Gauss	0.003	7
K	766.490	1.0	990	Gauss	0.003	5
Mg	285.213	4.0	640	Max	0.003	1
Mn	257.610	4.0	560	Max	0.003	1
Na	589.592	1.0	660	Gauss	0.003	5
Ni	231.604	4.0	930	Max	0.002	1
P	178.229	4.0	990	Max	0.003	1
Si	251.611	1.0	580	Gauss	0.003	5
Sr	407.771	1.0	700	Gauss	0.003	5
V	292.402	1.0	890	Gauss	0.003	7
Y	371.029	4.0	620	Max	0.003	1
Zr	343.823	1.0	640	Gauss	0.003	5
Ti	334.941	1.0	620	Gauss	0.003	5
Nb	316.340	1.0	550	Gauss	0.003	5
Sc	361.384	0.5	620	Gauss	0.002	5

Notes: Reported settings are stored in the software. Entrance and exit slits are the same for each element, 20/15 nm, respectively. \* = the interval between each of the calculation points in Gaussian mode or the calculation window that constitutes the single point in Max mode. N = number of calculation points. This table is also available in [ASCII](#).



**Table T14.** Example run sheet for hard rock inductively coupled plasma–atomic emission spectroscopy run, Hole 1256D.

Analysis number	Cell ID	Hard rock sample	Analysis type
1		Drift 1	Drift
2	1	Std 3	Standard analysis
3		Drift 2	Drift
4	2	Unk 3	Sample analysis
5	3	CkStd 1	Check standard analysis
6		Drift 3	Drift
7	4	Unk 2	Sample analysis
8	5	Std 2	Standard analysis
9	6	Blank	Blank analysis
10		Drift 4	Drift
11	7	Unk 4	Sample analysis
12	8	Unk 1	Sample analysis
13	9	Std 4	Standard analysis
14	10	Unk 7	Sample analysis
15		Drift 5	Drift
16	11	Std 1	Standard analysis
17	12	CkStd 2	Check standard analysis
18	13	Unk 5	Sample analysis
19	14	Unk 6	Sample analysis
20		Drift 6	Drift
21	15	Std 5	Standard analysis
22	16	Unk 4	Sample analysis
23	17	Std 3	Standard analysis
24	18	Unk 3	Sample analysis
25		Drift 7	Drift
26	19	Unk 5	Sample analysis
27	20	CkStd 1	Check standard analysis
28	21	Std 5	Standard analysis
29	22	Unk 1	Sample analysis
30		Drift 8	Drift
31	23	Std 2	Standard analysis
32	24	Unk 7	Sample analysis
33	25	Std 1	Standard analysis
34	26	Blank	Blank analysis
35		Drift 9	Drift
36	27	Unk 2	Sample analysis
37	28	Std 4	Standard analysis
38	29	CkStd 2	Check standard analysis
39	30	Unk 6	Sample analysis
40		Drift 10	Drift

Notes: The run contained five certified standards (Std), seven unknown samples (Unk), two check standards (CkStd), and a full procedural blank (Blank). The drift monitor was typically analyzed more frequently at the beginning of each run. Cell ID = the position of each solution in the auto-sampler; the drift solution was kept in a 500-mL beaker. All analyses were run at least in duplicate, spaced randomly throughout the run. This table is also available in [ASCII](#).

**Table T15.** Precision and accuracy of inductively coupled plasma–atomic emission spectrometry analyses on the JY-2000, Leg 206. (Continued on next page.)

Standard:	All-92-29-1			BAS-140			BAS-148			BIR-1			BOB-1			JA-1		
	Average for all runs	Precision (%)	Published value	Precision (%)	Published value*	Precision (%)	Published value†	Precision (%)	Published value‡	Precision (%)	Published value‡	Precision (%)	Published value‡	Precision (%)	Published value‡	Precision (%)	Published value‡	
Major element (wt%):																		
SiO <sub>2</sub>	48.31	2.4	49.39	51.06	1.1	50.28	49.03	2.1	49.31	48.35	1.5	47.15	50.83	0.6	50.48	64.20	1.4	64.10
Al <sub>2</sub> O <sub>3</sub>	15.97	0.5	15.30	14.29	0.6	14.57	15.65	1.8	15.59	15.33	1.8	15.15	16.23	1.6	16.57	14.72	2.4	14.99
TiO <sub>2</sub>	1.79	2.4	1.73	1.02	0.4	0.99	0.90	5.2	0.90	0.96	2.6	0.95	1.29	5.2	1.27	0.82	2.1	0.87
Fe <sub>2</sub> O <sub>3</sub>	10.95	5.3	10.72	10.73	0.2	11.17	10.26	8.2	9.96	10.92	8.6	11.11	8.82	4.7	8.48	7.84	15.9	6.95
MgO	7.66	3.1	7.32	8.27	0.0	8.13	8.66	8.6	8.61	9.39	5.1	9.56	7.44	4.3	7.69	1.77	3.7	1.61
MnO	0.17	2.9	0.18	0.17	1.7	0.18	0.16	7.0	0.17	0.15	6.8	0.17	0.13	0.2	0.13	0.14	1.6	0.15
CaO	11.41	2.0	11.02	12.53	3.5	12.47	12.93	2.7	12.80	13.06	2.4	13.07	11.36	1.6	11.07	5.70	1.9	5.68
Na <sub>2</sub> O	3.31	2.2	3.03	1.78	0.6	1.70	2.17	4.2	1.97	1.70	3.9	1.73	3.26	4.8	3.06	3.80	0.5	3.86
K <sub>2</sub> O	0.18	3.4	0.17	0.00	141.4	NR	0.09	60.0	0.02	0.01	24.9	0.03	0.39	1.3	0.36	0.76	5.4	0.78
P <sub>2</sub> O <sub>3</sub>	0.17	41.5	0.16	0.06	141.4	0.08	0.05	111.3	0.07	0.02	173.2	0.05	0.15	49.4	0.16	0.17	15.7	0.16
Trace element (ppm):																		
Cr	255.6	6.7	233.1	205.7	1.9	191.5	431.3	27.2	343.7	395.1	2.9	377.1	282.6	4.6	236.6	6.9	3.5	7.3
Ni	125.0	1.7	101.8	110.8	13.4	80.8	135.3	14.9	109.5	210.4	5.3	163.9	115.4	15.8	104.5	0.0	BDL	1.8
V	329.3	12.7	300.3	327.9	3.2	NR	290.9	3.7	NR	303.8	4.2	309.0	253.5	15.8	NR	121.8	7.6	105.1
Sc	40.1	16.5	30.7	40.7	4.5	43.9	44.2	4.0	NR	39.0	8.4	43.4	32.6	13.7	NR	32.5	16.7	28.4
Ba	10.7	85.2	NR	7.5	71.3	NR	6.2	63.7	NR	7.9	98.3	6.9	42.4	4.1	57.2	309.6	5.7	307.2
Sr	143.9	1.6	131.4	57.1	1.7	46.9	78.9	5.1	62.8	112.7	0.7	106.6	208.3	4.9	196.2	254.0	0.7	266.2
Y	35.9	2.0	42.5	26.8	4.4	29.9	25.8	1.4	28.1	16.2	3.4	15.8	26.9	6.6	26.6	28.3	9.8	30.6
Zr	123.3	4.5	133.4	48.4	8.9	48.9	48.6	12.4	48.3	22.3	11.7	15.3	102.2	5.1	100.6	85.9	4.6	88.4
Nb	6.6	6.0	NR	0.0	BDL	NR	0.1	222.3	1.5	0.0	BDL	0.6	1.7	9.1	4.9	0.0	BDL	1.7

Notes: Standards analyzed as a check on precision and accuracy. Precision is calculated as the standard deviation of *n* analyses divided by the average value. BDL = below detection limit; NR = not reported. For elements with near background concentrations, the precision is artificially high (i.e., the actual precision is much better than suggested by the numbers). All values have been normalized to 100% volatile free. \* = Sparks and Zuleger (1995), † = Bach et al. (1996), ‡ = following Govindarasu (1994). This table is also available in [ASCI](#).

**Table T15 (continued).**

Standard:	JP-1		
	Average for all runs <i>n</i> = 3	Precision (%)	Published value
Major element (wt%):			
SiO <sub>2</sub>	44.55	2.4	41.45
Al <sub>2</sub> O <sub>3</sub>	3.16	2.0	0.61
TiO <sub>2</sub>	0.01	7.0	NR
Fe <sub>2</sub> O <sub>3</sub>	8.18	7.8	8.16
MgO	42.72	3.5	43.73
MnO	0.12	6.5	0.12
CaO	0.84	1.4	0.55
Na <sub>2</sub> O	0.00	BDL	0.02
K <sub>2</sub> O	0.00	112.6	0.00
P <sub>2</sub> O <sub>3</sub>	0.00	89.6	NR
Trace element (ppm):			
Cr	2978.4	5.7	2904.2
Ni	2779.9	1.3	2405.5
V	33.4	5.9	28.4
Sc	13.3	2.7	6.9
Ba	13.4	30.8	16.6
Sr	16.0	1.3	NR
Y	4.5	18.0	NR
Zr	14.7	28.1	6.2
Nb	0.0	BDL	1.2

**Table T16.** Setup parameters used for the cryogenic magnetometer software, Leg 206.

Parameter	Setting
SQUID configuration:	
SQUID-x response (cm)	6.071
SQUID-y response (cm)	6.208
SQUID-z response (cm)	9.923
SQUID-x calibration (emu)	8.21E-05
SQUID-y calibration (emu)	-8.34E-05
SQUID-z calibration (emu)	4.32E-05
SQUID filter data (x, y, and z) (Hz)	10
SQUID range data (x, y, and z)	1 x range
SQUID slew data (x, y, and z)	Disable fast slew
SQUID feedback data (x, y, and z)	Close feedback loop
Degausser configuration:	
Ramp rate	3
Tracking timeout (s)	40
AF field maximum (mT)	80
AF field minimum (mT)	2
Coil calibration constant (x, y, and z)	1
Character delay	50
Sample handler configuration (right-hand home and right-hand tray):	
Home switch type	Limit switch
Home offset (cm)	0.0
Tray offset (cm)	2.2
Track length (cm)	599.3
Full tray length (cm)	160.3
Scale (steps/cm)	1572
Sample handler positions:	
SQUID (cm)	255.85
Magnetic susceptibility (not applicable)	0
Degauss stage 1 (cm)	190.0
Degauss stage 2 (cm)	435.0
DG coil center (cm)	410.0
IRM stage (not applicable)	0
IRM coil center	0
Background stage 1 (cm)	300.0
Background stage 2 (cm)	30.0
Load/unload (cm)	0.0
Sensor velocity (cm/s)	10-25
Degauss velocity (cm/s)	10-25
Background velocity (cm/s)	10-25
Load velocity (cm/s)	10-25
Discrete configuration:	
Max number of sample positions	4
Center offset (cm)	20
Center separation (cm)	40

Notes: SQUID = super-conducting quantum interference device. AF = alternating field. IRM = isothermal remanent magnetization.

**Table T17.** Acronyms and units used for wireline logging tools.

Tool	Output	Tool name/explanation of output	Unit
APS		Accelerator Porosity Sonde	
	APLC	Near array porosity (limestone calibrated)	%
	SIGF	Formation capture cross section ( $\Sigma_f$ )	Capture units
	STOF	Tool standoff (computed distance from borehole wall)	in
DLL		Dual Laterolog	
	LLD	Deep resistivity	$\Omega$ m
	LLS	Shallow resistivity	$\Omega$ m
DSI		Dipole Sonic Imager	
	DTCO	Compressional wave delay time ( $\Delta t$ )	ms/ft
	DTSM	Shear wave delay time ( $\Delta t$ )	ms/ft
	DTST	Stoneley wave delay time ( $\Delta t$ )	ms/ft
FMS		Formation MicroScanner	
	C1, C2	Orthogonal hole diameters	in
	P1AZ	Pad 1 azimuth	Degrees
		Spatially oriented resistivity images of borehole wall	
GPIT		General Purpose Inclinator Tool	
	DEVI	Hole deviation	Degrees
	HAZI	Hole azimuth	Degrees
	$F_x, F_y, F_z$	Earth's magnetic field (three orthogonal components)	Degrees
	$A_x, A_y, A_z$	Acceleration (three orthogonal components)	m/s <sup>2</sup>
HLDT		Hostile Environment Litho-Density Tool	
	RHOB	Bulk density (corrected)	g/cm <sup>3</sup>
	PEF	Photoelectric effect	b/e-
	CALI	Caliper (measure of borehole diameter)	in
	DRHO	Bulk density correction	g/cm <sup>3</sup>
HNGS		Hostile Environment Gamma Ray Sonde	
	HSGR	Standard (total) gamma ray	gAPI
	HCGR	Computed gamma ray (HSGR minus uranium contribution)	gAPI
	HFK	Potassium	wt%
	HTHO	Thorium	ppm
	HURA	Uranium	ppm
SGT		Scintillation Gamma Ray Tool	
	ECGR	Environmentally corrected gamma ray	gAPI
TAP		Temperature/Acceleration/Pressure tool	°C, m/s <sup>2</sup> , psi
UBI		Ultrasonic Borehole Imager	
		Spatially oriented acoustic images of borehole wall	
		Acoustic arrival times and amplitude	ms
		Borehole diameter	in
		Borehole azimuth	Degrees
WST		Well Seismic Tool	
		Acoustic arrival times	ms

**Table T18.** Specifications of the BGR oriented bore-hole magnetometer.

Parameter	Specification
General:	
Length (m)	6.25
Diameter (mm)	92
Weight (kg)	250
Maximum temperature (°C)	230
Maximum pressure (bar)	800
Maximum cable length (m)	10,000
Cable type	Schlumberger 7-46P
Operating voltage (V DC)	55
Operating current (mA)	250
Cable head	GO 7
Magnetometer:	
Range (each component) (nT)	±85,000
Resolution (nT)	1
Tiltmeters:	
Range (°)	±87
Resolution (°)	0.2
Gyro:	
Resolution (mdeg/s)	1

Note: V = volts, DC = direct current.

**Table T19.** Measurements made by wireline tool strings.

Tool string	Tool	Measurement	Sampling interval (cm)	Approximate vertical resolution (cm)
Triple combination	HNGS	Spectral gamma ray	15	51
	APS	Porosity	5 and 15	43
	HLDT	Bulk density	2.5 and 15	46
	DLL	Resistivity	15	61
	TAP*	Temperature	1 per s	NA
		Tool acceleration	4 per s	NA
Pressure		1 per s	NA	
Formation MicroScanner (FMS)-sonic combination	SGT	Total gamma ray	15	NA
	FMS	Microresistivity	0.25	0.5
	GPIT	Tool orientation	0.25 and 15	NA
	DSI	Acoustic velocity	15	61
Ultrasonic Borehole Imager	UBI	Ultrasonic imaging	Variable	1.5–8
	GPIT	Tool orientation	0.25 and 15	NA
	SGT	Total gamma ray	15	46/NA
WST (stationary measurement)	WST	Sonic traveltime	Variable	NA

Notes: All tool and tool string names (except the TAP) are trademarks of Schlumberger. For additional information about tool physics and use consult ODP Logging Services at [www.ldeo.columbia.edu/BRG/ODP](http://www.ldeo.columbia.edu/BRG/ODP). See Table T17, p. 92, for explanations of acronyms used to describe tool strings and tools. \* = not included on every run. NA = not applicable.